UNIVERSITY OF BELGRADE
FACULTY OF TECHNOLOGY AND METALLURGY

Rabab Salih

LIGNIN MICROSPHERES AS ADSORBENTS FOR TEXTILE DYES REMOVAL AND SUPPORTS FOR IMMOBILIZATION OF ENZYMES

Doctoral Dissertation

Belgrade, 2023

Univerzitet u Beogradu
Tehnološko Metalurški fakultet

Rabab Salih

LIGNIN MIKROSFERE KAO ADSORBENTI ZA UKLANJANJE TEKSTILNIH BOJA I NOSAČI ZA IMOBILIZACIJU ENZIMA

Doktorska disertacija

Beograd, 2023

Supervisor:

prof. dr Aleksandar Marinković, Full professor, University of Belgrade, Faculty of Technology and Metallurgy

dr Katarina Banjanac, Research Associate, University of Belgrade, Innovation center of Faculty of Technology and Metallurgy

Members of committee:

dr Maja Djolić, assistant professor, University of Belgrade, Faculty of Technology and Metallurgy

prof. dr Dejan Bezbradica, Full professor, University of Belgrade, Faculty of Technology and Metallurgy

dr Jelena Gržetić, Assistant research professor, Military Technical Institute

Candidate: _____

In Belgrade: _____

LIGNIN MICROSPHERES AS ADSORBENTS FOR TEXTILE DYES REMOVAL AND SUPPORTS FOR IMMOBILIZATION OF ENZYMES

ABSTRACT

In this doctoral dissertation, starting material lignin was modified in order to synthesize lignin microspheres to obtain a material that will be used for the adsorption of dyes as organic pollutants, and as a carrier for the immobilization of the laccase which will be used for the degradation of textile dyes Lanaset® violet B, Lanaset® blue 2R, and Acid Green 40, Ciba®, present in industrial wastewater.

In the first part of the dissertation, procedures for the synthesis and modification of lignin microspheres are described (as result of applied procedures three different b-LMS microspheres are created (LMS-DEGDMA, b-LMS and b-LMS-OSO_3H).

The first step of kraft lignin (KfL) modification is the reaction of suspension copolymerization with acrylic acid, where acrylic modified kraft lignin (KfL-AA) is obtained. Acrylic acid was obtained by multi-step synthesis from natural sources-fructose, whereby levulinic acid was obtained, which is it further oxidized to 3-hydroxypropanoic acid (3-HPA). Acrylic acid is obtained by dehydration of 3-hydroxypropanoic acid. The KfL-AA obtained in this way reacts with diethylene glycol dimethacrylate (DEGDMA), whereby lignin modified microspheres (LMS-DEGDMA) are obtained, which will be used as a carrier for the immobilization of laccase from *Myceliophthora thermophilia* expressed in *Aspergillus oryzae* (commercial laccase preparation Novozyme® 51003).

Furthermore, the acrylic modified kraft lignin (KfL-AA) from the process of inverse suspension copolymerization reacts with an acrylic reactant - bio trimethylpropane triacrylate (TMPTA), whereby porous microspheres (b-LMS) are formed. And finaly, by reacting of b-LMS with chlorosulfonic acid, a sulfate group is incorporated into the structure of the microsphere and b-LMS-OSO_3H microspheres are created, and this material will be tested for the adsorption of cations and cationic dyes from water.

In the second part of the dissertation, three synthesized samples of lignin microspheres (LMS-DEGDMA, b-LMS and b-LMS-OSO_3H) were characterized using instrumental characterization techniques. The experimental techniques used are: Fourier Transform Infrared Spectroscopy (FT-IR), X-ray Diffraction Analysis (XRD), X-ray Photoelectron Spectroscopy (XPS), Raman Spectroscopy, Scanning Electron Microscopy (SEM), Nuclear Magnetic Resonance (NMR), Thermographic analysis (TGA) and Specific Surface Area and Porosity Analysis (BET). In order to better understanding the structural and surface characteristics of the synthesized adsorbents, the quantification of functional groups (phenolic, hydroxyl) and the point of zero charge (pHpzc) was performed. Process of laccase Novozyme® 51003) immobilization on LMS-DEGDMA microspheres, ,is also described in detail. Key parameters that define immobilization process such as the protein loading and immobilization yield, stability and catalytic activity of the immobilized preparation were also determined. Optimization of the immobilization process made it possible to desing LMS-DEGDMA-laccase preparation which could be used for decolorization of textile dyes present in industrial wastewater. As result of the immobilization process optimization, it was showed that laccase immobilization on LMS-DEGDMA exhibited the best results (protein immobilization yield of 70 %, activity yield of 27 %, and catalytic activity of 262 IU/g of support) when the immobilization was perform at pH 5.0 and 100 mg of offered protein per g support during 1 h.

The results for degradation of the crystal violet, aniline blue dyes and acid green (such as Lanaset® violet B, Lanaset® blue 2R (C.I. Acid Blue 225 (AB 225) and C.I. Acid Green 40, Ciba®) showed that LMS-DEGDMA-laccase have good prospects to be used for removal of textile dyes from wastewater with efficiecy of about 85% during 45minutes, 2 h and 3 h in case of Acid Green 40, Lanaset® blue 2R and Lanaset® violet B, respectively. Experiments on the reusability of the LMS-DEGDMA-laccase showed satisfactory stability, from 5 to 7 cycles depending of used dye in reaction. Also, it has been showed that decolorization of dyes with LMS-DEGDMA-laccase occurs dominatly as result of laccase activity and the contribution of dye adsorption on LMS-DEGDMA microspheres process after one repeated use could be neglected.

On the other hand, in order to examine the adsorptive performance of the synthesized materials, various adsorption studies were performed, such as adsorption kinetics study, adsorption isotherms and pH effect. The laccase Novozyme® 51003 adsorption kinetics on LMS-DEGDMA microspheres was also examined. Obtained results indicated that laccase molecules adsorb on LMS-DEGDMA according to a first-order adsorption kinetics and the experimental data are fitted well with Langmuir isotherm model. The intra-particle diffusion process was also studied by applying of Weber–Morris model on the experimental data. The obtained experimental results during various adsorption studies performed on b-LMS and b-LMS-OSO_3H were fitted with different theoretical models to examine their agreement and suppose the adsorption mechanism. Statistical analysis of the results was performed using the analysis of variance (ANOVA) method. In order to test the reusability of adsorbents, adsorption/desorption experiments were performed in several cycles of wastewater treatment, where they showed satisfactory adsorption efficiency of the b-LMS sample after 5 consecutive cycles of adsorption/desorption.

In the third part of the dissertation, the adsorptive properties of synthesized materials for dyes removal: Methyl Red (MR), Tartrazine (T) and Malachite Green (MG) from aqueous solutions were examined. Adsorption experiments showed that b-LMS has a higher affinity and better adsorption performance for removing Malachite Green than Methyl Red and Tartrazine, which was confirmed by theoretical modeling. The regeneration and competitive adsorption results showed satisfactory b-LMS sample performance. The introduction of a sulfate group into the structure of the b-LMS sample resulted in higher affinity and better selectivity for cationic dyes and cations of b-LMS-OSO_3H sample.

These results show modified kraft lignin's potential application in wastewater treatment processes. Bearing in mind the global trend of environmental pollution, research from this dissertation can contribute to solving the wastewater pollution problem, which will be key to preserving environmental protection in the future.

Keywords: Kraft lignin, lignin microspheres, laccase immobilization, lignin modification, removal of dyes from water, degradation of textile dyes, competitive adsorption, adsorbate/adsorbent interactions

Scientific field: Environmental engineering

LIGNIN MIKROSFERE KAO ADSORBENTI ZA UKLANJANJE TEKSTILNIH BOJA I NOSAČI ZA IMOBILIZACIJU ENZIMA

SAŽETAK

U ovoj doktorskoj disertaciji polazni materijal lignin je modifikovan u cilju sinteze lignin mikrosfera da bi se dobio materijal koji će se primenjivati za adsorpciju boja kao organskih zagađivača i kao nosač za imobilizaciju enzima lakaze koji će se koristiti za degradaciju tekstilnih boja (Lanaset® violet B, Lanaset® blue 2R, and Acid Green 40, Ciba®) koje se nalaze u industrijskim otpadnim vodama.

U prvom delu disertacije opisani su postupci sinteze i modifikacije lignin mikrosfera (b-LMS). Prvi korak modifikacije lignina predstavlja reakciju suspenzione kopolimerizacije sa akrilnom kiselinom gde se dobija akrilni modifikovani kraft lignin (KfL-AA). Akrilna kiselina je dobijena višestepenom sintezom iz prirodnih izvora, iz fruktoze pri čemu je dobijena levulinska kiselina koja se dalje oksiduje do 3-hidroksipropanske kiseline (3-HPA). Dehidratacijom 3-hidroksipropanske kiseline dobija se akrilna kiselina. Ovako dobijeni KfL-AA reaguje sa dietilen glikolom dimetakrilatom (DEGDMA) pri čemu se dobijaju lignin modifikovane mikrosfere (LMS-DEGDMA) koje će se koristi kao nosač za imobilizaciju lakaze Novozyme® 51003.

Dobijeni akrilni modifikovani kraft lignin (KfL-AA) postupkom inverzne suspenzione kopolimerizacije reaguje sa akrilnim reaktantom – bio trimetilpropanom triakrilatom (TMPTA) pri čemu nastaju porozne mikrosfere (b-LMS). Reakcijom sa hlorsulfonskom kiselinom se inkorporira sulfatna grupa u strukturu mikrosfere i nastaje b-LMS-OSO_3H, materijal koji će se ispitivanje adsorpcije katjona i katjonskih boja iz vode.

U drugom delu disertacije, tri sintetisana uzorka lignin mikrosfera (LMS-DEGDMA, b-LMS i b-LMS-OSO_3H) su okarakterisana primenom instrumentalnih tehnika karakterizacije. Eksperimentalne tehnike koje su korišćene su: Infracrvena spektroskopija sa furijeovom transformacijom (FT-IR), Rendgenska difrakciona analiza (XRD), Rendgen fotoelektronska spektroskopija (XPS), Ramanska spektroskopija, Skenirajuća elektronska mikroskopija (SEM), Nuklearna magnetna rezonanca (NMR), Termogravimetrijska analiza (TGA) i Analiza specifične površine i poroznosti (BET). Pored navedenih tehnika, u cilju boljeg sagledavanja strukurnih i površinskih karakteristika sintetisanih adsorbenasa, rađena je kvantifikacija funkcionalnih grupa (fenolne, hidroksilne) i tačka nultog naelektrisanja (pH_{pzc}). Takodje je detaljno opisan postupak imobilizacije lakaze na nosaču LMS-DEGDMA koji se koristio za uklanjanje tekstilnih boja. Određen je prinos imobilizacije, stabilnost enzima i odredjena katalitička aktivnost materijala. Optimizacija procesa imobilizacije omogućila je izradu preparata LMS-DEGDMA koji bi mogao da se koristi za dekolorizaciju tekstilnih boja u industrijskim otpadnim vodama. Kao rezultat optimizacije procesa imobilizacije pokazano je da je imobilizacija lakaze na LMS-DEGDMA dala najbolje rezultate (prinos imobilizacije proteina 70%, prinos aktivnosti 27%; i katalitička aktivnost 262 IU/g nosača) kada je imobilizacija vršena na pH 5.0 i 100 mg proteina/g nosača tokom 1h. Rezultati degradacije ljubičate, anilinsko plave i zelene boje (Lanaset® violet B, Lanaset® blue 2R (C.I. Acid Blue 225 (AB 225) i C.I. Acid Green 40, Ciba®) pokazali su da LMS-DEGDMA-lakaza poseduje dobre adsorptivne mogućnosti za uklanjanje ovih boja iz otpadnih voda sa efikasnošću oko 85% tokom 45 min, 2h i 3h u slučaju Acid Green 40, Lanaset® blue 2R i Lanaset® violet B, respektivno. Eksperimenti ponovne upotrebe LMS-DEDGMA-lakaza dali su zadovoljavajuće rezultate i stabilnost od 5-7 ciklusa regeneracije. Takođe je pokazano

da dekolorizacija boja LMS-DEGDMA-lakaza se javlja pretežno kao rezultat aktivnosti lakaze a doprinos adsorpciji boje na LMS-DEGDMA nakon jedne ponovne upotrebe može se zanemariti.

Sa druge strane da bi se ispitale adsorptivne perfomanse sintetisanih materijala urađeni su eksperimenti adsorpcije: kinetika adsorpcije, adsorpcione izoterme i pH zavisnost. Kinetika adsorpcije Novozyme® 51003 na LMS-DEGDMA mikrosfere je takodje ispitana. Dobijeni rezultati pokazali su da molekuli lakaze adsorbuju na LMS-DEGDMA u skladu sa kinetikom adsorpcije prvog reda i pokazuju dobro fitovanje sa Lengmir izotermom. Model unutar čestične difuzije je takođe ispitan primenom Weber-Morris modela. Dobijeni rezultati tokom različitih eksperimenata adsorpcije b-LMS i LMS-DEGDMA fitovani su sa različitim teorijskim modelima da bi se ispitalo njihovo slaganje i pretpostavio mehanizam adsorpcije. Analiza varijanse (ANOVA) je korišćena za statističku obradu rezultata. U cilju ispitivanja ponovne upotrebe adsorbenasa uradjeni su eksperimenti adsorpcije/desorpcije u nekoliko ciklusa tretmana otpadnih voda gde su pokazali dobru efikasnost adsorpcije na b-LMS uzorku nakon 5 uzastopnih ciklusa adsorpcije/desorpcije.

U trećem delu disertacije ispitane su adsorptivne osobine sintetisanih materijala za uklanjanje boja: Metil crveno (MR), Tartrazin (T) i Malahit Zeleno (MG) iz vodenih rastvora. Takodje je ispitana mogućnost degradacije antrahinonske boje Lanaset® violet B iz industrijskih otpadnih voda lakazom imobilizovanog LMS-DEGDMA. Da bi se postigao maksimalni prinos imobilizacije lakaze Novozyme® 51003, process je optimizovan, i dobijena je efikasnost od 70% prinosa i 27% aktivnosti na pH 5.0 I 100 mg proteina po gramu nosača. Rezultati degradacije boje Lanaset® violet B pokazali su izuzetnu efikasnost imobilizovanog LMS-DEGDMA, tokom 24h adsorbovano je oko 90% boje. Eksperimenti regeneracije i ponovne upotrebe adsorbenta pokazali su zadovoljavajuću stabilnost, posle 7 ciklusa adsorpcije/desorpcije, adsorbuje se više od 60% zagađivača. Adsorpcioni eksperimenti pokazali su da b-LMS ima veći afinitet i bolje adsorpcione performance za uklanjanje Malahit zeleno (MG) od Metil crvenog i Tartrazina, što je potvrđeno teorijskim modelovanjem. Rezultati regereneracije i kompetitivne adsorpcije pokazali su zadovoljavajuće performance b-LMS uzorka. Uvođenje sulfatne grupe u strukturu b-LMS uzorka rezultiralo je većim afinitetom i boljom selektivnošću za katjonske boje i katjone uzorka b-LMS-OSO_3H.

Dobijeni rezultati pokazuju potencijalnu mogućnost primene modifikovanih kraft lignina u procesima za prečišćavanje otpadnih voda. Imajući u vidu globalni trend zagađenja životne sredine, istraživanja iz disertacije mogu doprineti rešenju problematike zagađenja otpadnih voda što će biti krucijalno za očuvanje zaštite životne sredine u budućnosti.

Ključne reči: Kraft lignin, lignin mikrosfere, imobilizacija lakaze, modifikacija lignina, uklanjanje boja iz vode, degradacija tekstilnih boja, kompetitivna adsorpcija, interakcije adsorbat/adsorbent

Naučna oblast: Inženjerstvo zaštite životne sredine

LIST OF ABBREVIATIONS AND SYMBOLS

M1G – Coniferyl (4-(3-hydroxyprop-1-en-1-yl)-2-methoxyphenol)

M1S – Sinapil (4-(3-hydroxyprop-1-en-1-yl)-2,6-dimethoxyphenol)

M1H – p-coumaryl alcohol (Phenol, 4-((1Z)-3-hydroxy-1-propenyl)-)

LMS – Lignin-based microspheres

KfL – Kraft lignin

^{1}H NMR – Proton Nuclear Magnetic Resonance Spectroscopy

^{13}C NMR – Carbon Nuclear Magnetic Resonance Spectroscopy

Laccase (EC 1.10.3.2)

Monophenol monooxygenase (EC 1.14.18.1)

UV/Vis – Ultraviolet Visible Spectroscopy

EPR – Electron Paramagnetic Resonance

T1 – Copper Type I

T2 – Copper Type II

T3 – Copper Type III

Leu – Leucine

Phe – Phenylalanine

His – Histidine

Cys – Cysteine

$ABTS^{\bullet+}$ – 2,2'-Azino-bis(3-ethylbenzothiazoline-6-sulfonic acid)

DMP – 2,6-Dimethoxyphenol

pI – Isoelectric point

PAHs – Polycyclic aromatic hydrocarbons

POPs – Environmental pollutants

IUBMB – International Union of Biochemistry and Molecular Biology

CGPM – Conference on Weights and Measures

U – Total enzyme activity

Cat (Catal) – Catalytic activity of enzymes

IU (IJ) – International unit

U, mg^{-1} – Enzyme activity per weight unit

U, ml^{-1} – Enzyme activity per volume unit

SA – Specific activity

A – Activity (activity expressed in enzyme units)

SP, mg^{-1} – Protein content in the enzyme preparation,

IU, g^{-1} – Activity of immobilized enzyme per weight unit of the dry support

BOD – Biological oxygen demand

COD – Chemical oxygen demand

FT-IR – Infrared Spectrometry with Fourier Transformation

SEM – Scanning Electron Microscopy

XRD – X-ray Diffraction method

RSM – Response Surface Method

R^2 – Correlation coefficient

K_L, L g^{-1} – Langmuir constant

C_0, mg l^{-1} – Initial adsorbate concentration

C_e, mg g^{-1} – Concentration of adsorbate at equilibrium

q_e, mg g^{-1} – Amount of adsorbate per unit weight of adsorbent in the equilibrium state

Q_{max}, mg g^{-1} – Maximum adsorption capacity

b, $Jmol^{-1}$ – Temkin constant related to the heat of sorption

1/n – Constant of expressing the adsorption intensity

K_f, mg g^{-1} – Freundlich constant

K_t, L g^{-1} – Temkin isotherm constant

q_m, mg g^{-1} – Maximum adsorption capacity

β, $mmol^2J^{-2}$ – Coefficient related to the mean of free adsorption energy

ε – Polanyi potential

T, K (°C) – Temperature

R, J mol^{-1} K^{-1} Universal gass constant

β_s – Sips isotherm exponent

K_s, L g^{-1} – Sips isotherm model constant

a_s, L g^{-1} – Sips isotherm model constant

A, L g^{-1} – Redlich-Peterson isotherm constant

ΔG_0, kJ mol^{-1} – Gibbs energy change

ΔH_0, kJ mol^{-1} – Enthalpy change

ΔS_0, kJ mol^{-1} – Entropy change

K_L, mol^{-1} – Langmuir equilibrium constant

k_1, min^{-1} – Pseudo-first-order adsorption rate constant

q_t, mg g^{-1} – Amount of adsorbate per weight unit of adsorbent in time t

k_2, g mg^{-1} min^{-1} – Pseudo-second-order adsorption rate constant

t, min – Time

α_E, mg g^{-1} min^{-1} – Initial adsorption rate

β_E, g mg^{-1} – Desorption coefficient

B_t – Boyd's constant

k, mg^{-1} $min^{-1/2}$ – Intraparticle diffusion rate constant

C – Constant proportionally of the thickness of the boundary layer

K, min^{-1} – Constant adsorption rate

HSDM – Homogenous surface diffusion model

D_s – Intraparticle diffusion coefficient

E_a, J mol^{-1} – Activation energy

k_0, g mg^{-1} min^{-1} – Proportionality factor temperature independent

k_B – Boltzmann constant

$c^{1/2}$ – Half-saturation concentration of active sites

c_s – Pollution solubility

k_{th}, cm^3 min^{-1} mg^{-1} – Tomas constant

m, g – Mass of adsorbent in column

Q_0, cm^3 min^{-1} – Wastewater flow through the column

t, min – Flow through the column time

C_0 (C), mg dm^{-3} – Input/output pollutant concentration

$k_{BA,}$ dm^{-3} mg^{-1} min^{-1} – Kinetic constant

F, cm min^{-1} – Linear rate

Z, cm – Column fill thickness

N_0, mg dm^{-3} – Time is the time needed for 50% adsorbate breakthrough

t, min – Time of the breakpoint or sampling

A (r) – Clark's parameters

n – Freundlich parameter

k_{YN}, min^{-1} – Yoon-Nelson flow constant

θ – Saturated concentration

PSDM – Pore Surface Diffusion Model

XPS – X-ray photoelectron spectroscopy

BET/BJH – Brunauer-Emmett-Teller method of gas adsorption and Barrett-Joyner- Halenda method

TGA – Thermogravimetric analysis

λ, nm – Wavelength

ν_{max} – position intensity

SE – Secondary scattered electrons

BE – Backscattered electrons

BET – Brunauer–Emmett–Teller method (Brunauer–Emmett–Teller adsorption isotherms)

D_2O – Deuterated water

DMSO-d6 – Deuterated dimethyl sulfoxide

AIBN – α,α'-azoiso-bis-butyronitrile

TMP – trimethylolpropane

EHL – 2-ethylhexyl levulinate

MG – Malachite green

T – Tartrazine

MR – Methyl red

DEGDMA – Diethylene glycol dimethacrylate

KfL-AA – Acrylic modified kraft lignin

AA – Acrylic acid

AIBN – Azoiso-bis-butyronitrile

LA – levulinic acid (4-oxopentanoic acid)

3-HPA – 3-hydroxypropanoic acid

RSM – Response Surface Methodology

ATR – Attenuated Total Reflectance

TMS – Tetramethylsilane

J, Hz – Coupling constant

FESEM – Eield Emission Scanning Electron Microscopy

SBET, m^2/g – Specific surface area

S_{meso}, m^2/g – Mesoporosity surface area

V_{mic} (V_{micro}), cm^3/g – Specific micropore volume

dV(r), nm – Pore size distribution

pH_{pzc} – point of zero charge

m_M, g – weight of the dry sample

m_W, g – weight of the wet sample

V, dm^3 – volume of the wet sample

Qs, g dm^{-3} – ethanol density

TnBAH – tetra-butylammonium hydroxide

AV – Acid value

TOC – Total organic carbon

IU – One unit (amount of the laccase that oxidized 1 μmol of $ABTS^{\bullet+}$ substrate per min)

IY_a, % – Activity immobilization yield

q, mg g^{-1} – Adsorption Capacity

C_i, ppm – Initial concentration of dyes

C_f, ppm – Final concentration of dyes

R, % – Removal efficiency

RE, % – Efficiency of regeneration

ANOVA – Analysis of variance

H_α – α protons

β-O-4 – arylethers

k_{id1}, k_{id2}, [mg/(g min^{-1})] –diffusion rate constants

HBD – Hydrogen donating site

A_T, L g^{-1} – Equilibrium binding constants in Temkin isotherm model

Re – Reynolds number

S – Lignin surface

BCS – Bed column study

B-A – Bohart-Adams model of fitting

Y-N – Yoon-Nelson model of fitting

TABLE OF CONTENTS

1. INTRODUCTION

Environmental and water pollution is currently one of the biggest challenges for humanity. The release of toxic substances, including textile dyes, from various sources into recipients represents a serious threat to the living world [1]. Dyes reach the water through various human activities and are subject to a certain extent to biological degradation, and it is known that they can accumulate in tissues. Until now, methods used to remove pollutants from water, such as sedimentation, coagulation, membrane processes, nanofiltration, ion exchange, advanced oxidation processes, and electrochemical methods, all have many disadvantages concerning efficiency and economy. Because of this is a need to develop new and improved techniques such as adsorption and biosorption. Development of natural materials based on lignocellulose is necessary [2]; lignin derivatives [3], as well as chitin and chitosan [4] due to their biorenewability. Chemical modification is one possible way to increase natural material adsorption effectiveness. Under chemical modification, it means introducing new functional groups (amino, carboxyl, phosphate, sulfate/sulfonic, etc.) on the material surface, which increases their adsorption potential and the possibility of using them as support for enzyme immobilization.

Generally, the possibility of wider application of enzymes in industry, among other things in water bioremediation processes, is limited because under extreme experimental conditions (ionic strength, temperature, pH, presence of various reagents of organic origin) enzyme denaturation can occur, whereby it loses its catalytic properties [5]. There is the problem of the impossibility of separating free enzymes from the reaction mixture and their reusability during several reaction cycles. One of the ways to overcome these problems is by physically or chemically binding enzymes to natural and synthetic supports surface or by "trapping" enzymes within the support matrix, i.e. using the enzyme immobilization procedure [6]. Application of enzyme immobilization procedure, it is possible to obtain a preparation with improved catalytic activity, stability, and selectivity towards the substrate compared to the free enzyme. Enzyme immobilization facilitates the separation from the reaction mixture and enables their use in multiple reaction cycles, which directly leads to reducing the costs of the enzymatic process at the industrial level [6]. Considering the fact that most synthetic materials and commercial carriers (such as polymethacrylate and polystyrene resins) used for enzyme immobilization are not environmentally friendly (problem with disposal after the procedure) and economically acceptable, in recent years research has been focused on the application of biomaterials (agarose, cellulose, chitosan, alginate, etc.) and agro-industrial waste (coconut, egg, cereal and pistachio shells, animal feathers, etc.)) as support for enzyme immobilization [7]. Considering that it is need to create a material that will be economically and environmentally acceptable, it is necessary to point out that natural materials are primarily biodegradable, cheap, easily available, easy to synthesize, possess different functional groups on their surface to which enzymes can be directly attached, as well as which can be easily modified by applying various modifying agents, it is understandable that an increasing investigations for this subject. As part of this doctoral dissertation, the possibility of applying natural material based on lignin to support enzyme immobilization will be studied [8].

The aim of this doctoral dissertation will be to investigate the possibility of applying the natural material lignin, chemically modified with acrylic acid (lignin-acrylate) with a crosslinker obtained from natural resources, in the synthesis of lignin microspheres, b-LMS, which will be used as pollutant adsorbents, primarily textile dyes (Lanaset® blue 2R, Acid Green 40, Ciba® Lanaset® violet B). Additionally, the possibility of using b-LMS, obtained by copolymerization of lignin-acrylate and

diethylene glycol-dimethacrylate (DEGDMA), as a support for enzyme immobilization, and above all, the commercial laccase preparation Novozyme® 51003, will be considered.

The scientific contribution based on the results from this dissertation will in the following:

- Synthesis of acryloyl-modified lignin derivatives (lignin-acrylate) and TMPTA based on renewable materials,
- Synthesized b-LMS microspheres, based on lignin-acrylate and bio-TMPTA, as new adsorption materials with improved properties, will be applied for the effective removal of Malachite Green (MG), Tartrazine (T), and Methyl Red (MR) textile dyes.
- Characterization of starting and modified materials before and after textile dyes adsorption from water,
- Optimization of material modification and synthesis and adsorption processes will be studied.
- Modeling of adsorption data using adsorption and kinetic models, as well as calculation of thermodynamic and activation parameters,
- Interpretation of the adsorption mechanism, influence of material properties and experimental conditions on adsorption efficiency,
- Applied semi-empirical and quantum-chemical calculations will contribute to defining the contribution of non-specific and specific interactions between adsorbents and adsorbates to the overall mechanism of adsorption,
- Modeling of the adsorption process in the column,
- Determination of desorption properties and solving the issue of wastewater after desorption,
- Optimization of the immobilization conditions (pH, time, temperature, initial protein concentration) of the laccase enzyme on the support (lignin of microspheres),
- Determination of laccase binding kinetics to synthesized lignin microspheres,
- Determination of catalytic activity, operational and thermal stability of the obtained immobilized laccase preparations,
- Synthesized b-LMS microspheres, based on lignin-acrylate and DEGDMA, for the immobilization of the selected enzyme, will be applied in the reaction of degradation of textile dyes (Lanaset® violet B, Lanaset® blue 2R, C.I. Acid Green 40),

It is expected that the results from this doctoral dissertation will significantly contribute to solving the problem of removing textile dyes from water using natural (biodegradable) materials based on lignin. Obtaining an economically accepted and environmentally friendly adsorbent and enzyme support from a natural polymer obtained from waste raw materials, is in accordance with sustainable development and circular economy principles and represents a very useful solution for water purification.

2. THEORETICAL PART

2.1. Lignin-origin, physicochemical properties, and structure

Main polymers in wood biomass are cellulose (35-50%), hemicellulose-cellulose (20-30%), and lignin (20-30%). Hemicellulose and cellulose are linked by hydrogen bonds, while covalent bonds link lignin and cellulose. Lignin represents the main structural polymer in the cell wall of trees, and contributes to the rigidity of the cell walls, which ensures the plant's growth in height. Covalent bond between lignin and wood polysaccharides provides rigidity and reduces cell wall permeability. It is the second most common natural polymer after cellulose. Its role for the plant is to provide strength, impermeability, and resistance to microorganisms because it represents a physical barrier in the attack of microbial enzyme systems. Lignin has a very branched structure built of phenylpropanoid units derived from coniferyl (M1G), sinapil (M1S) and p-coumaryl alcohol (M1H) as monomers and contains aromatic and aliphatic functional groups. Structure of lignin is complex and depends on the origin; lignin is made up of 63 - 67% carbon, 6% hydrogen, and 28.5% oxygen. One of the possible classifications of lignin can be performed according to the representation of phenyl propane units incurred from monomeric precursors: p-hydroxyphenylpropane, guaiacylpropane and syringylpropane units. Lignin contains more than two-thirds of phenylpropane units bounded by ether bonds, and the other is carbon-carbon bonds [1–4].

Lignin is thermally stable, low toxic, has antioxidant and antimicrobial effects, and is also very reactive precisely because the presence of different functional groups in its structure and the possibility of additional functionalization. The most important groups that lignins contain and which define their reactivity are phenolic hydroxyl groups, hydrogen atoms in addition to phenolic hydroxyl groups, hydroxyl groups in the side chains, ether bonds in the side chains, and methoxy groups [13]. Besides natural biomass, lignin can also be found in the waste streams from the paper industry or biomass pretreatment process. For this reason, lignin is an inexpensive resource available in large quantities. Thanks to the branched structure, if it is necessary to improve specific characteristics, relatively simple chemical modification by different functional groups makes lignin suitable for various purposes. Adler proposed the complete structure of lignin in 1977. (Figure 1) [13–17].

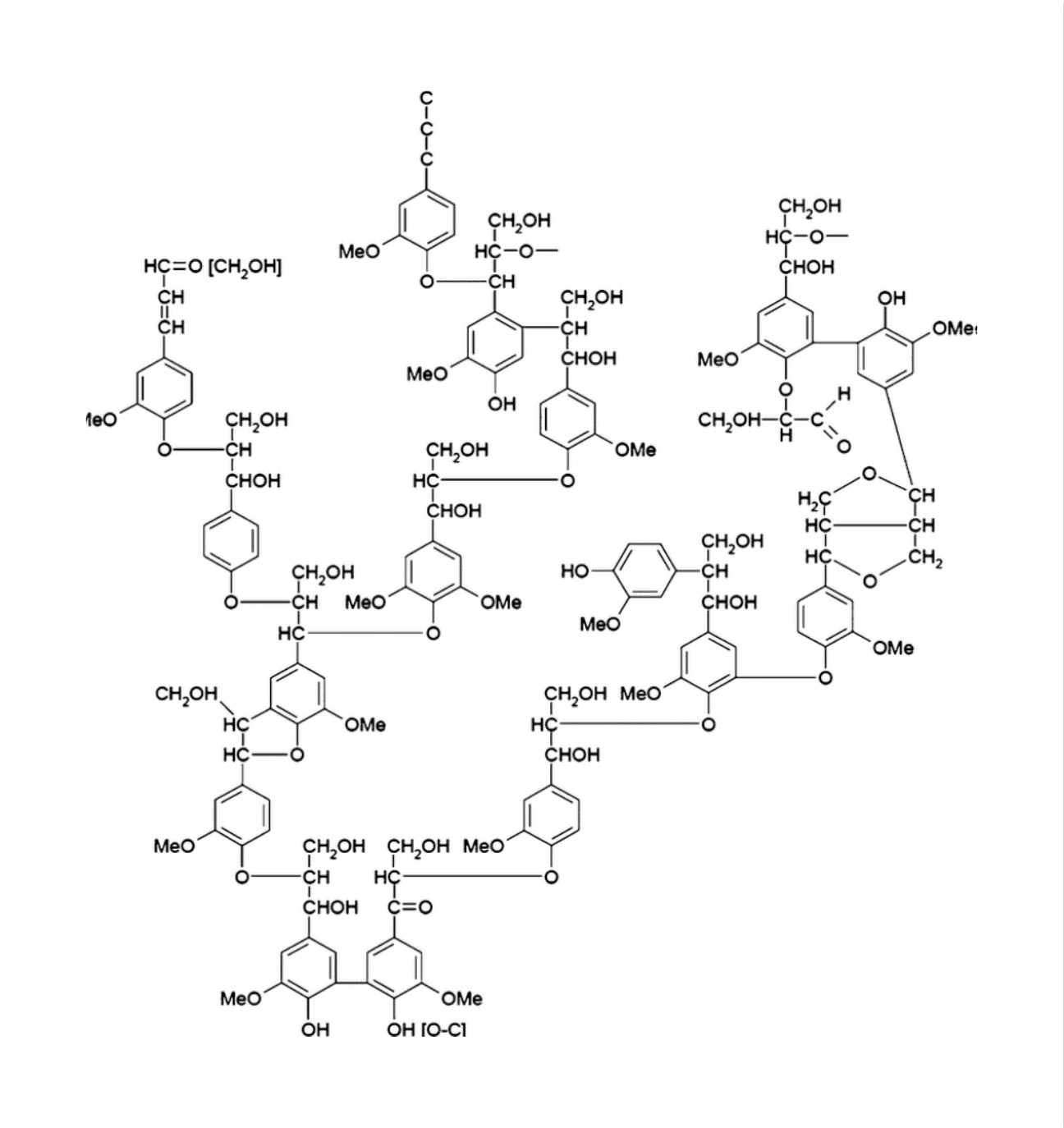

Figure 1: Adler's model of lignin structure [13]

2.2. Utilization of lignin

As a consequence of the growing challenges in the environmental protection field due to the inefficiency of resource use and the effects of climate change, awareness of the value of using natural materials is growing, as well as the utilization of waste as new raw materials, both for reuse, or recycling energy production. Lignin can be used directly in pure form, relatively limited, and with various potential modifications, thanks to its chemical nature and aromatic structure with the existence of phenolic and aliphatic hydroxyl groups [15], and can also be successfully isolated from

waste streams. As estimated, world annual lignin production is up to 5 × 1014 t, and it is further considered an underutilized resource[18–20].

Lignin is used for obtaining energy as a low-energy fuel (98% of the produced lignin in the paper industry) and for developing many chemical products: additives, emulsifiers, binders, dispersants, epoxy resins, carbon fibers, and various nanomaterials [21–23]. The paper and board industry estimation is that only 2% of the total lignin produced is used for commercial purposes [24]. The use of lignin in polymer applications remains challenging due to a complex macromolecular structure and a high degree of lignin heterogeneity, depending on the origin and isolation procedure [15,25].

2.3. Lignin isolation procedures

Physicochemical properties and composition of lignin depend on the type of extraction, plant origin, purity of waste raw materials, and the process of lignin isolation, which affect the formation of various forms and possibilities for further chemical functionalizations. Thus, the structure and properties of the obtained lignin differ. [15]

2.3.1. Kraft Lignin

For experiments in this work, alkali kraft lignin KfL such as precursor b-LMS microspheres synthesis with high content of hydroxyl groups was used.

In the production of the kraft lignin, for the solubilization of lignin and hemicellulose in the ,,black liquor" aqueous solution of NaOH and Na_2S heated on 155–175^{0}C was used. The resulting black liquid contains 35-45 wt.% of lignin. The Kraft lignin is further obtained by precipitation and neutralization with an acidic solution (pH 1-2) and drying [16]. The Kraft lignin is rich in phenolic $^-$OH groups, mainly because of the cleavage of aryl ether bonds in lignin [25], and is very susceptible to modifications. Although the procedure performs in the presence of sodium sulfide, the residual sulfur content is low (less than 1-2%). Traditionally, kraft lignin was burned in boilers; however, since kraft lignin production exceeds energy production needs, new industrial processes are developed to isolate kraft lignin from waste process streams [26]. The availability of large quantities of technical kraft lignin is an important step in further research toward developing low-budget adsorbents from natural materials [14]. Aliphatic hydroxyl ($^-$OH) functional group in commercial kraft lignin determined by 1H NMR and 13C NMR spectroscopy is in the range of 9.8 - 10.09 wt.%, The phenolic (-OH) group content determined by potentiometric analysis and aminolysis is between 4.54 and 4.60 wt.% because these methods are considered the most reliable for the determination of phenolic (-OH) groups [27].

2.3.2. Lignin sulfonates

Lignin sulfonates are produced from softwood liquid waste processing, using various sulfuric acid salts (sulfite or bisulfite) for lignin extraction from the pulp by the sulfite-pulping production process. Lignin sulfonates have hydrophilic and hydrophobic properties; they are soluble in water and can be chemically modified with sulfonate groups, carboxylic groups, and certain inorganic compounds. They are most often prepared in the form of Ca, Mg, and ammonia salts. The synthesis process is less aggressive compared to obtaining kraft lignin, and the final product's molecular mass is higher than kraft lignin, which gives a structure more similar to the original lignin [16].

2.3.3. Organosolv Lignin

Organosolv lignin has been developed from various procedures based on a mixture of organic solvents and other mixtures and solvents. In short, lignin is extracted from biomass by a mixture of organic solvents and water at high temperatures and pressure. The most common solvents used in these processes are acetic acid-water, acetic acid-HCl, ethanol-water, alkaline sulfite-anthraquinone-methanol, acetic acid-formic acid-water, formic acid-hydrogen peroxide etc.[16]. Organosolv lignin is finally isolated by acid deposition. The organosolv lignin structure has less potential modifications than kraft lignin, and most organosolv lignin does not contain sulfur. It is cleaner than other types of lignin, soluble in organic solvents, and practically insoluble in water due to high hydrophobicity.

2.3.4. Soda Lignin

Soda lignin is obtained by lignin extraction from the pulp by the *soda pulping* process. In this procedure, sodium hydroxide solution is heated to the temperature of 150–170^{0}C and pH values in the range of 11-13. This way, soda lignin does not contain sulfur and is relatively more difficult for chemical modification than other types of lignin [15]. Temperature of soda lignin degradation is much higher than 160^{0}C (this is the degradation temperature of industrial lignin). Analytical measurements show that the highest content of functional groups (such as $^-$OH is in the range 14,34-14,69 wt.%) is in kraft lignin compared to organosolv, soda lignin and other technical lignins[27]. This phenomenon indicates a higher potential adsorption capacity for kraft lignin, which is chosen as alkaline material for efficient adsorption possibilities [14]

2.4. Application of lignin in wastewater treatment

Due to their economy, environmental friendliness, and good adsorption characteristics, natural adsorbents from biomass based on polymers are used in wastewater treatment. In addition to hemicellulose, lignin-based materials are also used [19,28–30]. Adsorption is the simplest, most efficient, and cost-effective pathway for wastewater treatment. Adsorption method's characteristics are flexibility in design, adsorbent regeneration potential and sludge-free operation[31–33].

Many research papers have investigated different ways for the synthesis of low-cost adsorbents based on lignin which could be used for wastewater treatment and removal of various heavy metals and other pollutants [24,25,30,34,35]. The newest lignin modifications such as lignin-based composites with xanat-bentonite, has been successfully tested for adsorption.

Researchers also investigated the adsorption mechanism of heavy metal ions removal by lignin and it was concluded that no unique mechanism could define the pollutants removal from wastewater, but rather it may be a combination of several processes. Many physical and chemical processes are involved, including ion exchange, surface adsorption, and complexation [11]. Detailed studies are necessary in order to fully understand the adsorption process by lignin.

Studies showed that complexation processes dominate the adsorption of the metals on the hybrid amino-modified adsorbent with the lone electron pair of nitrogen and chelate interaction with the oxygen atom [36]. It was also confirmed that heavy metals ions is complexing and hydrolysis during adsorption. Oxyanion adsorption is more complex than cations' adsorption mechanism and depends on pH[37,38]. Chen et al. investigated the mechanism of cadmium adsorption on a mesoporous biosorbent and determined that chemisorption was the dominant mechanism that occurred on ion exchange between the sorbent and cadmium ions. They concluded that functional and aromatic

groups on the surface of the bio-sorbent provide a lone electron pair and π electrons that participate in adsorption [39].

2.4.1. Functionalization of lignin

Lignin functionalization can be classified into two groups:

- First, without chemical modification, where lignin is used directly or it is incorporating in hybrid matrices giving new or improved properties
- With chemical modification where the many phenolic compounds are synthesized, monomers, oligomers, and differents adsorbents from polimers materials which are incorporated in hybride matrices.

In order to increase adsorption properties and capacities in wastewater treatment, lignin modification is performed by binding various functional groups: amino groups, hydroxymethyl and epoxy groups [40], carboxymethyl [41], sulfonate [42], vinyl [22], alkyl and nitrite groups [15] with addition of various oxides of iron (FeII, FeIII)), aluminum (Al_2O_3), zinc oxide (ZnO), manganese (IV) -oxide (MnO_2) [3,22,24,43], etc. Physicochemical properties of lignin, such as hydrophobicity, solubility and thermostability, depends on the introduced functional group and can be significantly improved, as well as the reactivity of lignin, due to the increase of active sites. Many aliphatic and aromatic hydroxyl groups make lignin applicable for chemical functionalization by various methods to increase structural, morphological, and adsorption characteristics. Besides hydroxyl groups, hydrogen atoms from ether bonds and methoxy groups are also susceptible to chemical modification and contribute to their reactivity [14].

An amine modification gives lignin amino groups $^{-}NH_2$, which adsorbed the heavy metal ions by interacting with alkaline amino and acid metal ions [24,44]. For this purpose, diethylamine and formaldehyde, with or without epichlorohydrin, are used.

Figure 2 shows the scheme of kraft lignin functionalization with vinyl groups by esterification using methacryloyl chloride, achieved through aliphatic ^{-}OH groups kraft lignin. Podkoscielna and co-workers [22] are vinyl functionalization of kraft lignin significantly increased their reactivity by introducing new active sites in the macromolecule which can participate in copolymerization with other monomers. Vinyl functionalized kraft lignin was copolymerized with the addition of divinylbenzene and triethoxy-vinylsilane, and thus highly porous, hybrid microspheres based on lignin were obtained (Figure 3).

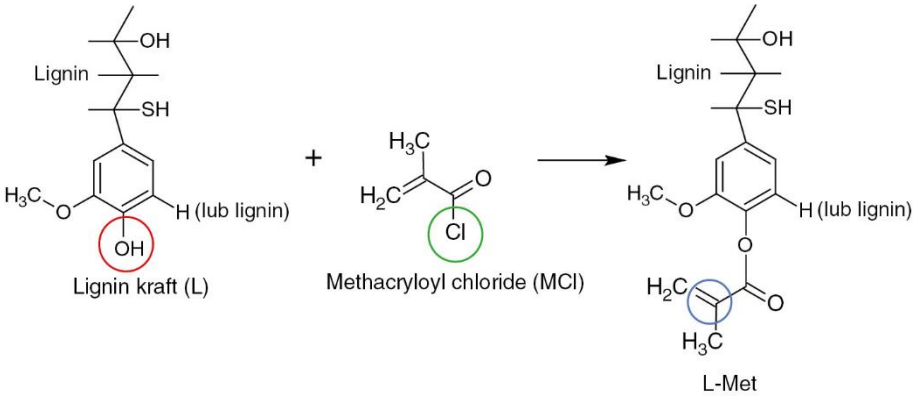

Figure 2: Scheme of synthesis of methacrylate lignin derivative [22]

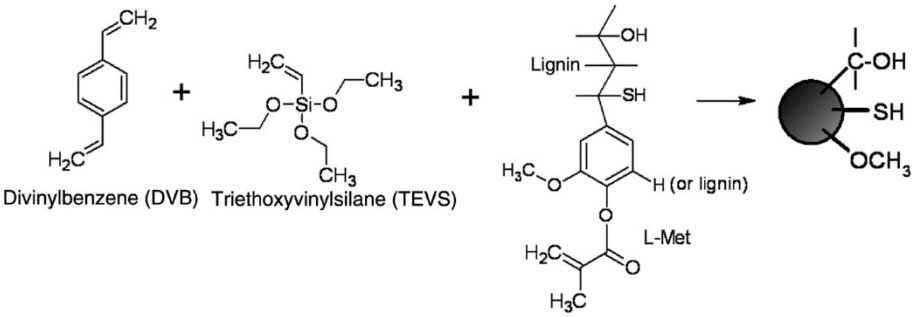

Figure 3: Scheme of copolymerization [22]

Iron oxides are compounds that make up different oxides, oxyhydroxides, and hydroxides of iron that contain Fe and O and/or OH groups in their structure [45]. They impregnate porous adsorbents with a large active surface originating from natural macromolecules, thereby creating composite adsorbents [31,46]. The adsorption properties of different types of iron oxides have been investigated in several studies: goethite [47], magnetite[37], hematite [48], iron hydroxide [49].

Magnetite (Fe_3O_4) is a black oxide widely distributed in nature. At atmospheric pressure, it is thermodynamically unstable, which is why it is found in crystalline form in rocks and soil [45]. Synthetic magnetite can be obtained in two ways:

- Using Fe(II) salt solution ($FeSO_4$ or $FeCl_2$ in hydrated form), with KNO_3 in basic medium, at a temperature of 90°C and
- By precipitation of a mixture of Fe(II) and Fe(III) chloride solutions [45].

Application of magnetite nanoparticles in environmental protection is quite widespread. Also magnetite is used to improve adsorption processes for heavy metals removal and due to its super magnetic properties, it can be easily separated from the aqueous solution with a low magnetic field [35,37,41,50]. Zhang and co-workers synthesized new lignin-based hybrid nanoparticles using epichlorohydrin as a cross-linker between amino-functionalized magnetic nanoparticles with tetraethoxysilane (TEOS) and carboxymethylated lignin [41]. Functionalization of lignin with amino-functionalized magnetic nanoparticles contributed to the high adsorption capacity for heavy metals removal and ultra-fast adsorption (30 s) due to the nanostructure, but also the contribution of a high number of active sites carboxymethylated lignin [41].

Lignin functionalization with MnO_2 is a supplementary mechanism of already modified, activated lignin to improve their adsorption characteristics [51]. MnO_2 minerals occur in three forms (α-, β-, and δ-MnO_2). Different shapes and sizes of manganese oxides can be found in the literature, while the α-MnO_2 nanorod structure offers the greatest possibilities thanks to the "insertion" phenomenon [52]. MnO_2 is an important and interesting material widely used in adsorption due to its large surface area, plenty of active and passive sites, high redox potential, negatively charged surface at neutral pH values, and possible layered structures [53]. Manganese oxides are considered effective adsorbents for heavy metal cations, such as Pb(II), Cu(II), Cd(II), Ni (II), whereby heavy metal ions are adsorbed on the surface and the interlayers in the MnO_2 structure [53–55]. Experiments are also carried out on applying micro- and nano-particles of manganese dioxide in wastewater treatment, heavy metals remediation, and applications in the electronic industry [55–57]. Synthesis of manganese dioxide nanoparticles is most often done using potassium permanganate and ethyl alcohol.

2.4.2. Synthesis of lignin-based microspheres

In addition to increasing the adsorption efficiency in the column and the higher exploitation possibility of lignin in the adsorption process, their synthesis is carried out in functional microspheres of higher porosity. Microspheres provide a higher specific surface area and have a better ability for diffusion, dispersion, and mass transfer, and because of that, they are more efficient in the adsorption process [3,24,58]. Some microspheres' synthesis methods are based on kraft or organosolv lignin and include inverse suspension of polymerization, functionalization, and copolymerization with different reactants [3,24,59]. Then, esterification with the anhydride of maleic acid with additional magnetite functionalization or emulsion solvent evaporation in two phases with various organic solvents such as methylene chloride and ethyl acetate are also used [35,60]. Inverse lignin polymerization using formaldehyde, ammonia, and hexamethylene-tetramine, results of the porous homogeneous particle size distribution of lignin-based microspheres with an emulsifier, which has a vital role in size distribution control and surface morphology of synthesized microspheres [59]. Synthesis of lignin-based microspheres by evaporation of emulsion solution with dichloromethane or ethyl acetate gave a uniform spherical shape and a narrow particle size distribution. More recently, the mussel-inspired chemistry process is used for the chemical functionalization of lignin through $^{-}$OH groups to adapt structural, morphological, and adsorptive characteristics, which could also be applied to base-based microspheres lignin. Also, the mussel-inspired chemistry process synthesizes functional composites for adsorption, forming several functional groups, such as $^{-}$OH and $^{-}NH_2$[50,61,62]. However, copolymerization from suspension provides a controlled shape and size of the adsorbent, with a porous microstructure that contains each other connected pores required for good adsorption performance in the column.

2.5. LACCASES

2.5.1. Laccases: discover, natural sources and cell function

In 1883, Japanese scientist Yoshida discovered laccases, enzymes that catalyze the rapid hardening process of latex present in the Japanese and Chinese trees of *Rhus vernicifera* species in the presence of air. A decade later, Bertrand optimized process for their isolation and purification, giving them their name [63]. Fungi that participate in the process of wood rot produce the most laccases and are isolated from *Ascomycetes*, *Deuteromycetes*, and *Basidiomycetes*. *Basidiomycetes* are represented the most in the decomposition of lignin lichens, and these include white-rot fungi and fungi that transform litter, for example *Trametes Versicolor*, *Trametes hirsute*, *Trametes Ochracea*, *Trametes Villosa*, *Trametes Gallica*, *Cerena Maxima*, *Coriolposis Polyzona*, *Lentinus Tigrinus* (Figure 4), *Phlebia Radiate* and *Pleurotus Ostreatus* [64–66] as well *as Phanerochaete Chrysosporium*, *Theiophora Terrestris* and *Lenzites Betulina* [67,68].

Figure 4: *Lentinus Tigrinus, source of laccasa* [69]

Fungi from *Trichoderma Genus, T. Longibrachiatum* or *T. Atroviride* and *T. Harzianum* [70]) are also laccase producers. Saprophytic ascomycetes as laccases producers occur, among others, in *Myceliophtora Thermophila* and *Chaetomium Thermophila,* and are involved in the humification process of compost [19]. Laccase obtained from *Monocillium Indicum* represents the first laccase from ascomycetes that was characterized by peroxidase activity [71].

In fungi, laccases are involved in the process of lignin degradation, sporulation, and mushroom formation [72]. Most of the fungi in which the laccases were found belong to higher fungi, while their presence has never been proven in lower fungi, for example, *Zygomycetes* and *Chytridiomycetes* [67]. In ascomycetes and basidiomycetes, laccases were isolated from the human pathogen *Cryptococcus (Filobasidiella) neoformans* [73]. Laccases can also be found in some bacteria, lichens, insects, and prokaryotes, moreover in higher plants they are very important for the process of lignin synthesis [74–76]. They are also found in cabbage, turnips, radishes, apples and other vegetables.

Bacterial laccases were first found in the *Azospirillum lipoferum* [77], then in *Streptomyces Lavendulae, Streptomyes Cyaneus* and *Marinomonas Mediterranea* [78,79]. In insects, laccase has been found in several genera, some of which are *Calliphora, Drosophilia, Manduca, Oryctes, Papilo, Sacophanga* and others [65]. In order to improve their characteristics, laccases are isolated, purified and cloned from basidiomycetes (*Polyporus pinsitus* and *Rhizoctonia solani*, but also from ascomycetes *Myceliophthora thermophila* and *Scytalidium thermophilum*), whereas their expression is carried out in the *Aspergillus oryzae* system [80]. Bearing in mind that the presence of the laccase enzyme in nature have been detected in a large number of different sources, it is necessary to characterize each laccase obtained from a particular source. Catalytical properties of enzymes define their suitability for biotechnological and industrial applications and depend on the origin and source from which enzyme it was isolated. It is possible to obtain laccases with different properties isolated from the same source, for example, from the same genus of fungi, on the other hand it is also possible to isolate laccases with similar properties from different sources. The localization of the enzyme in the cell is an important characteristic of the enzyme, which makes it easier or more difficult to isolate it. Since laccases primarily participate in the process of lignin degradation, that is conditioned by their localization, so it is expected that laccases be extracellular enzymes. In addition, the other enzymes obtained from white-rot fungi, which belongs to of the same group as laccases, are extracellular lignin and manganese peroxidases. The amount of laccase produced extracellularly represents up to 98% of the total amount of enzyme produced by cells [67]. However, Localization of laccase in the cell depends on the type of substrate available. It is believed that intracellular laccases participate in the

transformation of certain phenolic compounds into compounds of smaller molecular masse. Laccase, bound to the cell wall, possibly participates in forming protective components of the cell wall, such as melanin [67,81]. To date, all laccase used for industrial applications are extracellular.

2.5.2. Laccases properties

One of the most important properties of laccase is its low specificity towards the substrate, which also includes organic pollutants, resulting in their detailed characterization in the literature. But since the specific properties of laccases are very dependent on their origin and source, only some can be stated as general for all laccases. Large spectrum of substrates that laccases can oxidise (e.g. para-diphenols, polyamines, aminophenols, polyphenols, and aryl diamines under mild optimal reaction conditions, as well as the manifestation of activity without the presence of cofactors, the usage of the oxygen as the final electron acceptor, without the formation of harmful catalysis products recomends them for application in biotechnological processes and bioremediation. Bearing in mind increasing environmental pollution, the ways to reduce it is one of the most important topics today, scientific research is focused on developing green technologies, such as removing organic or inorganic pollutants without producing impurities or more waste. Because of all this, laccases are very interesting to scientists as a potential green catalyst, and genetically production of laccases with specific characteristics that would have a specific purpose are very much sought after.

2.5.2.1. Laccases classification

Laccase (benzenediol: oxygen oxidoreductases; EC 1.10.3.2) belongs to the class of polyphenol-oxidase. Polyphenol-oxidases are copper-containing proteins making them metalloenzymes, and their typical property is the ability to oxidize aromatic compounds. According to three types of activity, this group of enzymes is further classified as:

- Catechol oxidases or *o*-diphenol: oxygen oxidoreductases (EC 1.10.3.1)
- Laccase or *o*-diphenol: oxygen oxidoreductases (EC 1.10.3.2), or *p*-benzenediol: oxygen oxidoreductase (EC 1.10.3.2)
- Cresolase or monophenol monooxygenase (EC 1.14.18.1)

According to the substrate activity, tyrosinases also have cresolase and catechol-oxidase activity, because of that they are widespread and contribute to the melanin formation in organisms from bacteria to mammals. Both laccases and tyrosinases can oxidize diphenolic compounds and posses low substrate specificity, making their classification difficult [82]. Catechol-oxidases or tyrosinases have a both *o*-diphenol and cresolase activity, i.e. the ability to oxidize L-tyrosine, while laccases has stronger ortho- and para-diphenol activity. In addition, the differentiation of these enzymes is based on specificity toward the substrate and sensitivity to certain inhibitors. The most important difference is that only tyrosinases have cresolase activity, and only laccases can oxidize methoxy-activated phenols. With regards to inhibition, tyrosinases are strongly inhibited by tropolone, cinnamic and salicylic acid [72]. The only significant difference from other laccases is that they can oxidize a wide range of substrates such as diphenols (hydroquinone, catechol, 2,6-dimethoxyphenol), para-phenylenediamine, which is a specific substrate only for laccase, polyphenols, diamines, and other compounds, depending on the organism that produces laccase [67].

2.5.2.2. Structural characteristics of laccases and catalytic mechanism

The structure of an enzyme is the most important for its biological function. The development of proteins is carried out to increase their stability under unfavorable industrial conditions, which are often significantly different from the biological environment of the enzyme itself. The structural characteristics of laccase were derived based on the characterization of purified enzymes, mostly from white-rot fungi, which belong to basidiomycetes. The literature can find data on the structure of enzymes based on more than a hundred species examined from different sources [67].

2.5.2.2.1 Molecular weight and dimensions of laccases

The laccase derived from fungi is a protein with an approximate molecular weight of 60 kDa to 70 kDa. They often appear as isozymes by forming oligomerized multimeric complexes. More significant variations in mass occur with laccases obtained from ascomycetes. Laccases are monomeric proteins. However, laccases have homodimeric structures consisting of two identical monomers with the same mass as monomeric lacases. Several structures of laccases were discovered in the wood-rotting fungi *Phellinus ribis, Pleurotus pulmonarius* and *Trametes villosa* as well as in the ascomycete *Rhizoctonia solani* [83–85]. Some laccases from ascomycete are also oligomers, whose structural units have masses of approximately 60 kDa. Structurally, mushroom laccases are extracellular proteins and contain a carbohydrate fraction [63,86] . More significant mass changes are observed after laccase purification and are associated with the glycosylation degree of a specific laccase from a certain source [63]. Besides the fact that they are in the majority mostly glycosylated monomers, some laccases have a heterodimeric, oligomeric, or homodimeric structure with a mass range from 50-130 kDa to 130 kDa.

The dimensions of the laccase molecule depend on its origin. Thus, the dimensions of laccase from *M. thermophila* are 6.74 nm x 12.84 nm x 16.36 nm [87], while the dimensions of laccase from *T. versicolor* are 6.5 nm x 5.5 nm x 4.5 nm [88]. Knowing the exact dimensions of the molecule is of great significance when choosing a support for immobilizing enzymes.

2.5.2.2.2 Chemical structure of laccases

Laccase is a type of cuproprotein (containing copper in its structure) from a group of enzymes called blue oxidases. As already mentioned, laccase is a glycoprotein, whereas the laccase molecule as an active holoenzyme may be in the form of a monomeric, dimeric and tetrameric glycoprotein. The content of saccharides in the carbohydrate fraction of laccases produced by fungi and bacteria is 10-25% and can be higher in laccases produced by plants. Laccase isolated from *Botrytis cinnerea* contained 49% saccharides, while other preparations isolated from the same species contained up to 80% saccharides [63,89]. Monosaccharides included in the composition of laccase play an important role in the enzyme's proteolytic sensitivity, secretion, thermostability and activity; and they are mainly galactose, glucose, fructose, mannose and arabinose. Mannose is most abundant in laccase. In addition to these, there are laccases with a low saccharide content, for example, laccases isolated from *Pleurotus eryngii* (7% and 1% of bound saccharides).

Laccases have four copper ions per monomer in their structure, and they are bound to three redox sites in the enzyme that play an important role in the catalytic activity. Copper ions are divided into three types, distributed in different places in the enzyme, and they are classified according to the characteristics determined by UV/VIS spectrophotometry and electron paramagnetic resonance spectroscopy (EPR). When they are in Cu^{2+} form, they can be divided into the following [90]:

- Copper Type I (T1, connected to at least one cysteine and two histidine ligands), source of the intense blue color of the enzyme, with absorption at approximately 600 nm and can be detected by the EPR method;
- Copper Type II (T2, connected to two histidine ligands) is colorless and does not show absorption in the visible spectrum but can be detected by the EPR method;
- Copper Type III consists of a pair of anti-ferromagnetically coupled copper atoms (T3, each linked to three histidines) that show a slight absorption at 330 nm in the Cu^{2+} form but cannot be detected by the EPR method [65,91].

Figure 5 shows the arrangement of copper atoms in the laccase. Copper atoms T2 and T3 with distances at most 0.4 nm form a trinuclear copper cluster where the molecular oxygen is reduced with water addition. A hydroxide bridge interconnects them. While for most laccases, the coordination of the T2 or T3 centers is similar for all poly copper oxidases. There are differences in the ligands. In the axial position, in laccases isolated from fungi, leucine (Leu) or phenylalanine (Phe) appears more often than methionine in the copper T1 axial position. However, these amino acids do not contain functional groups to bind to T1 copper and are too large to allow water molecules to bind at this site.

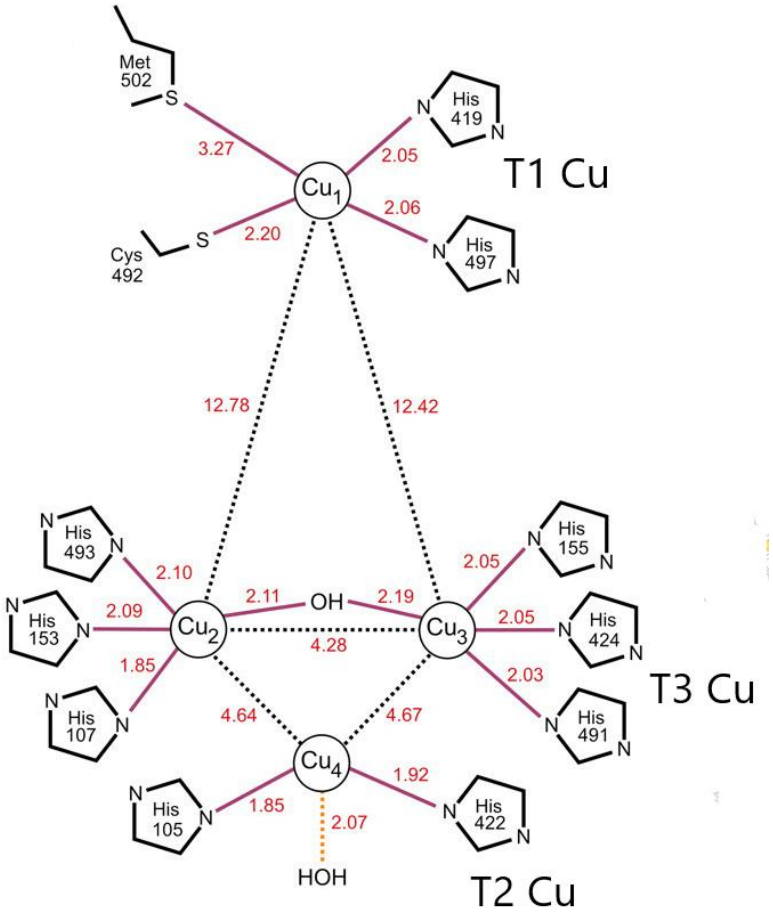

Figure 5: Schematic representation of the four copper atoms' position in the CotA laccase from *Bacillus subtilis,* including interatomic distances among all the relevant atoms [92]

However, the latest studies confirm that the Cu ion in the T1 position has a trigonal orientation, with equatorial ligands that are smaller molecules, i.e., two histidines and one cysteine, while in the axial position at a distance of less than 0.4 nm, there are non-polar residues, for laccases from fungi, bacteria and plants. Methionine is usually found in this position [93,94].

2.5.2.2.3. Redox-potential of laccase

Redox potential indicates the enzyme's oxidation ability and is determined in relation to a reference standard hydrogen electrode, which is expressed in mV. A higher value of the redox potential indicates a higher oxidation capacity. Redox potential (E_0) ranged from 450-480 mV (*Myceliophthora thermophila*) to 760-790 mV (*Polyporus Pinsitus*). Researchers who have investigated the properties of laccases hypothesize that these large differences in the redox potentials of laccases from different sources can be attributed to structural differences in the coordination of the Cu atom in the T1 position [67]. Redox potential is of great importance for the biotechnological application of laccases and based on its value, laccases are divided into laccases with low E_0 (as 500mV) and laccases with higher E_0 (700-800mV) [88].

Certain hypotheses describe the connection between the coordination distances of the CuT1 atom and its redox potential, where with increasing distance, E_0 increases. In this way, by stretching the Cu-N bond, the contribution of the one electron pair of nitrogen would be reduced, making the Cu T1 bond electron deficient [88]. In the literature can be found data about CuT1 atom distance for the laccase from *T. Versicolor*, the distance of Cu1-Nδ2 (His458) was determined to be 0.017 nm longer than in case of the laccase *from Coprinus cinereus*, which confirms the hypothesis. The stretching of Cu-N occurs in the spatial distribution of amino acids in the vicinity of T1 and the creation of hydrogen bonds between them, which leads to the destabilization of higher oxidation states and an increase in the redox potential of copper. An increase in redox potential of copper could be also explained by the appearance of two hydrophobic residues Phe460 and Ile452 in the CuT1 area. Additionaly residue Phe460 is surrounded by many other hydrophobic residues. These two facts, together contribute to an increase in the redox potential of CuT1 atom [95]. The literature confirmed that variations in the redox potential of CuT1 of laccases from different sources are not a direct consequence of structural features but rather several factors such as T1 coordination geometry and the nature of the residues present in the shell of T1 cave, thus affecting the substrate access to CuT1. Stereo interference during substrate binding also has a major impact on the redox potential of laccase [96].

2.5.2.3. Active center and the catalytic cycle of laccase

Laccases catalyze oxygen reduction in water using a hydrogen donor, and for complete catalytic activity, all four Cu atoms per active protein unit connected by a polypeptide chain are necessary. During catalysis, four substrate oxidations are carried out 4 electrons are exchanged, and water molecule is reduced. Copper is an electron acceptor within the T1 zone during oxidation processes catalyzed by laccase. Further, the electrons move to T1 and T2, and after water reduction, two oxygen atoms are bonded - one to Cu^{2+} ions between the T2 and T3 zones and the other to T3 zone, where peroxide as an intermediate is formed [97]

Laccase-catalyzed oxidation begins by receiving an electron on the CuT1 atom. Electrons are transferred *via* the His-Cys-His tripeptide to the trinuclear cluster composed of Cu T2 and T3 atoms. The reduction of oxygen to water completes the process. Figure 6 shows the triangular spatial orientation of copper, and the coordinate bonds that are formed between Cu atom the sulfur atom from cysteine and the Nδ1 nitrogen from two histidines, resulting in formation a cavity. The Cu in the T1 position, the cavity is large which allows access of many substrates to enzyme catalytic site, meaning that this is a plase where electrons from the substrate come into catalytic site of enzyme. The copper atom in position T1 also determines the rate of catalysis during the entire process [96]. The

protein-ligand hydrophobic interactions formed between residues present on the cavity surface near location of T1 copper and the residues which subtend cavity and are part of the enzyme structure.

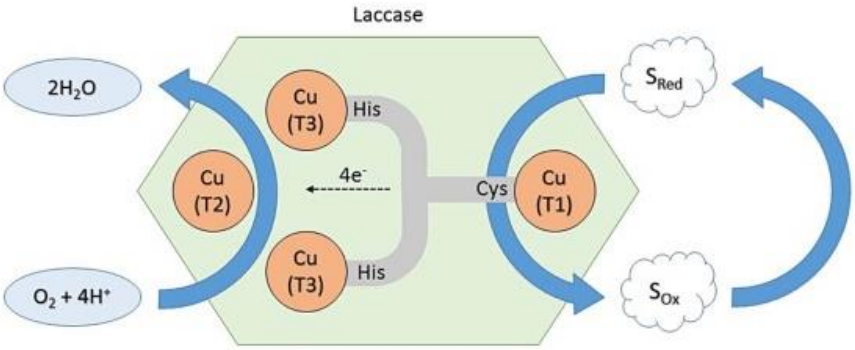

Figure 6. Reaction mechanism of laccase oxidation of the suitable substrate. [90]

Figure 7 shows the proposed laccase catalytic cycle mechanisms. Starting from the "native intermediary," the substrate reduces the copper T1 center, by transfering an electron to the trinuclear center. Two possible mechanisms for the reduction of the trinuclear center are shown: (A) together T1 and T2 centers reduce a pair of T3 Cu atoms, or (B) each copper ion in the trinuclear center is successively reduced by electron transfer from Cu T1 , in which case the T3 center is no longer active as a two-electron acceptor. Slow disintegration of the "native intermediate" leads to a formation of completely oxidized form. In this state, the T1 center can still be reduced by substrate, but electron transfer to the trinuclear center is too slow to be catalytically significant [98].

Due to the fact that laccases couple the one-electron oxidation of the substrate with the reduction of oxygen molecules in which four electrons participate, it can be assumed that laccases act as a kind of battery, as well as the action mechanism that cannot be simple and easily explained [72].

Laccases use oxygen as an electron acceptor for removing protons from phenolic hydroxyl groups. As a result of this reaction, radicals are formed, which can spontaneously rearrange, leading to the breaking of C-C or C-O bonds of alkyl side chains or splitting of aromatic ring [76].

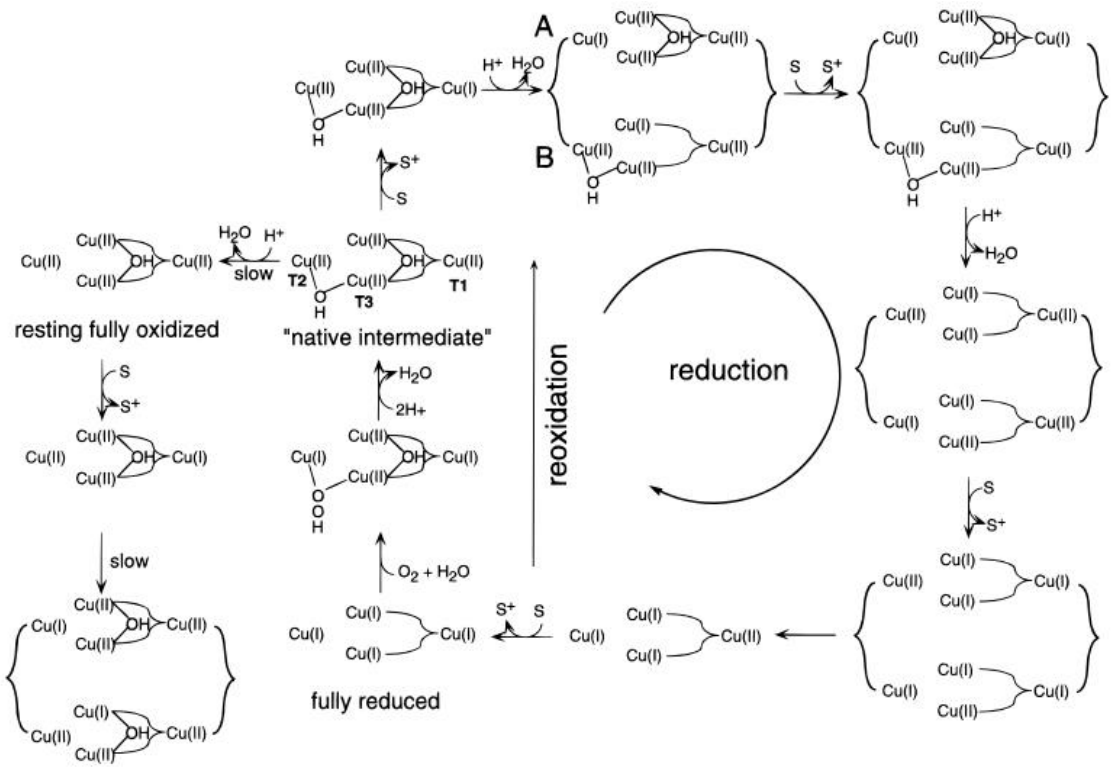

Figure 7: Schematic representation of proposed catalytic cycle mechanism of laccase [98]

2.5.2.4. Catalytic constants

Catalytic constants were determined in reaction of laccase with several substrates, for example ABTS, guaiacol, phenolic compounds, syringaldazine, 2,6-dimethoxyphenol. These constants were determined for many laccases from different sources and are shown in Table 1 for the substrate ABTS [76].

Table 1: Kinetic constants of laccase and the pH values at which the constants were measured:

Substrate	pH	k_m (μM)	k_{cat} (min^{-1})	K_s ($min^{-1}μM^{-1}$)	Laccasa source
ABTS	4.0	106	1000	9.43	*Bacillus subtilis*
	5.5	23	1090	47.39	*Coprinus cinereus Lcc1*
	4.5	270	4690	17.37	*Melanocarpus albomyces*
	6.0	290	790	2.72	*Myceliophthora thermophile Lcc1*
	5.5	45	620	2.14	*Trichophyton rubrum*
	5.3	58	2700	46.51	*Trametes villosa Lcc1*
	3.4	30	198	6.6	*Trametes trogii POXL3*
	3.0	14	41400	2957.14	*Trametes pubescens LAP2*
	4.5	75	4130	50.1	*Thielavia arenaria Lcc1*

By comparing k_{cat} and K_m, which represent a measure of enzymatic activity, it can be seen that there are few differences between them, which indicates that laccases from different sources have different preferences toward the substrate. Laccases have a high affinity for syringaldizine and ABTS, which can be seen based on higher specificity constants (K_s) that reach values of 3888.9 min^{-1} $μM^{-1}$ for ABTS (Table 1) and 3623 min^{-1} $μM^{-1}$ for syringaldazine in case of laccase from *Melanocarpus albomyces*. On the other hand, the oxidations of guaiacol and DMP are significantly slower with laccase from *Melanocarpus albomyces* sincethe corresponding K_s constants are 4-times lower than in case of ABTS and syringaldizine , The Ks value of 832 min^{-1} $μM^{-1}$was obtained in the oxidation of 2,6-DMP. The K_s of guaiacol oxidation by laccase from *Trametes pubescens* LAP2 was 300 min^{-1} $μM^{-1}$ [76].

2.5.2.5. Laccasa inhibitors

Individual anions (azide, hydroxide, cyanide, halide) are bound to the Cu atoms present in the T2 and T3 center and thus disrupt the electrons transfer within the enzyme active center. In this way, the inhibition occurs. Halide ion inhibition is related to the trinuclear vent channel size where oxygen binds. Hydroxide ion acts as an inhibitor by preventing substrate oxidation in a basic environment.

Other inhibitors can modify amino acid residues, cause conformational changes in the glycoprotein or in the copper ion complex. Such inhibitors are hydroxyglycine, fatty acids, mercury, or quaternary ammonium detergents [76] .

2.5.2.6. Heterologus laccase production

Laccases obtained from mushrooms are produced in small quantities and in order to increase the production yield, gene cloning and heterologous gene expression are carried out. Until now, bacterial laccases have been expressed in *Escherichia coli*, while laccases from fungi have had heterologous expression in *Aspergillus nidulans, Saccharomyces cerevisiae, Aspegillus oryzae, Aspergillus niger, Trichoderma reesei* [76]. Since 1990. gene mapping has been done. Today, several hundreds of laccase genes have been sequenced, and most of them represent smaller sequences of genes found in large gene sequencing projects and assigned to laccases based on sequence homology with known laccases. The number of laccase genes for which the corresponding protein products have been characterized is about 20, mostly for fungal laccases [76].

2.5.3. Laccase characterization

Three chemical parameters are important for enzyme characterization: pH value, isoelectric point, and temperature.

Optimal pH value for laccases depends on the substrate and environment. Laccases from fungi displays pH optimum for phenolic substrates in therange of 3-7, while the pH optimum is around pH 9 for laccases from plants. Optimal pH for different laccase and substrates varies greatly due to changes in the reactions caused by the substrate, enzyme, or oxygen. At higher pH values, there is a higher difference in the redox potential of phenolic substrates and CuT1, which increases possibility for oxidation of the substrate. However, if the $^{-}$OH ion concentration is high, the OH^{-} ion binds to T2/T3 copper atoms, and as result laccase inhibition occurs. These two factors play an important role during determination of the optimal pH value [65].

Isoelectric point (pI) is the pH value of the environment at which the enzyme is not electrified (bears the same amount of negative and positive electricity at its surface), and pI is one of the basic properties of the enzyme. For laccase from mushrooms, the isoelectric point ranged from pH 3 to pH 7, depending on source, mostly around pH 4, indicating that acidic amino acids predominate in the enzyme's primary structure [65,67]. Enzyme's surface is negatively charged at the pH value higher than pI of the enzyme. The enzyme surface is positively charged at the pH lower than pI of the enzyme. This behavior is a very important property for selection of the support for enzyme immobilization and for determination of the optimal pH at which immobilization process will be performed.

Laccase's optimum temperature can vary considerably for laccases from different sources. For example, laccase from *Ganoderma lucidum*, have a temperature optimum of 20°C to 25°C [65], laccase from *Trematosphaeria mangrovei* have a temperature optimum of 65 °C [99], while in the case of bacterial laccase isolated from *Bacillus tequilensis*, the temperature optimum is of 85 °C [100]. Bacterial laccases have higher values of pH optimum and temperature optimum than laccases from fungi, as well as tolerance to salt in the reaction mixture. However, in bacteria, they are present mostly as intracellular enzymes. Therefore, it is more difficult to isolate bacterial laccases and to have a wider industrial application meaning that their favorable properties could not be adequately used.

2.5.4. Application of laccases in industry

Due to the specific favorable properties of laccases and their availability in nature, it has been given great importance to their industrial application (Figure 8). Until now, their industrial application in paper production has been as a pulp bleaching agent and biosensors for the detection of phenolic compounds; as well as for removal of xenobiotics and various pollutants from industrial wastewater and contaminated soil; PAHs degradation; decolorization of azo dyes; bioremediation of wastewater from the food industry etc [76,90,101–103]. Considering that they are extracellular enzymes, they can tolerate high concentrations of substrate in a reaction mixture, which is an asset for industrial application [104,105]. More about their most important uses will be described in following sections.

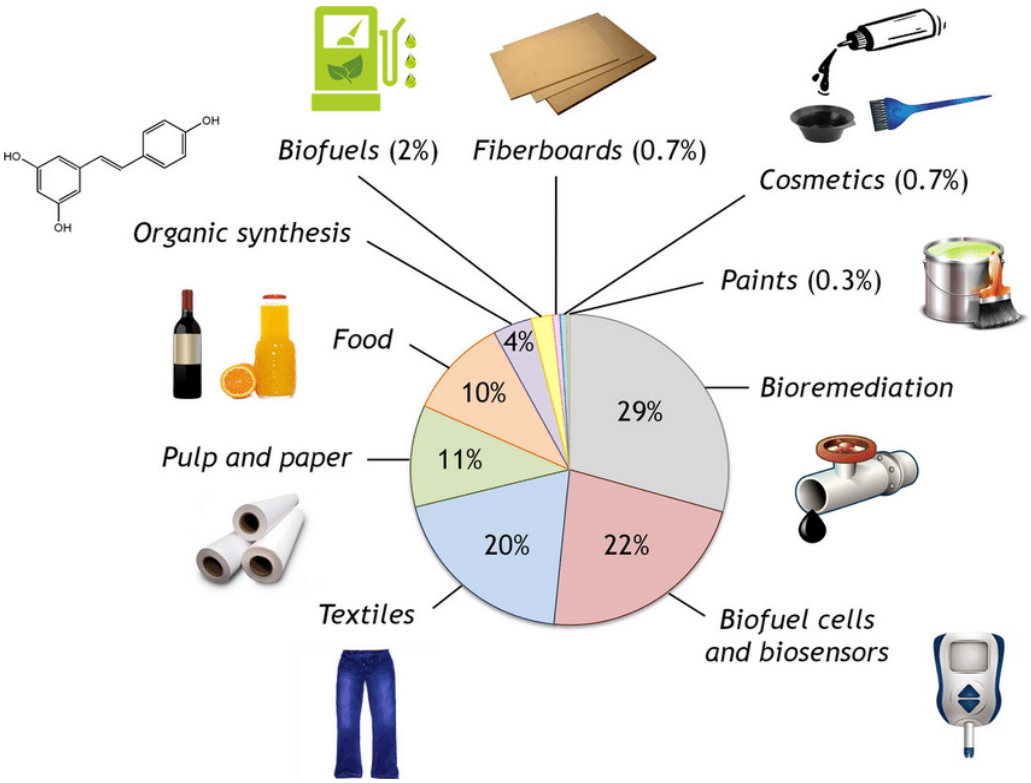

Figure 8. The biotechnological applications of laccases [106]

2.5.4.1.Application of laccases in the paper industry

Laccase plays a very important role in paper production as a bleaching agent. The producing paper process from wood is such that in a certain step, it requires the separation of wood fibers and their merging into sheets. Lignin enables this bonding, so its degradation and removal are necessary either by physically separating the fibers or by chemical or mechanical pulping. Considering that wood is susceptible to decomposition, new possibilities for lignin biodegradation involving laccase have emerged. The chemical structure of lignin is such that pulping removes about 90% of lignin, and the last 10% is removed by degradation or bleaching. The bleaching process involves using highly toxic chlorinated compounds that end up as industrial waste and become a big environmental problem. Laccase can be used as an eco-friendly variant. Laccases degrades lignin by acting on small phenolic fragments resulting in partial lignin degradation, and then laccases degrade on the lignin fibers and break them it down. In this way the pulp is decolored, and the process has already been tested with laccase from *T. Versicolor*, using N-hydroxy compounds for the pulp degradation obtained by kraft pulping in a pilot plant [65].

2.5.4.2. Application of laccase in the food processing industry

Laccases are used in wastewater bioremediation, beverages, bakery, and fruit juice production in the food processing industry. Laccase from *T. Versicolor* polymerizes phenol from wastewater obtained during process of olive oil production, which is very important for environmental protection [107]. Laccases immobilized on organogel can be used for removing of xenobiotics and aromatic compounds, which are toxic to human health from water [108]. Polyphenols also can be found in wastewater from the brewing industry. Laccase from *Coriolopsis gallica* decomposes tannin compounds, as result reducing of the concentration of polyphenols and guaiacol occurs. Wastewaters from distilleries also contain a large amounts of organic pollutants, which causes the water's brown color. The decolorization of these wastewaters using laccase from *Trametes sp*. was achieved [108].

Laccase is also used in wine stabilization. It is known, that the wine color and taste depend on the composition of phenolic compounds. During the wine aging, various oxidation processes take place that include polyphenols, and as a result, cloudiness and change in color, aroma and taste of the wine occur. Removal of polyphenols which is the cause of this phenomenon, is possible by using laccase to provide the decomposition of polyphenols, it also has the advantage since laccase optimum pH is in an acidic environment which reverses sulfite inhibition

2.5.4.3. Application of laccases in the textile industry

In the textile industry, laccases are added to detergents. In this way, they quickly decolorize the water during washing and save time, energy, and water for the process [76]. Also, one of the purposes is to prevent the creation of back-staining on dyed or printed textiles. These stains are created due to the dye deposition during the textile washing in places that were not dyed (inside, folds, pockets, seams) due to a poor-quality of dyeing process.

In denim processing, laccases have found application in the bleaching of synthetic indigo dye, which achieves different bleaching effects on the material. For this process, a mediator is also needed. The reaction product is indigo oxidation to isatin and further to anthranilic acid, which follows a reduction of oxygen to water. This combined laccase mediator system ensures that neither the denim sulfur-black color nor beige color is degraded, which gives the natural look of faded-away denim. Reaction stops when the mediator in the system is used up, so the process can be easily controlled to the desired effect [65].

2.5.4.4. Application of laccases in the PAHs degradation

Polycyclic aromatic hydrocarbons (PAHs) are organic compounds with multiple aromatic rings. They belong to the persistent organic environmental pollutants (POPs) distributed in the air, soil, water, and marine environments. They occur in wastes from processing of oil, crude oil, wine and the production of paints and textiles [90]. PAHs do not degrade in nature but accumulate in the soil and sediments. Their insolubility in water makes the bioremediation process difficult where they have remained in higher concentrations. Lignolytic enzymes from white rot fungi, including laccases, oxidize PAHs to quinones and CO_2. Laccases can oxidize most of the 16 PAHs listed by the US EPA as priority pollutants[65]. It has been proven that the laccase from *T. Versicolor* oxidized PAHs with 3-5 rings in the presence of mediators ABTS and HBT [109].

PAHs are considered toxic compounds for aquatic and living organisms, have a mutagenic and carcinogenic effect on humans, and are therefore subject to regulation as organic pollutants by the European Commission, the USA, and the Republic of Serbia. Chlorinated phenols and their

derivatives are chemicals that stimulate hormonal activity in wild animals and humans and have negative impact on their reproductive function [55].

2.5.4.5. Application of laccases in medicine and personal care

In medicine, laccases are widely used to relieve dermatitis symptoms caused by contact with poison ivy, which contains the urushiol toxin. This derivative of catechol, laccases polymerize, oxidize, and remove. Another possible application is in situ iodine preparation, which is used as a disinfectant,by oxidation with laccases. Iodides are much more suitable for storage than iodine. This way, only the necessary amounts of iodine can be produced, controlled by the used laccase concentration. With this system, it is possible to sterilize and disinfect drinking water, swimming pools, and small body wounds [110].

Due to their ability to oxidize various thiols and other sulfur compounds, laccases have been investigated for possible use in air fresheners (in antiperspirants), i.e., for removing unpleasant odors. For this purpose, laccases would not only mask unpleasant odors with aromas, as most deodorants do today but would also degrade the odor molecules and possibly act on the microbes that produces odor compounds [65]. Also, laccases are used as catalysts in anticancer production drugs and as ingredients in some cosmetic products [76].

2.5.4.6. Application of laccases for diagnostics and biosensors

The laccases also are widely used in nanobiotechnologies. Laccase catalysts, with other instruments, can be used as a biosensor for oxygen detection or substrate detection (aniline phenol and other compounds). Biosensors which monitor the changes in laccase spectrum in the VIS region at 600 nm were developed. Another type of biosensor monitors current or voltage changes on a modified oxygen electrode, on which the electrocatalysis of immobilized laccase enhances oxygen reduction. Several biosensors exist for detecting aniline and phenolic compounds in which free or immobilized laccases are used, together with a transducer (optical, amperometric, or based on the piezo effect). Laccases are covalently bound with biomolecules and can be used on histochemical, immunochemical, cytochemical analysis and detection as biomarkers for enzymes [65].

2.6. ENZYME IMMOBILIZATION

Enzymes are biological catalysts, and they significantly affect industrial processes. However, for their wide industrial application, including bioremediation, enzymes must be reusable and stable under extreme process conditions[76]. Free enzymes are susceptible to denaturation at high temperatures and are influenced by pH value, ionic strength, or the presence of certain chemicals in the solution [104]. In order to overcome these problems, enzyme immobilization as one of the techniques is necessary for most industrial applications. This way, by reducing enzyme mobility, possible limitations in the use of enzyme is diminished, increasing their stability and resistance and enabling continuous use. Immobilization of enzymes ensures their repeated use, facilitated physical separation from the reaction medium, greater enzyme selectivity toward substrate, and prevention of proteins product contamination [74,111,112]. Two most important criteria for selecting immobilization supports are immobilization capacity and achieved activity yield.

2.6.1. Basic characteristics of free and immobilized enzymes

Enzymes as biocatalysts are widely used in industry, whether they are part of a living cell or isolated from it, in free or immobilized form. They can be characterized by three quantitative dimensions: activity, specificity, and stability.

2.6.1.1. Enzyme activities expression

The enzyme activity represents the reaction rate catalyzed by the enzyme, which is the substrate oxidation reaction rate in the case of laccase. Various instrumental methods to determine enzyme activity are used. Most commonly used are chemical, polarimetric, spectrophotometric, viscosimetric, fluorimetric, and others. Method selection depends on the measured quantity nature and the physicochemical change that is examined and monitored. Enzyme activity is most often expressed by the enzyme unit marked with „U'' i.e., the unit that represents the quantity of enzyme that catalyzes the transformation of one micromole of a substrate under strictly defined environmental conditions (pH, temperature), and is expressed in units of μmol min^{-1}. International Union of Biochemistry and Molecular Biology (IUBMB) defined the enzyme unit in 1964. In 1978. the general Conference on Weights and Measures (CGPM) recommended the introduction of a new unit for enzyme activity since the minute, which is in the definition of an enzyme unit, is not an SI unit. That recommendation, which was officially accepted in 1999., introduced a new SI unit for the catalytic activity of enzymes, catal, (cat). Catal is the amount of enzyme that converts 1 mole of substrate per second. The relationship between U and kat was established so that the enzyme unit 1U has a value of 0.017 μ_{kat}, i.e. 16.67 n_{kat}. However, today the enzyme unit, U, often called the international unit, IU ("international unit," English) or the international unit IJ, is still widely used in the literature. International unit IU is mainly used in pharmacy and is a unit for the substance quantity based on the measurement of biological effects. This unit uses is used for the quantification of the activity of several biologically active compounds such as hormones, drugs, vitamins, enzymes, vaccines, and other biologically active substances. It can have the same meaning as the unit in terms of enzyme activity, but in most cases, it does not. Precise definition of IU or IJ differs from substance to substance and there is an international agreement for each substance in particular. Enzyme activity can be more expressed as total activity (U), activity per weight unit (U mg^{-1}), or as activity per volume unit (volumetric activity or enzyme activity concentration – U ml^{-1}) [113].

Specific activity of an enzyme is the quantity that represents the number of activity units per one milligram of protein in the enzyme preparation (SA [U mg^{-1} protein]=A/SP, where SA is the specific activity, A is the activity expressed in enzyme units, and SP is the protein content in the enzyme preparation in milligrams), whereby enzyme preparations represent products obtained from animal, plant or microbiological sources that contain one or more enzymes. Enzyme preparations are commercially available as liquids, in the form of concentrates or powders, and as immobilized enzyme preparations. For comparison of different the results for enzyme activity it is necessary to specify the environmental conditions under which reaction was performed, such as pH value, temperatures, organic solvents, etc [113].

2.6.1.2. Specificity and stability

Enzyme specificity expresses the enzyme's ability to catalyze only one of many possible reactions. In this sense, the specificity can be: *strict or absolute* (the enzyme catalyzes a particular reaction of only one substrate); *group* (the enzyme acts on several substrates with a particular atomic group or bond in the molecule); *type of reaction* (the enzyme catalyzes certain reactions regardless of the substrate chemical structure); *stereochemical* (the enzyme acts only on one of two possible stereochemical forms of the substrate); *regiospecificity* (catalytic changes occur only in a certain region of the substrate) and enantiospecificity (specificity towards optically active substances) [64]. It has been mentioned that the laccases catalyze the oxidation of many substrates and have a low specificity toward the substrate thus their industrial application is highly possible. Stability is an essential characteristic of an enzyme for its application. In order for enzyme to catalyse reaction, it have to be present in its native conformation and natural conditions should be ensured, since most often enzymes are sensitive to minimal changes in environmental parameters (temperature, pH, ionic strength, organic solvents concentration). Changes in these parameters can also cause changes in the enzyme's secondary and tertiary structure, causing loss of catalytic activity and its denaturation. Enzyme immobilization can greatly increase enzyme stability, which will significantly expand the industrial application of enzyme in otherwise unfavorable environmental conditions for free enzyme (high temperature, pressure, etc.) [114,115].

2.6.2. Methods for enzyme immobilization

Selection of the immobilization method could significantly affect the properties of obtained immobilized preparation. For the correct choice of immobilization method, it is necessary to know the enzyme and support structure, and define the intended use of the obtained immobilized preparation. Enzyme immobilization methods can be classified into two groups based on the type of bonds that occur between the enzyme and support: *physical*, based on non-covalent interactions between the enzyme and support, and *chemical*, involving the formation of one chemical bond between the enzyme and support, mostly irreversible. After formation of a chemical bond between enzyme and support, the enzyme cannot be removed from support surface without disrupting its molecular structure and catalytic ability. Unlike chemical immobilization, the enzyme attached to the support surface by physical methods can be easily removed after its activity decreases due to repeated use, additionally a new amount of enzyme can be attached to the support after their removal. These methods have considerable advantages from an economic point of view due to the high prices of the supports, since this way they can be used repeatedly. Immobilization methods can be classified into several groups (Figure 9) [115,116]:

- Enzyme adsorption on a solid support,
- Covalent immobilization (linking enzyme molecules to support by covalent bonds),
- Enzymes entrapment (enzymes immobilization and cross-linking in polymer matrices),
- Cross-linking immobilization,
- Inclusion of enzymes in one of the two-phase systems, and
- Enzyme microencapsulation (enzyme placement in a semi-permeable membrane or behind it)

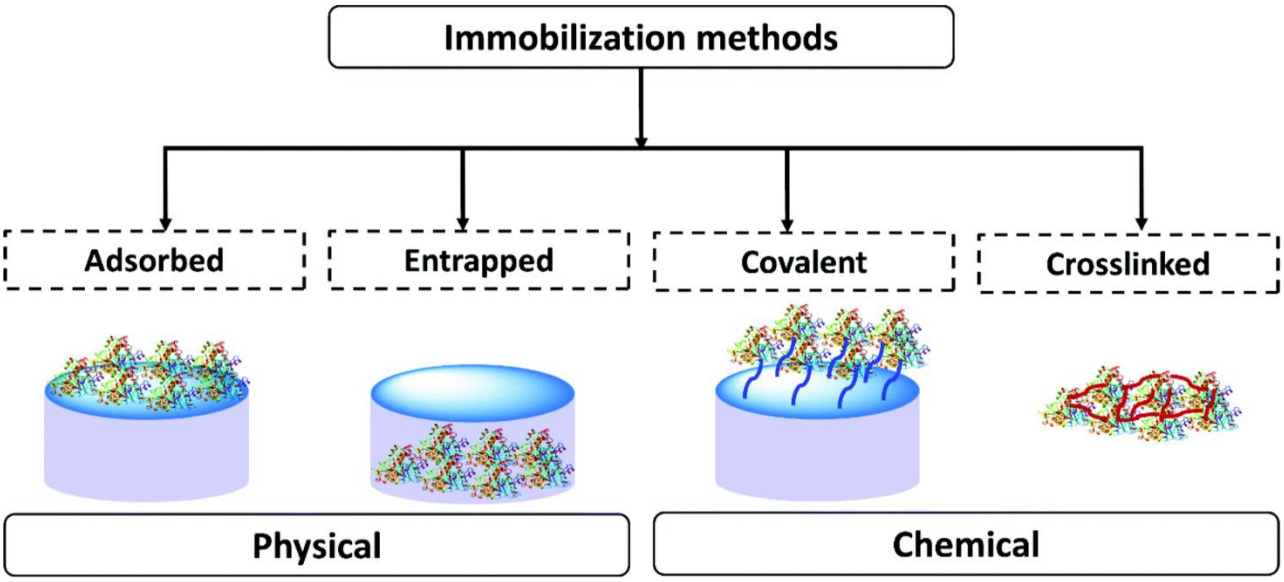

Figure 9: Immobilization methods of the enzyme [117]

2.6.2.1. Enzyme immobilization via adsorption on solid supports

This immobilization method is based on forming weak attractive forces between the enzyme and support. Their advantages are the low price of adsorbents, accessibility, simple procedures, and the possibility of support regeneration. Method takes place in mild conditions while preserving enzyme activity and specificity. Some disadvantages of this method are loss of enzyme during desorption and difficult standardization. Adsorption can be divided according to the connections formed between the enzyme molecules and the support [118]

- **Ionic adsorption** - based on formation electrostatic interactions between opposite charges present on enzyme and support surfaces, the most common application in industry.
- **Non-specific physical adsorption** – could occur on any support, without pretreatment and modifications, by forming weak hydrogen bonds, van der Waals forces, and hydrophobic interactions.
- **Hydrophobic adsorption** – occurs due to the creation of hydrophobic interactions between hydrophobic groups in the support skeleton and hydrophobic areas of the enzyme molecule. Formation of hydrophobic interactions is influenced by optimizing environmental conditions: pH, ionic strength, and temperature.
- **Affinity adsorption** - is achieved by introducing an affinity ligand (transition metal ions, antibodies, coenzymes, substrate analogs, or specific dyes) into the support for stronger binding of a specific enzyme and is based on the binding of molecules based on biocompatibility.

2.6.2.2. Covalent immobilization of enzymes onto solid supports

This method is based on establishing covalent bonds between surface functional groups of the enzyme and the surface of solid support. Great advantage of this immobilization type is the formation of real chemical bonds between the enzyme and support, meaning that leaching of enzyme from support surface could not occur. This advantage of covalent immobilization provaded its widely usage. Other advantages of this method are the possible target change of the immobilized enzyme properties, small activity losses due to diffusion limitations, and suitability of this method for wide range of reactions. This method's disadvantages are high costs, no possibility for enzyme regeneration, and complex support regeneration procedures [119].

Covalent immobilization process mainly consists of two steps: first, the activation of enzyme or modification of support, while the second step consists of is only the covalent binding of the enzyme to support surface. Activation of enzymes specific functional groups is achieved by modifying the free groups present on enzyme surface. Support modification implies the introduction of functional groups on the support surface, which can create a covalent bond with the amino acid enzyme residues. Electrophilic groups are often introduced to the support's surface, making it possible for them to react with solid nucleophilic groups of enzymes. Epichlorohydrin, glutaraldehyde, sulfonyl chloride, cyanogen bromide, epoxides, and others are used to modify the support surface. Binding can be achieved through amino groups of enzymes (α- and ε-lysine), carboxyl groups (C-terminal, aspartic and glutamic acids), and sulfhydryl groups of cysteine residues, imidazole groups of histidine residues, hydroxyl groups (serine, threonine residues) or phenolic core tyrosine [120].

Enzyme's covalent immobilization process must carefully took place, in order not to be formed covalent bonds between the amino acid residues present in the enzyme active site and the support, resulting in reduced enzyme activity.

2.6.2.3. Characteristics of immobilized enzymes

Same parameters characterize free and immobilized enzymes (activity, specificity, and stability). In order to monitor success of performed enzyme immobilization, special parameters are defined and followed, such as [115,116,121]:

- Concentration of immobilized proteins (mg g^{-1}).
- Protein immobilization yield (%) is the ratio of immobilized enzyme mass to the free enzyme's mass at the beginning of immobilization.
- The concentration of enzyme immobilized activity (IU g^{-1} of support) - the activity of immobilized enzyme" - per weight unit of the dry support introduced into the immobilization process.
- Activity immobilization yield (%) - represents the ratio of the activity of the immobilized enzyme and the activity of the free enzyme at the beginning of the immobilization process.
- Working stability of immobilized enzymes.

Enzyme concentration in the solution at the beginning of the immobilization greatly affects on immobilization extent and the enzyme's activity. Immobilized enzyme activity and stability depend on the concentration of immobilized proteins. Maximum activity of the immobilized enzyme when its concentration is equal to the concentration required to form a monolayer on the support surface is accomplished in the case of immobilization by adsorption. Yield of activity immobilization quantitatively determines how much of the enzyme activity is retained from initial activity during the

immobilization procedure. Immobilized enzymes' operational stability is tested using the obtained immobilized preparation in several consecutive reaction cycles. For each cycle, the immobilized activity concentration is determined and expressed in relation to the activity of the immobilized enzyme in the zero cycle. Stability of the obtained immobilized enzyme is assessed by monitoring the activity decrease of the immobilized enzyme.

2.7. ORGANIC DYES AND PIGMENTS AS A POLLUTANTS

Dyes and pigments represent organic pollutants primarily found in industrial wastewater environments. Production processes produce industrial wastewater; it has variable characteristics and is, therefore, more difficult to process. Many parameters determine the quality of industrial and municipal wastewater, which is important for the processing industry. Some parameters that are determined are flow rate, water amount (per hour, per day, per month), water temperature, color, pH, odor, dry residue, and biological and chemical oxygen demand (BOD and COD).

Parameters which determine the quality of wastewater are defined by law. At the European Union they are given in the directive 91/271/EEC and its annex 98/15 EEC on treating wastewater from settlements and setting effluent quality standards. In the Republic of Serbia, the Regulative ("Sl. glasnik RS ". 30/2010 and 93/2012) and the Regulation on the priority limit values and priority hazardous substances that pollute surface waters and deadlines for achieving them ("Sl.glasnik RS," 24/2014) and the Guidelines on method and conditions for measuring the quantity and testing the quality of wastewater and content of the report on performed measurements ("Sl.glasnik RS, "no. 33/2016).

For the world needs of various industries, over 15000 dyes are available, used in the textile industry, printing and food industry, cosmetics, paper processing, pharmacy, and other industries. It is estimated that the annual world production of synthetic dyes is about 7 x 105 tons [122]. In textile industry, large amounts of water are consumed for material processing and up to 100 liters of water for 1 kg of textile material [123,124]. Therefore, this industry's wastewater is significant.

2.7.1. Physicochemical properties of dyes and pigments

Pigments are typically insoluble and chemically unaltered by the vehicle or media inserted into them. In contrast, dyes are colored chemicals that are liquid or dissolve following application and transfer their color by selective light absorption. Absorption of electromagnetic radiations in a molecule's ultraviolet and visible ranges induces electronic excitation, and an electron attains a greater degree of electronic energy. A chromophore is a covalently unsaturated group responsible for UV or visible light absorption, such as C=O, C=C, CC, N=N, CN, or NO_2. If a chemical absorbs visible light (400–800 nm), it will only look colored. Depending on whether the chromophore absorbs photons in the visible or UV area, a chromophore may or may not provide color to a molecule. There are no defined guidelines for identifying a chromophore, since the wavelength and absorption intensity vary on a number of variables. Chromogen, chromophore, and auxochrome were the three primary components of organic dye molecules.[125,126]:

- Chromogen is a chemical substance that is either colored or might be colored with the addition of an appropriate substituent. Additionally, auxochrome(s) and chromophores are components of chromogen.
- A chromophore is a chemical group that imparts color to compounds in which it is present. Colorants are also occasionally categorized based on their primary chromophore.

- Auxochromes are substituent groups present in chromogens that affect their color. The chromophore or chromophoric group is responsible for the chromogen will be colour.

Dyes and pigments are colored because they: contain a single chromophore; absorb light in the ultraviolet range (400-800 nm); display electron resonance, a stabilizing factor in organic compounds; and have a conjugated system, i.e. a structure with alternating single and double bonds. azo (Methyl orange), nitro (Martius Yellow), Methine (Basic Yellow 11), Anthraquinone (Alizarin-Turkey Red), Triarylmethane (Ethyl Violete), Indigo (Tyrian purple), Phthalocyanine (Pigment green 7) and others are examples of chromophores found in organic dyes.[127].

Some differences between dyes and pigments are: dyes form a bond with the substrate, pigments do not; dyes are soluble in medium, pigments do not; auxochrome groups are present only in dyes; for dyes, the chemical composition is important for an application while pigments are that a size and physical form. Also, dyes are used for coloring textile materials, foodstuffs, and paper, while pigment is used for printing and coloring paints and is cheaper than dyes [127].

2.7.2. Pollution sources

Many dyes from pulp, textile, pharmaceutical, and paper industries are introduced as contaminants into natural water sources or wastewater treatment facilities. The textile industry and its dye-containing wastewaters are one of the leading causes of severe pollution. Due to the presence of carcinogens such as benzamine, naphthalene, and other aromatic compounds, the color, released dyes, and breakdown products of toxic and carcinogenic dyes make effluents which containing dyes in water undesirable. Without treatment, these dyes become persistent in the environment for an extended period. Water use by the textile industry was also a significant concern. Due to the high levels of pollution caused by the dying process, it is necessary to recycle treated wastewater. Due to the negative environmental impact of synthetic dyes, a global transition to natural dyes has begun. However, the effluent may become very hazardous due to the usage of heavy metals, such as chromium, to fix color onto the cloth. Additionally, natural dyes need a considerable amount of water. In addition, around 70 % of the dyestuff remains on the fabric, while the remainder is lost to the environment. [125]

2.7.3. Consequences of dyes and pigments pollution

Synthetic industrial dyes are aromatic compounds soluble in water, are dispersive, and classified as: heterocyclic, azo dyes, anthraquinone, triphenylmethane, or phthalocyanine dyes [128]. Reactive dyes can be covalently fixed to textile fibers which are important for industrial [129]. However, some dyes are harmful to the respiratory system, with allergies possibly. A small number of dyes, such as benzedrine, are considered to be potential carcinogens. Long-term exposure leads to more serious diseases such as cancer, extensive skin damage, and chronic obstructive pulmonary diseases. Unfortunately, these conditions are difficult to detect since their manifestations require years of exposure to the influence of dyes. Due to their complex aromatic structures, industrial dyes are resistant to light effects, moisture, and oxidants, which is a favorable industrial characteristic. However, they are also mutagenic, carcinogenic, and toxic, and their degradation can create products that are dangerous to the environment. Synthetic dyes in the water cause a decrease in biological diversity, preventing the sunlight spread through the water and thereby creating obstacles for photosynthetic aquatic plants and algae. Also, dyes can accumulate in sediments and leach groundwater systems [130].

2.7.4. Analytical method for dyes and pigments determination

Since dyes and pigments are divided according to their chemical structure into organic and inorganic, instrumental techniques normally used for testing substances can be used for testing and analyzing colors. First, these include UV/VIS spectrophotometry and FTIR spectroscopy, which are very important for the qualitative analysis of colors by comparing the spectrum of the sample with the spectra from the base, thus providing information about dyes. Also, chromatographic techniques (liquid and gas chromatography) are widely used for dyes analysis. In order to identify the pigments present in painting paints, scanning electron microscopy and X-ray diffraction techniques are usually applied. To choose the right method, it is necessary to know the sample nature, the chemical properties, and potential interferences during analysis.

2.7.5. Application of laccase for the pollutants removal

Laccases have found application in oxidative detoxification and removal of many organic pollutants from industrial waste such as contaminated soil or waters. Their action ensures polymerization and the direct decomposition of compounds. Activity of laccase in mineralizing PAHs or direct removal of Cl^- has been investigated. In the laccase polymerization process, polymers of polluted compounds are created, which become insoluble and can be removed more easily by physical ways [65]. Laccases can degrade plastic waste by oxidizing them with mediators' help. They can also remove unpleasant odors from landfills or livestock farms [63]. Phenolic compounds also can be found in wastewater from the coal processing, petroleum, or organic chemical industries. Possibility of removing oil stains on water surfaces, as a result of spills from ships, with the help of lacquers was investigated. Also, it has been proven that they can reduce the concentrations of synthetic heterocyclic compounds, such as halogenated organic pesticides, in the soil [76].

2.7.6. Application of laccase for purification of dyes contaminated water

Physico-chemical methods of dye removal from water are costly and complex. To eliminate industrial and synthetic dyes, such as azo, triphenylmethane and anthraquinone, preferred processes are based on a biological method using microorganisms or their enzymes (laccases, peroxidases or azoreductases). Due to their complex aromatic structures, these dyes are resistant to the effects of light, moisture, and oxidants, which accumulate in the environment, as previously emphasized [130,131].

Application of white-rot fungi in the purification and decomposition of dyes such as azo has been proven effective. However, for industrial applications for the same purpose, it is much more suitable to use enzymes as a laccase due to the possibility of catalyzing the oxidation of both phenolic and non-phenolic compounds and, therefore, a wide range of synthetic dyes. Because of the increasingly strict regulations on wastewater from the textile industry, this bioremediation technology has been increasingly researched in recent years [65].

2.7.7. Methods for removal of dyes and pigments from water

As a priority pollutant, the dyes' have special importance for their removal. Most current methods used for dyes removal of fall under three main groups [132]:

- *Physical methods* (adsorption with natural adsorbents, agricultural and industrial adsorbents, surfactants, irradiation, filtration process)
- *Chemical methods* (includes advanced oxidation method using Fenton's reagent, ozonization, oxidation with H_2O_2, oxidation with sodium hypochlorite, Photochemical oxidation, solvent-extraction method, and electrocoagulation)
- *Biological methods* (includes application of algae, bacteria, and fungi species)

This work used adsorption as a removal method and they will be described below.

2.7.7.1. Adsorption

Adsorption is a process that indicates changes in components concentration on the surface boundary phases of a heterogeneous system due to the existence of attractive forces of molecules, ions, or atoms that are not saturated on the surface. In the adsorption process, retention occurs of adsorbate (a compound that is adsorbed) on the adsorbent surface (on phase surface increases the concentration compound of interest). Because those component systems are adsorbed on the phase boundary, their presence reduces the system's specific surface energy, which is why the adsorption process is spontaneous. In relation to the bond nature between the adsorbate and adsorbent, the adsorption process can be physical (physisorption) and chemical (chemisorption) [133,134] .

Physisorption implies the occurrence of weak physical force, such as the attractive Van der Waals forces, and the chemical bonds are not broken. Due to the small enthalpy change (10 to 20 kJ/mol), physical adsorption is usually a reversible and fast process. The adsorbed substance can also be adsorbed in several molecular layers. Adsorbed substance amount decreases with increasing temperature. Ion exchange is also physisorption and represents a process in which ion exchange occurs between the solid phase and the solution, and it is based on electrostatic interactions between the charged surface of the adsorbent and ions from the solution.

Chemisorption forms strong, covalent, ionic, or coordination chemical bonds on the boundary layer between adsorbate and surface functional groups, where a monolayer is most often formed. Based on the thickness of the adsorbed layer, it can be concluded whether it is chemical or physical adsorption. Chemisorption enthalpy ranges from 40 to 400 kJ/mol. Increasing the temperature, the rate of chemisorption can increase, which is a characteristic of the process that requires activation energy [135].

Factors that affect the adsorption process can be: process parameters (temperature, pH value, composition and concentration of present ionic species, adsorbent concentration, etc.); properties of the adsorbent (pore size, total porosity, active surface, shape, and dimensions.)

In order to determine the adsorption mechanism, electrostatic interaction analysis is performed, surface complexes between adsorbent and adsorbate are formed and determined, and chemical reactions, equilibrium constants, and mass charge balance are also determined. Results are analyzed as a function of parameters such as pH value and ionic strength of the solution, temperature, and adsorbent surface coverage. Solution's pH value determines the material's adsorption capacity and regulates the removal degree of organic compounds and pharmaceuticals from aqueous solutions [14].

Adsorbent nature is characterized by its chemical composition, specific surface area, structure, and porosity. There are organic, inorganic, natural, or synthetic adsorbents with structures that can be crystalline, amorphous, or combined. Adsorption degree is proportional to the active specific surface of the adsorbent (the adsorbent's effectiveness increases by increasing the specific surface area), and the specific surface area of the adsorbent increases with the increased porosity and depends on the pore size. A spherical adsorbent is the most favorable for adsorption, and by increasing active surface area and porosity, adsorption is more efficient.

Adsorption rate is proportional to the free adsorbent surface and is the largest at the beginning because the free adsorbent surface is also the highest. After a certain time, between the adsorption and desorption processes, a balance is established. Adsorption kinetics also depends on various physicochemical parameters such as pH value, temperature, initial concentration of pollutants, adsorbent mass, presence of other cations and anions (competitive adsorption), contact surface, ion exchange, contact time as well as and characteristics and type of adsorbent (dimensions, shape, active surface, number of pores).

Pore size has an important effect on adsorption and is classified as micropore (pore size ≤ 2 nm), mesopores (pore size 2-50 nm), and macropores (pore size > 50 nm).

pH values strongly influence the present ionic species, the surface charge, and the adsorbent surface properties. Thus, pH affects the adsorption efficiency. A change in the pH value may result in protonation or dissociation of adsorbent surface functional groups. Pollutant particles' orientation also significantly influences adsorption since the number of particles that can bind to the surface unit depends on the orientation of asymmetric ionic and molecular species. Finally, the adsorbent and adsorbate contact time affect adsorption efficiency. The faster phase is characterized by a larger number of active centers on the adsorbent, while in the slower phase, with the gradual occupation of active sites, adsorption becomes less efficient [133,134] .

2.7.7.2. Process optimization

Process optimization of adsorption and adsorbent synthesis is carried out to be as precise as possible optimization of variable parameters (weight and used reactants concentration) and processes parameters (reaction time temperature, pH values), which is important for obtaining better product quality and increasing the efficiency of synthesized adsorbents, as well as from the aspect of environmental protection. It is possible to create process simulation models to predict the adequate concentrations and variable ratios to obtain synthesized products' most favorable required properties. The optimization goal is to maximize resource use while improving the adsorbent properties.

2.7.4.2.1 Response surface method

Response surface method (RSM) is an empirical statistical method used to analyze the simultaneous relationship between experimental parameters (reactants amounts and reaction time) and measure defined factors' effects on system response (adsorbent functionality) using a minimal number of experiments [31,136]. RSM is applied for adsorbent synthesis optimization, adsorption experiments, the definition of optimal conditions, and the prediction of adsorption results. To apply the RSM method, selecting the variables that have the largest impact on synthesizing adsorbents with the best adsorption properties or on the adsorption process itself is necessary. Minimum and maximum number of changes (from 3 to 5) were determined for each defined variable. When this is completed, an experimental design is made according to the experiments performed. Defined plan

leads to an improved model for adsorbents synthesis while performing as few experiments as possible. Result of applying the RSM method is the connection between the independent input variables (process parameters) and the output dependent variable, as well as the possibility of predicting the minimum and the maximum response values for any combination variable parameters in the examined range.

2.7.4.2.2 Statistical analysis and error function

Statistical analysis assesses the significance of differences in the obtained experimental data and results. Tests used are: Analysis of Variance (*ANOVA*), regression analysis, Fisher's t-test, Paired t-Test, Mean Square Error, Non-linear Chi-square (χ^2) test, agreement degree of the obtained results, as well as other error functions used to assess the experimental agreement data with theoretical models (47): correlation coefficient (R^2), Root Mean Squared Relative Error, Average Relative Error, Average Relative Standard Error, Sum Squares Errors, and others [137].

Regression analysis represents a statistical analysis of the relationship between a dependent variable and one or more independent variables. It provides an estimation model and predicts the dependent variable's values for certain independent variable values. Correlation coefficient, R^2, is a criterion of a particular model that shows how much the independent variable can represent variation in one dependent variable. R^2 represents the ratio of a particular sum of squares to total sum of squares and has a value between 0 and 1 ($0 \leq R^2 \leq 1$). Tested method is more applicable when the correlation coefficient is near 1. When $R^2=1$, other factors do not affect the behavior of the dependent variable. i.e., the dependent variable can be defined based on independent variables. If $R^2=0$, it can be concluded that the independent variable does not affect the dependent variable (Null hypothesis). Parameters of the used adsorption isotherms were analyzed by linear and nonlinear regression methods to check the agreement of experimental data and adsorption isotherm models. Nonlinear regression model is increasingly applied due to the need for more complex mathematical analysis to select the best model and develop appropriate software tools [137].

Analysis of variance (ANOVA) is a statistical method used to examine the effect of one or more independent variables on one dependent variable, that is, to define the impact of changing input variables on the system's response. It is used to compare means or parameters used in models for analysis. Depending on the number of examined factors, it can be single-factor or multi-factor. Each factor can contain multiple levels, groups, or parameters. It uses the ANOVA test, obtaining parameter values that define statistically significant parts representing input variables whose change affects the system response (output variable). ANOVA analysis uses the sum of squares and the F statistic parameter to calculate the relative significance of analyzed processable parameters, errors in measurements, and parameters that are not controlled [137].

A *paired t-test* is a statistical test for testing the significance of a difference between two samples or methods. It is used to compare the mean value of the results obtained experimentally (adsorption capacity values) using the dependence of the mean value of the difference between the two methods and the standard deviation of the obtained differences as a function of the experiment number. No significant differences exist if the t-parameter calculated value is less than the critical value. On the other side, if t parameter higher than critical value indicates that it significantly differs from zero, it defines that the difference in pairs of results is statistically significant [137].

Fisher's t-test is a statistical test of the absolute probability of the null hypothesis. Fisher's parameter value is calculated and compared with table values according to significance level and degrees of freedom number. When the calculated F-parameter is higher than the tabular, the null hypothesis is not accepted since an independent variable affects the dependent variable. Significance level is defined by the probability that up to some of the change in the value of the dependent variable randomly occured using the p parameter. Parameter has a value between 0 and 1 ($0 \leq p \leq 1$), which determines the upper limit and changes the value of the dependent variable [137].

2.7.8. Adsorption isotherms and thermodynamics

Adsorption isotherms represent the equilibrium difference between adsorbent and adsorbate, which is valuable for the mechanism optimization, expression of surface properties, adsorbent capacity, and efficient design of the adsorption system. Adsorption isotherm can be presented as a curve that describes the retention, mobility or release of a substance from an aqueous environment on a solid phase at a constant temperature and pH value of the solution. Physicochemical parameters and basic thermodynamic assumptions ensure insight into the adsorption mechanism, surface properties, and degree of affinity of the adsorbent. Adsorption capacity is one of the most important parameters for sorbent characterization because it represents the amount of pollutants that can remove the selected sorbent per weight unit (mg of pollutants per grams of sorbent). However, depending on applications, the sorption capacity is insufficient to describe the adsorbent sorption performance [138].

Langmuir adsorption isotherm was developed to describe gas adsorption on activated carbon and traditionally they have an application to quantify the properties of various biosorbents. According to its formulation, this empirical model represents adsorption in a single layer that occurs on a fixed number of defined adsorption sites that are identical and equivalent, without lateral interactions and steric obstacles between adsorbed molecules. Langmuir isotherm refers to homogeneous adsorption where each molecule has a constant adsorption activation energy and enthalpy (all sites have the same affinity to the adsorbate) without adsorbate transmigration in the plane of the surface. It is characterized by a plateau, i.e., equilibrium saturation where one molecule occupies one site after which no further adsorption occurs [138].

Webber and Chakravorti [139] defined the dimensionless constant R_L as represented by equation 1 (Eq1). In relation to the calculated value of the R_L constant, it can be concluded whether the adsorption process is: $R_L>1$ unfavorable, $R_L=1$ linear, $0<R_L<1$ favorable, or $RL=0$ irreversible [140]. The Langmuir isotherm is expressed in linear (Eq.2) and non-linear forms (Eq.3) as follows:

$$R_L = \frac{1}{1+ K_L C_e} \quad \text{(Eq.1)}$$

Where K_L (L g^{-1}) is the Langmuir constant, C_0 is the initial adsorbate concentration (mg l^{-1}).

$$\frac{C_e}{q_e} = \frac{1}{bQ_0} + \frac{C_e}{Q_0} \quad \text{(Eq.2)} \qquad q_e = \frac{Q_{max}\, bC_e}{1+bC_e} \quad \text{(Eq.3)}$$

Where C_e is a concentration of adsorbate at equilibrium (mg g^{-1}), q_e is the amount of adsorbate per unit weight of adsorbent (mg g^{-1}), Q_{max} is the maximum adsorption capacity (mg g^{-1}), b is the equilibrium constant related with the free adsorption energy.

Freundlich isotherm described reversible adsorption that is not limited to monolayer formation. This empirical model can be used to multilayer adsorption with a non-uniform adsorption distribution heat and heterogeneous surface affinity. Freundlich isotherm is widely used in heterogeneous systems, primarily for the adsorption of organic compounds or highly reactive species on activated carbon. Slope of isotherm, which can have values between 0 and 1, is a measure of adsorption intensity or surface heterogeneity. If slope value is near 0, it indicates the increasing heterogeneity of the system, while the slope value near 1 implies the chemisorption process. A value for 1/n above 1 is indicative of cooperative adsorption [138]. The Freundlich isotherm is expressed as linear (Eq.4) and non-linear (Eq.5) form as follows:

$$logq_e = logK_F + \frac{1}{n} + logC_e \qquad \text{(Eq.4)} \qquad\qquad q_e = K_F + C_e^{\frac{1}{n}} \qquad \text{(Eq.5)}$$

Where q_e is the quantity of adsorbate per unit weight of adsorbent (mg g^{-1}), C_e is a concentration of adsorbate at equilibrium (mg g^{-1}), 1/n is constant, expressing the adsorption intensity, K_f is the Freundlich constant (mg g^{-1}).

Temkin isotherm models described hydrogen adsorption on platinum electrodes in an acidic solution. This isotherm contains a factor explicitly included in the calculation of the adsorbent-adsorbate interaction. Despite extremely low and high concentration values, Temkin model assumes that the adsorption heat (a function of temperature) of all molecules in a layer decreases linearly rather than logarithmically with increasing coverage. Isotherm equation implies a uniform distribution of binding energy. Temkin equation is considered suitable for predicting gas equilibrium against complex systems that cannot be successfully described [138,141]. Linear (Eq.6) and non-linear (Eq.7) form of the Temkin isotherm is given by the following:

$$q_e = \frac{RT}{b_T} lnK_T + \left(\frac{RT}{b_T}\right) lnC_e \qquad \text{(Eq.6)} \qquad\qquad q_e = \frac{RT}{b_T} lnK_T C_e \text{ (Eq.7)}$$

Where b is the Temkin constant related to the heat of sorption (Jmol^{-1}), and Kt is the Temkin isotherm constant (L g^{-1})

Dubinin-Radushkevich isotherm is an empirical model originally developed for subcritical vapor adsorption on a solid microporous material. It is used to express the adsorption mechanism with Gaussian energy distribution on a heterogeneous surface and has the possibility of distinguishing between physical and chemical adsorption on metal ions. D-R isotherm can be expressed as follows (Eq.8) [138]:

$$\ln(q_e) = \ln(q_m) - \beta\varepsilon^2 \qquad \text{(Eq.8)}$$

Where q_m is the maximum adsorption capacity (mg g^{-1}), q_e is the amount of adsorbate per unit weight of adsorbent (mg g^{-1}), β is a coefficient related to the mean of free adsorption energy (mmol^{2}J^{-2}), ε is the Polanyi potential given as:

$$\varepsilon = RT\left(1 + \frac{1}{C_e}\right) \qquad \text{(Eq.9)}$$

Where T is temperature (K), and R is univerzal gass constant (8.314 J mol^{-1} K^{-1})

Hill's isotherm equation was developed to describe the binding of different species to a homogeneous substrate. The model assumes cooperative adsorption with the ability of the ligand to bind to one side of the macromolecule and the ability to affect different binding sites on the same macromolecule. Linear (Eq.10) and non-linear (Eq.11) form of Hill's isotherm model is given by the following [138]:

$$\log\left(\frac{q_e}{q_h - q_e}\right) = n_h log(C_e) - log(K_D) \qquad \text{(Eq.10)} \qquad q_e = \frac{q_h\, C_e^{n_H}}{K_D + C_e^{n_H}} \qquad \text{(Eq.11)}$$

Where K_D, n_h and q_h are constants.

Sips isotherm is a combined form of Langmuir and Freundlich models that were developed for heterogeneous adsorption systems and did not have the adsorbate concentration growth limitations associated with the Freundlich adsorption model. At low concentrations, Sips isotherm is reduced to a single-layer adsorption characteristic of Longmire. Parameters of the Sips equation depend on operating conditions such as changing pH, temperature, and concentration. Sips isotherm is expressed as linear (Eq.12) and non-linear (Eq.13) form as follows [138,142]:

$$\beta_s ln(C_e) = -ln\left(\frac{K_s}{q_e}\right) + ln(a_s) \qquad \text{(Eq.12)} \qquad q_e = \frac{K_s C_e^{\beta s}}{1 + a_s\, C_e^{\beta_s}} \qquad \text{(Eq.13)}$$

Where β_s is Sips isotherm exponent, K_s and a_s are Sips isotherm model constant (L g^{-1}).

Redlich-Peterson isotherm is a hybrid model that includes three parameters in the empirical equation in which the Langmuir and Freundlich models figure. Redlich-Peterson model has a linear dependence on the concentration in the numerator and an exponential function in the denominator, it describes the adsorption equilibrium in a wide concentration range, and due to its versatility, it can be used in heterogeneous and homogeneous systems. At high concentrations (when the exponent β tends to 0), this isotherm is reduced to the Freundlich model, and at low concentrations (β near 1) to the Langmuir model. The following expression defines this model [138] (Eq.14):

$$q_e = \frac{A\, C_e}{1 + B\, C_e^{\beta}} \qquad \text{(Eq.14)}$$

Where A is the Redlich-Peterson isotherm constant (L g^{-1}), B is constant (L mg^{-1}), and β is an exponent that lies between 0 and 1.

Thermodynamic parameters are used to define the spontaneously of an adsorption process, the reaction, and the type of adsorption. That parameters are Gibbs energy change (ΔG_0, kJ mol-1), enthalpy change (ΔH_0, kJ mol-1), and entropy change (ΔS_0, kJ mol-1). These parameters can be calculated using temperature-dependent equilibrium constants and using the following Van Hoff thermodynamic equations [37,143]:

$$\Delta G^0 = -RTlnK_L \qquad \text{(Eq.15)}$$

$$lnK_l = -\frac{\Delta H^0}{RT} + \frac{\Delta S^0}{R} \qquad \text{(Eq.16)}$$

$$\Delta G^0 = \Delta H^0 - T\Delta S^0 \qquad \text{(Eq.17)}$$

Where K_L is the Langmuir equilibrium constant (mol^{-1}), T is the absolute temperature (298K), R is the universal gas constant (J mol^{-1} K^{-1})

Negative ΔG_0 values indicate that a certain process takes spontaneously. With adsorption, the Gibbs energy is always negative. If the values of $\Delta H_0 > 0$, the adsorption process is endothermic; if $\Delta H_0 < 0$, the process is exothermic. At a ΔH_0 value of 20 up to 80 kJ mol^{-1} is physical adsorption. In chemisorption, ΔH_0 is usually between 100 - 400 kJ mol^{-1} since covalent bonds bind adsorbate particles. The disorder of the system is determined by measuring the entropy. An increasing ΔS_0 indicates spontaneous irreversible processes; if $\Delta S_0 > 0$, indicates a higher disorder degree between the adsorbent surface and adsorbate during the process.

2.7.9. Adsorption kinetics and activation parameters

Adsorption kinetics is important for performance evaluation and insight into the adsorption mechanism. From the kinetic analysis, time required to complete adsorption reaction can be determined, and adsorption kinetics is the basis for determining the properties of flow systems. Over the years, many mathematical models have been developed to describe the adsorption process.

Mathematical models describing adsorption kinetics can be divided into reaction and diffusion models. Both types of models have the same purpose, but they are different. Reaction models are based on considering the entire adsorption process without considering the steps in diffusion models. Diffusion models consist of three sequentially steps: the first step is diffusion through the liquid film surrounding the adsorbent particles (external or film diffusion); the second step represents diffusion in the pore fluid or pore walls along (internal or intra-particle diffusion); the third step is adsorption and desorption between adsorbate and active sites. Unlike reaction adsorption models, diffusion adsorption models represent real adsorption, provide useful information about the mechanism, and the intraparticle diffusion coefficient is useful in system design.

Pseudo-first order kinetic model describes adsorption rate, which is proportional to the number of vacant sites for adsorbate binding on the adsorbent's surface. According to this model, one type of adsorbate reacts with one active center forming an adsorption complex. Pseudo-first-order model best describes the early stages of adsorption processes, after which a significant change occurs concentration of adsorbate in the solution and reduction of the number of free sites for adsorption, so this model at that stage does not describe the process satisfactorily. Value of the constant k_1 can be obtained from the slope linearized curves by linear regression, depending on the initial concentration.It can be expressed based on the equation for the adsorption system in non-linear (Eq.18) and linear form (Eq.19) [144,145]:

$$q_t = q_e(1 - e^{-k_1 t}) \qquad \text{(Eq.18)} \qquad\qquad ln(q_e - q_t) = lnq_e - k_1 t \qquad \text{(Eq.19)}$$

where k_1 represents the pseudo-first-order adsorption rate constant (min^{-1}), q_e is the amount of adsorbate per weight unit of adsorbent in the equilibrium state (mg g^{-1}), and q_t (mg g^{-1}) represents the amount of adsorbate per weight unit of adsorbent in time t.

A *Pseudo Second Order* model implies that the degree of occupancy of adsorption centers is proportional to the square of the number of free ones and occupied sites, which is also proportional to the amount of adsorbed pollutants. When equilibrium is reached, the adsorption rate is very low. A model of the pseudo-other order is often expressed by non-linear (Eq.20) and linear (Eq.21) forms [145,146]:

$$q_t = \frac{t}{\frac{1}{k_2 q_e^2} + \frac{t}{q_e}} \qquad \text{(Eq.20)} \qquad\qquad \frac{t}{q_t} = \frac{1}{k_2 q_e^2} + \frac{1}{q_e} t \qquad \text{(Eq.21)}$$

Where k_2 is the pseudo-second-order adsorption rate constant (g mg^{-1} min^{-1}), q_e and q_t are the amounts of adsorbate per weight of adsorbent in an equilibrium state (mg g^{-1}) in time t (min). The values of the k_2 constant and the adsorption equilibrium capacity qe are obtained according to the experimental data by fitting the equation based on the intercept and slope from linear plot t/q_t versus t [146].

Elovich's model was primarily used to examine the chemisorption of gases on solids adsorbents, and later, for the description of adsorption kinetics in aqueous solutions, e.g., heavy metals on activated carbon [147], paint on natural adsorbents [147,148][150], etc. Model can also be expressed in the following equation (Eq.22):

$$q_t = \frac{ln^{(\alpha_E \beta_E)}}{\beta_E} + \frac{lnt}{\beta_E} \qquad \text{(Eq.22)}$$

where α_E is the initial adsorption rate (mg g^{-1} min^{-1}), β_E (g mg^{-1}) is the desorption coefficient.

Diffusion models of adsorption

In kinetic diffusion processes, we observed three basic stages of adsorption:

1) transfer the adsorbate from the solution to the adsorbent surface,

2) internal diffusion of adsorbate through the adsorbent (intraparticle diffusion),

3) adsorption on active sites inside the adsorbent.

When processes occur at the phase boundary or involve a transfer process through one or more stages, the mass transfer rate controls the overall process rate. Liquid film diffusion, through the adsorbent pores or in combination, is usually the slowest phase and determines the overall adsorption rate. In order to identify the mechanism and determine the diffusion coefficient during adsorption, the Boyd's, Weber-Morris model, Dumwald-Wagner model, and the diffusion model on homogenous surface diffusion model, HSDM were used [148].

Boyd's model describes intraparticle diffusion and is used when surface diffusion is the main rate-limiting step of the overall process and for t purpose of checking and comparing with the diffusion model on a homogeneous surface. Boyd model is expressed by equation [149] (Eq.23):

$$B_t = \left(\sqrt{\pi} - \sqrt{\pi - \frac{\pi^2 f(t)}{3}}\right)^2 \quad F(t) \leq 0.85 \quad [13] \quad \text{(Eq.23)}$$

Where B_t is Boyd's constant depending on the time constant, however, if the plot B_t versus t, a straight line passes through the coordinate start (0, 0), which confirms that the adsorption process is controlled by diffusion within the particles [150].

The *Weber-Morris* intraparticle diffusion model considers whether adsorbate diffusion through the adsorbent determines the adsorption rate. The model is based on the theory that adsorption capacity and √B values are in a proportional relationship [151]. Different mass transfer mechanisms are shown by the curves of the dependence of qt on √B. If a linear dependence passes through the coordinate start, it can be concluded that intraparticle diffusion represents the limiting degree of such adsorption. Slope may correspond to different adsorption degrees; in that case, the curve does not pass through the coordinate origin, or the dependence of qt on √B will not be linear. Following equation (Eq.24) expresses the model:

$$q_t = k\sqrt{t} + C \qquad \text{(Eq.24)}$$

Where k is the intraparticle diffusion rate constant (mg^{-1} $min^{-1/2}$), and C represents the constant proportionally of the thickness of the boundary layer. The high C value represents the higher boundary level thickness which means that the influence of diffusion on adsorption is significant.

Damwald-Wagner model [149] intraparticle diffusion is considered the slowest stage and thus determines the adsorption rate. Model can be presented as a linear equation (Eq.25):

$$log\left(1 - \left(\frac{q_t}{q_e}\right)^2\right) = -\frac{K}{2.303}t \qquad \text{(Eq.25):}$$

Where K is constant adsorption rate (min^{-1}).

Homogenous surface diffusion model (HSDM model) is applied to described mass transfer on the adsorbent, which characterizes amorphous and homogeneous spherical surfaces, and is often used in the adsorption analysis in fixed bed columns [152]. The model is expressed in the following equation (Eq.26):

$$\frac{6q_t}{6t} = \frac{D_s 6}{r^2 6r}\left(r^2 \frac{6q_t}{6r}\right) \qquad \text{(Eq.26):}$$

Where Ds is the intraparticle diffusion coefficient, and it depends on its adsorbent nature.

Determination of activation and adsorption energy

Temperature of the chemical reaction rate affects constant reaction rates. Activation energy E_a ($J\ mol^{-1}$) was calculated using the Arrhenius equation:

$$k_2 = k_0\, exp\left[\frac{-E_a}{RT}\right] \qquad \text{(Eq.27)}$$

where k_2 ($g\ mg^{-1}\ min^{-1}$) is the pseudo-second-order adsorption rate constant, k_0 ($g\ mg^{-1}\ min^{-1}$) proportionality factor temperature independent, R is ($8.314\ J\ mol^{-1}\ K^{-1}$) universal gas constant and T is the absolute temperature (298K). By linearizing the equation, plot $k_2 - 1/T$ gives a slope $-E_a/a$ where reading Ea values.

Adsorption energy was calculated by the following equation [153]:

$$\varepsilon = k_B\, Tln\left(\frac{c_s}{c^{1/2}}\right) \qquad \text{(Eq.28)}$$

Where k_B is the Boltzmann constant, $c^{1/2}$ is the half-saturation concentration active sites, and c_s is the pollution solubility [154,155].

2.7.10. Modeling of adsorption process in a column

Description of adsorbent and adsorbate dynamic behavior in the column is difficult to describe accurately because processes and reactions do not occur in a static state, and it is a challenge to choose the appropriate mathematical model in a flow system with a fixed-bed column [156] [157]. In this work, modeling was done using the appropriate mathematical models: Thomas model [157], June-Nelson model [158], Bohart-Adams model [159], Clark's model [160], as well as using, the Gnjelinski equation and PSDM model for calculation of the coefficient of external mass transfer.

The Thomas model [157] is used to evaluate the adsorption capacity and prediction of breakthrough points, assuming second-order kinetics and Langmuir adsorption isotherm [161]. The model is suitable for evaluating the adsorption processes, which occur with a low resistance to external and internal diffusion [162]. The following equation (Eq.29) expresses the model:

$$\frac{C}{C_0} = \frac{1}{1+exp\left[k_{Th}\left(\frac{q_0 m}{Q}-c_0 t\right)\right]} \qquad \text{(Eq.29)}$$

Where k_{th} is the Tomas constant ($cm^3\ min^{-1}\ mg^{-1}$), q_o is the adsorption equilibrium per weight unit of adsorbent (mg g-1), m is the adsorbent mass in column (g), Q_0 is wastewater flow through the column ($cm^3\ min^{-1}$), t is the flow through the column time (min).

The Bohart-Adams model is often used to describe adsorption under dynamic conditions [159]. The linearized form of the equation is given as follows (Eq.30):

$$ln\left(\frac{C_0}{C}-1\right) = k_{BA}\left(\frac{N_0 Z}{F}-c_0\, t\right) \qquad \text{(Eq.30)}$$

Where C_0 and C are input and output pollutant concentration (mg dm^{-3}), k_{BA} is the kinetic constant ($dm^{-3}\ mg^{-1}\ min^{-1}$), F is the linear rate (cm min^{-1}), Z is the column fill thickness (cm), N_0 time is the time needed for 50 % adsorbate breakthrough (mg dm^{-3}), and t is the time of the breakpoint or sampling (min).

Clark's model [160] is represented by the following equation (Eq.31) where A and r are Clark's parameters, and n is the Freundlich parameters.

$$\frac{C}{C_0} = \left(\frac{1}{1+A\ exp(-rt)}\right)^{\frac{1}{n-1}} \qquad \text{(Eq.31)}$$

The Yoon-Nelson model [163] is based on the adsorption probability for each adsorbate molecule and the adsorbate probability for the break-through point in the column in a dynamic, continuous process [158]. The model equation is general and does not contain specific characteristic data on the adsorbate nature, type of adsorbent, and physical properties of the adsorption layer in the column. A simplified equation is as follows (Eq.32) and their linearized form (Eq.33):

$$\frac{C_0}{C} = \frac{1}{1+exp[k_{YN}\,(\theta-t)]} \qquad \text{(Eq.32)} \qquad ln\left(\frac{C_0}{C}-1\right) = k_{YN}(\theta-t) \qquad \text{(Eq.33)}$$

Where C has adsorbed pollution concentration (mol dm^{-3}), C_0 is the initial adsorbate concentration (mol dm^{-3}) k_{YN} is the Yoon-Nelson flow constant (min^{-1}), and θ is saturated concentration.

The Pore Surface Diffusion Model (PSDM) is a diffusion surface model through the pores in which the analysis of experimental data and time-dependent study is carried out of adsorption process in the column with the prediction of the break-through curve using different models. Using adsorption results obtained experimentally and the Freundlich model isotherms, determination of the break-through point is possible after the verification process in a laboratory column [164]. The PSDM model describes a system with a fixed packing in a column. Also, the PSDM model considers surface diffusion and diffusion through the pores and at the same time, gives a good prediction of performance and breakdown point to assess the applicability of adsorbents in real conditions [165–168].

2.7.11. The adsorption materials methods characterization

Materials characterization determined their qualitative and quantitative properties; potential application requires confirmation of the properties and the presence of functional groups. The methods and instrumental techniques used for samples characterization are: infrared spectrometry with Fourier transform (FT-IR), X-ray diffraction analysis (XRD), spectroscopy X-ray photoelectron (XPS), scanning electron microscopy (SEM), determination of the specific surface area by the Brunauer-Emmett-Teller method of gas adsorption and Barrett-Joyner- Halenda method (BET/BJH) and thermogravimetric analysis (TGA) and they will be described below.

2.7.11.1. X-ray diffraction (XRD)

The X-ray diffraction (XRD) method is successfully used for the identification of monophasic and multiphase crystalline compounds, identification of mixtures of one or more crystalline compounds, determining the crystal structure of previously identified materials, determination of the degree of crystallinity, quantitative determination of the present phases based on ratios peak intensity, crystal size determination and crystallite shape determination. XRD method is characterized by: reliability and quick material identification, simple sample preparation, device availability, and relatively quick data interpretation. XRD method is based on the interaction of the tested material and X-ray radiation. Bypassing the X-ray, when the beam passes through the sample, it collides with atoms or ions, becoming the source of new X-ray radiation. X-rays of a particular wavelength λ will be usefully reflected from the parallel crystal planes when they fall on the plane at a certain angle θ. At a given X-ray wavelength, the maximum reflection will occur only at certain angles of rays. Measurement intensity of diffracted radiation, with a particular step and exposure in a different range of the angle 2θ, different values of radiation reflected from the crystal lattice due to stochastic orientation, are obtained of crystals in the analyzed sample [94]. Each crystalline compound has characteristic reflection positions, which can be identified from the data obtained by measuring and comparing with the base data [37,169–171].

2.7.11.2. Infrared spectrometry with Fourier transformation (FTIR)

Infrared spectroscopy with Fourier transform (FTIR) is used for qualitative analysis of functional groups and structural analysis of various organic and inorganic compounds. FTIR analysis is used to identify functional groups on the adsorbent surface, the type of bonds, and the interaction between the surface functional groups of the adsorbent and adsorbate. FTIR spectroscopy is applied in the infrared region of electromagnetic radiation with a wavelength of 2.5 - 400 μm, i.e., with a wavelength of 4000 - 400 cm^{-1}. Each maximum in the IR spectrum is characterized by its position (ν_{max}), intensity, and shape. The relative intensity and shape of the spectral band allow distinguishing the peaks of functional groups that absorb in the same spectral region. Absorption maximums, also called absorption bands, appear at the frequencies at which radiation is absorbed. The appearance of the IR spectrum is directly related to the molecular structure and the characteristic of each compound. Because of this, IR spectroscopy is used to identify inorganic and organic compounds and is one of the most reliable and simple methods for identifying functional groups. In addition, IR spectroscopy is characterized by: fast recording of spectra, high detection sensitivity, simple handling, the possibility of recording spectra regardless of the aggregate state of the sample, and relatively low cost of the instrument [172].

The FTIR spectrometer is an instrument that combines the methods of interferometry and Fourier transformation. The advantages of FTIR over the classical instrument are related to the much faster recording of spectra, greater sensitivity, higher frequency precision and significantly better decomposition, subsequent repair of spectra, the possibility of comparation the recorded spectra with spectra from the base, capture of a much broader spectral range and the possibility of recording the spectra of solid samples. Preparing a solid sample for analysis is performed by compressing the sample with KBr into a plate. The most common practice is making a KBr pill by grinding the solid compound with pre-irradiated KBr so that the sample concentration (to KBr) is in the range of 0.1 to 2%. This mixture is then pressed in a unique mold using a high-pressure hydraulic press. During compressing, the mold is connected to vacuum pump, which air removes, and in this way a round tile is obtained [172].

2.7.11.3. Scanning electron microscopy (SEM)

In the SEM method, the electron source is the tungsten spiral, since the anode voltage (40-100 kV) is higher than the tungsten spiral voltage, electrons are accelerated towards the anode with a strong force. Part of the electron passes at high speed through the anode opening and continues to the imaging object and the electromagnetic lenses, where it is focused as needed. The recording object is placed in the focal plane of the lens, and its image is further enlarged by a few more degrees. To not limit the movement of electrons, it is necessary to ensure a high vacuum in the microscope column. The focal length of the electromagnetic lens is variable and decreases with increasing magnetic field voltage. The analyzed sample must be completely dry, and living objects cannot be recorded [173].

The SEM method provides many advantages over conventional techniques and is characterized by relatively easy sample preparation and the possibility of direct observation of the sample structure in 3D. Modern electron microscopes reach a magnification of about 300,000 times. A focused electron beam directed by high voltage (50 to 300 kV) from the measurement sample to the film is accelerated and generates different signals as radiation of a certain wavelength from the surface of the solid sample. The signals provide information on the morphology, sample texture, the identity of the present phases, homogeneity, orientation, and defects of the material structure, porosity, adhesion, size, shape, and distribution of the dispersed phase in multicomponent systems, and the size and distribution of particles [173].

An imaging object is obtained with a scanning electron microscope by registering the scattered electrons from the sample and thus providing information about the material. According to the emission mode, scattered electrons can be divided into secondary (SE) and backscattered (BE). Primary electrons progress into the sample and undergo elastic and inelastic scattering. Secondary electrons are mainly emitted by a thin surface layer with a thickness of 1-10 nm, while backscattered electrons originate primarily from a reflection in deeper layers of the sample. Secondary electrons have low energy (0-30 eV) and are used to show the morphology and topography of the sample. Scattered electrons provide contrast between phases in multiphase samples, and if the device has a suitable detector, their diffraction image can also be obtained [173].

SEM analysis is non-destructive because when X-rays are emitted, the sample is not lost, so it is possible to repeat the analysis of the same material several times [234]. The sample preparation for SEM is not demanding since this method primarily provides information on the surface structure. Thus, samples up to several millimeters thick can be directly examined if the material has a high enough electrical conductivity to prevent electrification. If this is not the case, the sample is coated

with a thin layer of electrically conductive material by vaporizing it vertically or at an angle of 60° in a high vacuum chamber with carbon or metals of gold silver platinum, etc. Injection molding is increasingly used as a metallization method because it is relatively cheap, fast, and efficient [173].

2.7.11.4. Brunauer–Emmett–Teller (BET) adsorption isotherms

The BET method (*Brunauer, Emmett, and Teller*) is used to determine the textural properties of materials, such as volume, specific surface area, and pore diameter, based on gas adsorption capacity. The specific surface area obtained by this method represents the total surface area of the coarsely dispersed composition (including the surface area of pores within the material). The principle of BET instruments is the adsorption-desorption isotherm, based on determining the amount of gas that condenses on the sample's surface at the equilibrium vapor pressure. Specific surface area, pore size distribution and pore volume are determined based on the appropriate theory for describing adsorption and desorption data [174]. When determining the total specific surface area and pore size distribution of samples using the BET method, it is necessary to remove moisture and possible impurities that can clog or fill the pores before the same analysis [175].

2.7.11.5. X-ray photoelectron spectroscopy (XPS)

X-ray photoelectron spectroscopy (XPS) is a quantitative technique for measuring the material's elemental composition and determining the elements' binding state[176]. It is based on electron fluorescence excited X-ray and corresponding peaks analysis. Electrons in all elements have characteristic bond energy, te a series of peaks at certain kinetic energies appears in the photoelectron spectrum. The peak intensity depends on the concentration of elements, and the amount of present elements can be determined from the corresponding peak area and thus a quantitative analysis of the sample. Since the excitation radiation energy is known, the spectrum is usually shown depending on the bond energy. The value of the electron bond energy in an atom depends on the level of photoemission that occurred, as well as on the oxidation state of the atom, and the atom's local environment changes will cause small shifts in the position of the peaks in the spectrum, the so-called chemical shifts. Therefore, one of the high advantages of the XPS technique is the ability to differentiate different oxidation states and chemical environments. XPS also has found extensive use in the investigation of textile surfaces, which is now spreading to study plasma-treated textiles [177].

2.7.11.6. Thermogravimetric analysis (TGA)

Thermogravimetric analysis is a destructive method based on measuring the mass change of the sample as a function of temperature or as a function of time at a constant temperature. The method is widely used for identifying and characterizing materials, determining composition, sharing organic and inorganic content in the tested sample, and studying degradation mechanisms[178]. The TGA instrument is composed of precision scales and sample containers located inside the oven for sample heating control (depending on the type up to 2000^0C), and in order to precisely analyze the sample, it is combined with FTIR or mass spectroscopy. The analysis results are expressed by the mass dependence over temperature curve when the analysis is done by changing the temperature or by the mass dependence over time curve if during the analysis the temperature is constant [179].

3. EXPERIMENTAL PART

3.1. Materials and reagent

Kraft lignin - KfL (Sigma Aldrich), sodium hydroxide, (Zorka Pharma Stada), Sodium acetate, Ammonium acetate, Trisodium citrate and Tetrahydrofuran (Sigma Aldrich), Chlorosulfonic acid, deuterated water (D_2O) and deuterated dimethyl sulfoxide (DMSO-d6) (Sigma Aldrich), toluene (Sigma Aldrich), α,α'-azoiso-bis-butyronitrile (AIBN) (Sigma), trimethylolpropane - TMP (Fluka), Benzoic acid and 4-aminobenzoic acid (Merck), disodium laureth sulfosuccinate (Zschimmer & Schwarz, Germany (Setacin 103 Spezial). All chemicals are of p.a. quality. Levulinic was supplied by Sigma-Aldrich; 2-Ethylhexyl levulinate (EHL) was kindly provided by GFBiochemicals (http://www.gfbiochemicals.com/products/#existing-products). γ-Alumina was supplied by Sigma. Malachite green (MG; 4-{[4-(Dimethylamino)phenyl](phenyl)methylidene}-N,N-dimethylcyclohexa-2,5-dien-1-iminium chloride, Merck), Tartrazine (T; Trisodium (4E)-5-oxo-1-(4-sulfonatophenyl)-4-[(4-sulfonatophenyl)hydrazono]-3-pyrazolecarboxylate) and Methyl Red (MR; 2-{[4-(Dimethylamino)phenyl]diazenyl}benzoic acid), Methylene blue was provided by Sigma. Iprodione and Azoxystrobin were kindly provided without charge from Agrosava chemicals, Serbia. AAS standard single-element solutions of Ni^{2+} and Pb^{2+} produced by Carl Roth Gmbh, Germany, were used for adsorption experiments, deionized water (Milli-Q, 18 MΩ·cm) was used for preparation of working solutions. p-Toluenesulfonic acid (p-TSA), citric acid, Glucose and Fructose were also provided by Sigma Aldrich. Levidiagro rice producer in Kocani, Republic of North Macedonia provided rice husk for the preparation of silica nanoparticles. Commercial laccase from M. thermophila expressed in *A. oryzae* (Novozym® 51003) was kind gift of Novozymes (Basgvaerd, Denmark). alkali kraft lignin, diethylene glycol dimethacrylate (DEGDMA), 2,2′-Azino-bis(3-ethylbenzothiazoline-6-sulfonic acid) (ABTS) were also provided by Sigma Aldrich [180,181]

3.2. Synthesis of lignin-based microspheres (LMS-DEGDMA)

Acrylic modified kraft lignin (KfL-AA) was synthesized using modified version of the method by Podkoscielna et al. In a flask with a mechanical stirrer, dropper and thermometer, 3.0 g of kraft lignin was dissolved in 7 ml of deionized water, 1 ml of NaOH water solution (0.35 g NaOH), and 7 ml of tetrahydrofuran were mixed for 15 minutes. Then, 1.115 mL of acrylic acid (AA) synthesized from fructose was added drop by drop for 1 hour at -3 °C. The flask's contents were then agitated for 1 h at 0 °C and 1 h at 10 °C. After the reaction, cold deionized water and ice were added and the mixture was left overnight. The precipitate was then filtered and washed twice with deionized water and ethanol. The product was vacuum-dried at 50^0C for 12 hours. The iodine number (IN=42) verifies the efficency of the modification technique and quantifies the amount of double bonds in synthesized KfL-AA. Podkoscielna et al.'s [182] inverse emulsion-suspension copolymerization method was implemented in an aqueous medium with a number of changes. Usually, 32 mL of water and 0.35 g of disodium laureth sulfosuccinate (surfactant) were mixed 30 minutes at 80 °C in a 250 mL three-necked flask equipped with a stirrer, a water condenser, and a thermometer. Then, acrylic modified lignin (KfL-AA 0.5 g), DEGDMA solution, the initiator,-azoiso-bis-butyronitrile (AIBN, 1%), and the mixture of toluene and tetradecanol (pore-forming agents) were added, then this reaction mixture was agitated at 80 °C for 18 hours at 350 rpm. After centrifugation, the modified KfL-AA containing DEGDMA was extracted in a Soxhlet apparatus with acetone and washed with 1.5–2 L of hot distillate water. After vacuum drying, the LMS-DEGDMA product was further characterized and used as a support for laccase immobilization. The procedure for synthesis of acrylic acid (AA) from

fructose are desribed in literature [181]. The procedure of synthesis pore-forming agents and precursors, which are used for adsorbents synthesis, bio-based precursor included in levulinic acid synthesis (4-oxopentanoic acid, LA) from carbohydrates (glucose/fructose), oxidation of LA to 3-hydroxypropanoic acid (3-HPA) and dehydration of 3-HPA to Acrylic Acid (b-AA) are described in the literature [180] The synthesis procedure of triacetin as bio-based pore forming agent (propane-1,2,3-triyl triacetate), b-AA-modified KfL (KfL-AA) are also described in the literature [180]. The b-LMS was synthesized by inverse emulsion-suspension copolymerization of KfL-AA, TMPTA, initiator AIBN with mixture of pore-foriming solvents (triacetin:ethyl levulinate 1:1) and disodium laureth sulfosuccinate. Finally the b-LMS was extracted in a Soxhlet apparatus with acetone, and washed with ethanol. The b-LMS-OSO_3H was synthesized by the reaction of b-LMS and chlorosulfonic acid in chloroform. After reaction the b-LMS-OSO_3H microspheres were decanted and washed applying vacuum to evacuate air.

3.3. Synthesis optimization and exprerimental design

Response Surface Methodology (RSM) is used to describe the output responses that are determined by the input process parameters. RSM explain the connection between the variable input parameters and the related output parameters. RSM designs enable us to estimate an interaction and quadratic effects, and provide us with a notion of the shape of the investigated response surface. Box-Behnken design has the highest efficiency for an experiment with three components and three levels; also, it is required much less trials than a central composite design. The suggested Box-Behnken design requires 17 experimental runs for data collection and response surface modeling. The regression model was constructed and its ability to predict output values was validated. In addition, the model was verified by conducting tests with three random sets of input data. Experimentally observed output parameters (actual) closely match the model's projected output parameters. They used the commercial program Design-Expert, Version 9 (Stat-Ease, Inc. 2021 E. Hennepin Ave. Suite 480 Minneapolis, USA). The evolution of the RSM was shown in 2D and 3D. In addition to identifying the dominant process variable and the order of dominance, these plots illustrate the interaction pattern between variables in the process. [180]

3.4. Characterization methods

Fourier transforms infrared (FTIR) spectra were collected using a Nicolet™ iS™ 10 FT-IR Spectrometer (ThermoFisher Scientific) equipped with Smart iTR™ Attenuated Total Reflectance (ATR).

Raman spectra were recorded with aXploRA Raman spectrometer, which used laser at 532 nm (maximum output power was 20-25 mW).

1H and 13C NMR measurements were carried out on Bruker Avance III 500 spectrometer equipped with a broad-band direct probe. The spectra of KfL was recorded at ambient temperature in D_2O, while ones for KfL-AA in DMSO-d6. Chemical shifts are given on δ scale relative to tetramethylsilane (TMS) as an internal standard in 1H NMR spectra, while to residual solvent signal in 13C NMR. Coupling constants (J) were expressed in Hz.

The melting points of synthesized compounds were analyzed on a Stuart digital SMP-30 melting point apparatus. Elemental analyses (C,H,N) were performed by the standard micro-methods using an ELEMENTAR VARIO ELIII C.H.N.S.O analyzer.

The field emission scanning electron microscopy (FESEM) observed the particle size, distribution and morphology with Tescan Mira 3 XMU FEG equipment. Prior to the analysis, microspheres were gold-coated using a Polarion SC502 sputter coater.

The pore size distribution and specific surface area of samples was investigated by the low-temperature nitrogen adsorption-desorption isotherm using the Brunauer Emmett Teller (BET) method (Thermo Fisher Scientific, USA). The specific surface area, SBET, pore size distribution, dV(r), mesopore including external surface area, S_{meso}, and specific micropore volume, V_{mic}, were computed from the full adsorption/desorption isotherm. Pore size distribution dV(r) was computed from the desorption isotherm from Barrett, Joyner, and Halenda (BJH) method until a mesopore surface and micropore volume were asseseds using the t-plot method.

Thermal properties of samples were investigated by thermogravimetric analysis using a SDT Q-600 (TA Instruments). Mass of 10 mg of samples were heated from the room temperature to 400 °C at a heating rate of 10 °C min^{-1}, in a standard alumina sample under nitrogen (flow rate of 100 cm3 min^{-1}).

The point of zero charge (pH_{pzc}) was determined using the pH drift method.

3.4.1. Determination of porosity

For the estimation porosity of samples, procedure earlier described was used. Material and samples densities, Q_M and Q_P, were calculated using the Eq. 33 and 34, based on the determined weight/volume ratio of the dry and wet sample [183].

$$Q_M = {m_M}/{V - \left(\frac{m_W - m_M}{q_s}\right)} \quad \text{(Eq. 33)}$$

$$Q_P = {m_M}/{V} \quad \text{(Eq. 34)}$$

Where m_M and m_W – weights of the dry and wet sample, respectively; V – volume of the wet sample and qs – ethanol density. The porosity was determined from the material and the sample densities by Eq. 35 [184]:

$$\varepsilon_P = {Q_M - Q_P}/{Q_P} = 1 - {Q_P}/{Q_M} \quad \text{(Eq. 35)}$$

3.4.2. Determination of hydroxyl and phenolic hydroxyl group amount in LMS-DEGDMA

The amount of total OH groups in kraft lignin and LMS-DEGDMA was evaluated by acetylation with acetic anhydride/pyridine, followed by potentiometric titration of excess free acetic acid with 0.1 N NaOH in water (ISO 4326:1992) [184].

Determination of the phenolic hydroxyl group amount was performed by a non-aqueous potentiometric titration with tetra-butylammonium hydroxide (TnBAH). 0.15 g of dried kraft lignin or LMS-DEGDMA and 0.02 g p-hydroxybenzoic acid as internal standard were used. Aliphatic $^{-}$OH content in lignin was obtained from the difference of determined phenolic and total $^{-}$OH groups [181,184].

3.4.3. Determination of hydroxyl and carboxylic groups amount in kraft lignin

The amount of total ⁻OH groups in lignin was measured by acetylation of samples with acetic anhydride/pyridine and subsequent potentiometric titration of excess free acetic acid with 0.1 N NaOH in water. The carboxylic groups were determined using a non-aqueous potentiometric titration with tetrabutylammonium hydroxide (TnBAH). As an internal standard, 0.15 g of air-dried lignin and 0.02 g of p-hydroxybenzoic acid were used. UV spectrometry and aminolysis techniques were also utilized to determine total phenolic groups. Aliphatic hydroxyl content of lignin was evaluated by subtracting the total OH group from the phenolic group. [185] The acid value (*AV*) was evaluated according to ASTM D3644. Iodine value was determined by the Wijs method. [180]

The amount of sulfate group in b-LMS-OSO_3H was determined by the potentiometric titration. In a typical experiment, 60 mg of sulfonated microspheres were dispersed in 25 cm^{-3} deionized water and then the solution was titrated with 0.1 mol/L NaOH, with a few drops of phenolphthalein as an indicator. The content of the sulfate group was calculated according to the following equation (Eq.36):

$$C_{(-OSO3H)} = \frac{c_{NaOH}}{m_{b-LMS-OSO3H}} \; x \; V_{NaOH} \qquad \text{(Eq. 36)}$$

In adsorption experiments, the concentration of MG, T and MR was measured using UV-VIS Spectrophotometer 1800, Shimadzu, Japan.

3.5. Determination of Chemical oxygen demand (COD) in real samples

In order to define criteria for the successfulness of the adsorption process, in default of regulatory international and national data, the most relevant approach was to use limit values given by the Serbian national document related to limit values for the emission of pollutants at the site of discharge into surface water: Decree on limit values for the emission of pollutants into water and deadlines for their achievement, Sl. RS Gazette, no. 67/2011, 48/2012 and 1/2016 (COD = 200 mg dm^{-3}; BOD = 30 mg dm^{-3} and TOC = 60 mg dm^{-3}). For the determination of chemical oxygen demand, the standard technique ISO 6060 was used (COD). After treatment, water samples were analyzed spectrophotometrically to determine COD concentrations. Mercury (II) sulfate was used as a masking agent for chloride. The instruments used for COD determination:

1. Lovibond MD 600 spectrophotometer, Tintometer GmbH,

2. Lovibond RD 125 sample heating apparatus, Tintometar GmbH

Total organic carbon (TOC) was analyzed on a Zellweger LabTOC 2100 instrument using high-temperature combustion followed by infrared CO_2 detection.

3.6. Enzyme catalytic activity assay

The following procedure performed enzime catalytic activity assay:

*The activity of free enzyme and supernatant***:** The assay mixture contained 400 μL of 0.1 M Na-phosphate buffer of pH 6.5, 100 μL of 1 mM substrate solution and 500 μL of enzyme or supernatant. Absorbance was measured at 420 nm in a spectrophotometer against a suitable blank every 30 s for 3 minutes. One unit (IU) of activity was defined as the amount of the laccase that oxidized 1 μmol of ABTS substrate per min. [181]

The catalytic activity of immobilized preparation (IU/g of support) was determined by incubating 10 mg of immobilized preparation with 4 mL of substrate solution and 36 mL of 0.1 M Na-phosphate

buffer pH 6.5 (total volume of reaction mixture was 40 mL), under magnetic stirring. The activity was measured by sampling 1 mL of reaction mixture and measuring absorbance at 420 nm every 30 seconds for 3 min. After each measurement, 1 ml of sample was taken and returned to the reaction mixture in order to avoid the potential impact of volume reduction on the measurement results. [181]

The specific activity (IU/mg of proteins) is calculated as enzyme activity per actual mass of enzyme attached (Eq.37):

$$The\ specific\ activity = \frac{The\ catalytic\ activity\ of\ immobilized\ enzyme\ (\frac{IU}{g}\ of\ support)}{The\ protein\ loading\ \frac{mg\ of\ proteins}{g}\ of\ support)} \qquad \text{(Eq.37)}$$

The activity immobilization yield (*IYa*) was calculated using equation (Eq.38):

$$IYa\ \% = \frac{The\ catalytic\ activity\ of\ immobilized\ enzyme\ \left(\frac{IU}{g}\ of\ support\right) * mass\ of\ immobilized\ preparation\ (\ \ )g)}{The\ initial\ catalytic\ activity\ at\ the\ start\ of\ immobilization\ process} * 100 \qquad \text{(Eq.38)}$$

3.7. Protein assay

The content of bound enzyme (protein loading - mg of proteins per g of support) was determined indirectly from the deference between the initial enzyme concentration and the amount of enzyme remaining in the supernatant after the immobilization. Sorption data were fitted to the Langmuir adsorption isotherm model. For investigation of laccase diffusion from solution on LMS-DEGDMA surface the pseudo-first-order kinetic model was used. [181]

3.8. Laccase immobilization procedure

The mass of 10 mg of LMS-DEGDMA was mixed with 1 mL of enzyme dissolved in buffer for laccase immobilization. At 25^0C, the enzyme suspensions and microspheres in the buffer were placed on an orbital shaker at 150 rpm. Various buffers with pH values between 4.0 and 7.5 were used. For pH 4.0 and 5.0, 0.1 M Sodium citrate buffer was used, while for pH 6.5 and 7.5, 0.1 M Na-phosphate buffer was used. To examine kinetics characteristics for laccase immobilization on LMS-DEGDMA, the initial enzyme concentration varied from 30 mg of proteins/g of support to 1000 mg of proteins/g of support immobilization time changed from 0 to 5 hours. When the immobilization process was complete, the immobilized laccase was separated from the reaction mixture, and the derived supernatants were used to measure the catalytic activity and protein concentration, while the immobilized laccase were used to measure activity after three washes with the used buffer. All investigations involving the immobilization of laccase were completed in duplicate, and the findings are presented as the arithmetic mean.[181].

3.9. Desorption assay

Laccase immobilized on LMS-DEGDMA was desorption in two phases. First, the immobilized enzyme was incubated in a 1 M $CaCl_2$ solution at 25 °C for 1h under optimum conditions. After 1 hour, the immobilized preparation was rinsed twice with 1 mL of immobilization buffer, and its activity was measured.

3.10. Textile dye decolorization

Dye decolorization by LMS-DEGDMA-laccase was estimated. The optimally immobilized LMS-DEGDMA-laccase preparation (50 mg) was added to a 20 mg L^{-1} dye solution (prepared by dissolving dyes in 25 mL of 0.1 M Na-acetate buffer pH 5.0). Control samples containing the same quantity of dye solution and support without enzyme (50 mg) were prepared for each dye examined. Absorbance at χ_{max}=590 and 630 nm was measured spectrophotometrically at certain time intervals to track the sample's color change. As the absorbance ratio decreased to the dye solution's original absorbance, the overall decolorization efficiency (%) was computed.

3.11. Reusability study

In order to determine the recycling performance of immobilized laccase, an immobilized preparation was used in successive dye decolorization reaction cycles (2h and 3 h for LANASET® violet B and blue 2R, respectively, 45 minutes for CIBA Green and 3 h for model effluent). After each cycle, a 20 mg/L dye solution was separated, absorbance was measured, and the immobilized enzyme was rinsed twice with buffer. The same quantity of dye standard solution (25 mL, c=20 mg/L) was added to each tube to begin the next reaction cycle.

3.12. Leaching assay

The separated dye solution was analyzed for the presence of proteins after each sequential cycle using the Lowry technique to assess whether leaching occurred during the recycling research.

3.13. Batch Adsorption kinetics experiments

Batch adsorption kinetics experiments was evaluated using Shaking Drybath/Thermofisher scientific laboratory shaker. The mass of b-LMS and b-LMS-OSO_3H was 1, 2, 3, 4, 5, 7.5 and 10 mg, shaked with 10 ml of standard solutions of Tartrazine (T), Malachite green (MG) and Methyl Red (MR) (initial concentration is 20 ppm), and Pb^{2+} solution (concentration 10 ppm) and Ni^{2+} solution (concentration 5.75 ppm). pH vaules for adsorption of dyes was 6 for Methyl Red and Tartrazine; 7 for Malachite green; 7.5 for Ni^{2+} and 6.5 for Pb^{2+} solution. The pH value was adjusted with 0.1 mol/dm^3 NaOH and 0.1 mol/dm^3 HCl. The kinetic experiments were performed at 298, 308 and 318 K. Obtained meen value from three measurements was used for data processing. The contact times varied from 5 - 90 min, and 12 h, for the adsorption kinetics study performed at initial concentration 10 ppm. pH influence on the efficiency of adsorption process was performed at the following conditions: C_i[MG] = C_i[T] = C_i[MR] = 1 mg/l, m/V = 0.125 g/l, T = 308 K. [180]

The capacity of the adsorption was calculated using Eq. 39:

$$q = \left({}^{(C_i - C_f)}\!\!\diagup\!\!{}_{m} \right) V \qquad \text{(Eq.39)}$$

where q – the capacity of the adsorption (mg/g), C_i – initial concentration (ppm), C_f – final concentration of dyes (ppm), V –volume of solution (L), and m – mass of adsorbent (g).

The removal efficiency (R%) was calculated using Eq.40:

$$R(\%) = \left[\frac{C_i - C_e}{C_i} \right] \times 100 \qquad \text{(Eq.40)}$$

Where C_i and C_f are the initial and final concentrations of dyes (ppm).

3.14. Desorption and sorbent reusability

The efficiency of regeneration (% RE) for n^{th} cycle and overall RE was calculated using the Eq.41 and Eq.42:

$$(\%\ RE) = \frac{q_{n+1(d)}}{q_{n(a)}} \times 100 \quad \text{(Eq.41)} \quad \text{and} \quad (overall\ \%\ RE) = \frac{q_{n(d)}}{q_{0(a)}} \times 100 \quad \text{(Eq.42)}$$

where q_0, q_n and q_{n+1} are adsorption capacities (a)/quantity of desorbed dye (d) (mmol/g or mg/g) in the first, n^{th} and $(n+1)^{th}$ cycle. Desorption efficiency represents a quantity of the desorbed pollutant related to the quantity of adsorbed pollutant per the adsorbent mass unit. Ten consecutive adsorption/desorption cycles were finished. Effluent was separated from adsorbent by filtration in a vacuum with 0.22 μm pore diameter PTFE filter [180]

3.15. Full-scale system modeling using validated pore surface diffusion model

For the full-scale system simulation, a 1.5 x 12 cm column was used. The adsorbent was packed on a glass bead/glass wool support and then coated with glass wool to ensure uniform flow. As recommended by the literature (dcolumn/dp>40) the insignificant wall impact on mass transfer was determined using a dcolumn/dp ratio of 59 for b-LMS. Thus, the wall effect relevant to diffusional transport for b-LMS and b-LMS-OSO_3H. Influent water which contatins T, MG, and MR with concentration of 1 ppm and breakthrough time at effluent COD of 200 ppm of oxygen, recalculated to Ce/Ci > 95%; specified loading rate of 0.6 - 2.5 L m^{-2} s^{-1}; as suggested for full scale operations [25]. The applied high loading rate was sufficient to offer optimal conditions with little mass transport film limitation. Using PSDM, the system's performance at full scale was analyzed while running at the same load rates as in SBC testing. The packed bed length varied to achieve the desired EBCTs of 3.32, 1.66 and 1.10 minutes [180].

3.16. Statistical analysis and theoretical calculations

To validate the model's fit, it was essential to examine the data using error analysis and correlation coefficient (r) values derived through regression analysis. Using a linear and/or non-linear least-squares technique, the commercial software (Origin 8.0) estimated all kinetic, isotherm, and thermodynamic parameters together with their standard errors were used. Analysis of variance was used to identify the relationships between experimental results and models (ANOVA). ANOVA evaluated the significance of the models. The mean square values are obtained by dividing the total of the squares of the different sources, the model, and the error variance by their respective degrees of freedom. The model terms whose Prob. > F value is less than 0.05 are significant. ANOVA indicates that all models are significant. The greater value of parameter F means the better fit theoretical model with experimental data. All adsorption experiment was repeted in triplicate, and the mean value was calculated for further analysis [180].

The initial 3D structures of lignin, tartrazine, malachite green, and methyl red were obtained from PubChem. pKa values of lignin and dyes were predicted using the Marvin Sketch program (https://www.chemaxon.com) to assign the correct protonation state at adsorption pH experiment (pH = 6-7). The initial geometries of dye/lignin complexes were obtained by manually positioning dye molecules around the adsorbent to match their molecular electrostatic potential (MEP) maps. The AutoDock Vina software were generated several configurations[186], where lignin was treated as the receptor. Exhaustiveness was set to 100, and 20 binding modes were stored for the analysis. The geometries of 10 complexes for each dye were optimized on PM7 semiempirical level [187] in MOPAC 2016 HTTP://OpenMOPAC.net222. The COSMO implicit model of water (EPS = 78.4) was applied to treat the solvation effects. The MEP, semiempirical, and docking calculations were done using

Vega ZZ 3.2.0 [188] as GUI. The nature of adsorbent/adsorbate interactions was analyzed in LigandScout 4.4.7 [180] .

4. RESULTS AND DISCUSION

4.1. Production of microspheres based on lignin LMS-DEGDMA

For synthesis of microspheres based on lignin, an ecologically friendly kraft lignin (KfL) is utilized as the strating material (Scheme 1). KfL is often a byproduct of the process of pulping and is created the lignins post-sulfonation and acquired by process pulping of sulfate. In addition, kraft lignin is possibly readily transformed into materials tailored with chemical characteristics and physical propreties to a particular application. Consequently, KfL was modified via a multistep process represented at Scheme 1. First, kraft lignin was treated using acrylic acid obtained from fructose. [181]. Today, acrylic acid is made from several eco-friendly, cost-effective manner by microbes fermenting renewable sources. Both low toxicity and biodegradability of acrylic acid under aerobic and anaerobic environment are established [181]. In the second process (Scheme 1) acrylic acid-modified KfL-AA was suspended and copolymerized with diethylene glycol dimethacrylate (DEGDMA). The suspension and copolymerization method produced cross-linked LMS-DEGDMA spherical beads, ranging of 50–90 m in diameter (Scheme 1 and Figure 15). The fabrication of lignin-based beads (LMS-DEGDMA) has several prospects for development of biocompatible, eco-friendly materials that may serve as enzyme immobilization supports [181].

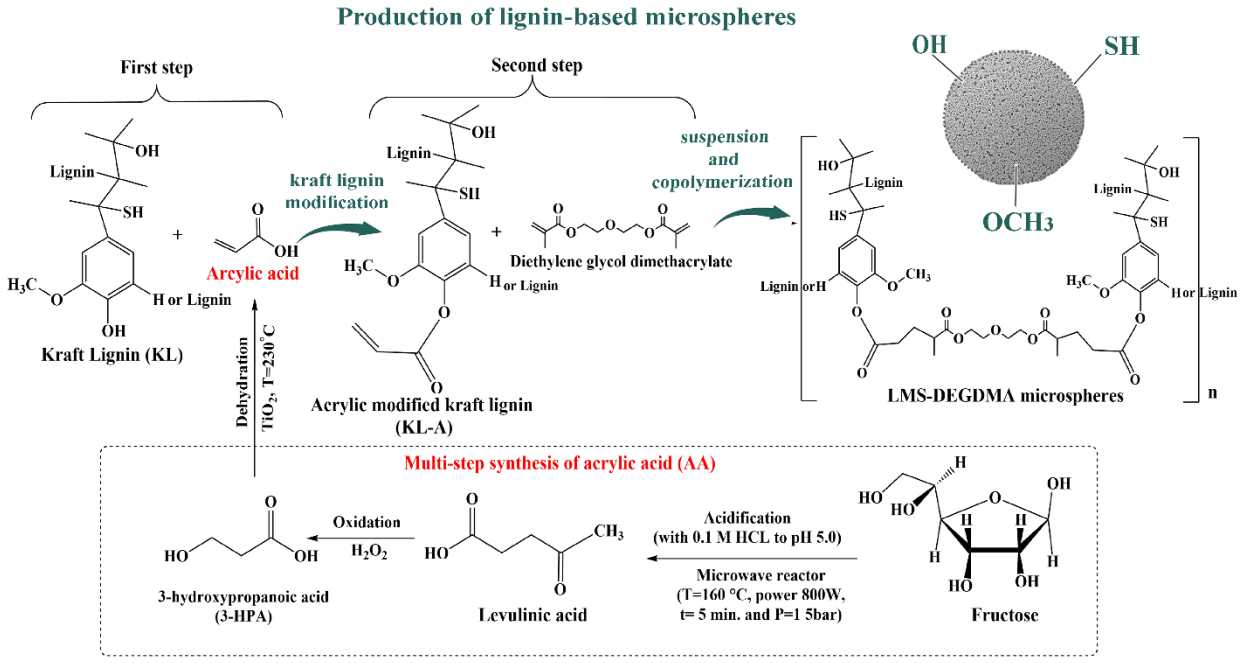

Scheme 1. Production process of KfL lignin-based microspheres [181]

4.2. Synthesis of KfL-based b-LMS microspheres and process optimization

Synthesis of microspheres based on kraft lignin and also its own sulfonated form (b-LMS-OSO_3H) were done by three step:

- Synthesis of acryloyl compounds based on bio-materials: KfL-AA ,b-AA, bio-TMPTA
- Optimization of synthesis from reactive precursor for b-LMS
- Sulfonation with sulfate group and formation b-LMS-OSO_3H

The synthesis sheme of b-LMS is presented in Figure 10.

4.2.1. Synthesis of acrylic acid (AA)

The first step on AA synthesis is getting levulinic acid from fructose. The next step is levulinic acid oxidation to 3-hydroxypropionic acid (3-HPA) with H_2O_2 by the following procedure [189]. Final step is 3-HPA dehydration to acrylic acid with nano-SiO_2 and χ alumina .

4.2.2. Synthesis of bio-TMPTA

Synthesis of trimethylolpropane triacrylate from acrlyc acid was performed by the following procedure. In the 1000 ml 4-neck round bottom flask coupled with Dean-strak separator, mechanical stirrer, nitrogen gas inlet tube, condenser and thermometer were added 134.7 g of trimethylolpropane, 216 g AA, 3.5 g p-TSA, 0.5 g hydroquinone and 75 ml of toluene, and heated at 90°C. When the acid value of the reaction mixture reach 30, the temperature was increased up to 95° C. Finally, toluene was acidified and removed by distillation. Catalyst was removed by washing two times with 2% NaOH, and washing with water under of pH 6. After drying product was obtained by vacuum distillation (150 Pa) at 70-72° C. The faint yellow TMPTA was obtained in 88% yield [180].

4.2.3. Synthesis of kraft lignin

KfL was synthesized using acrylic acid (AA) and produced using an optimized technique provided by Podkoscielna et al. [22] and Rusmirovic et al. [190]. Kraft lignin (10.0 g) and 1.1 g NaOH were dissolved in deionised water (25 ml) and put in an ice bath in a 3-neck 500 ml flask with a thermometer, condenser, and dropping funnel (0-5°C). After 30 minutes of stirring, AA (1.66 g) was dissolved in tetrahydrofuran (20 ml), which added drop-wise for 1 hour between -3 and 0^0 C. Additional stirring was performed for 1 hour at 0^0C and 1 hour at ambient temperature. The remaining dispersion was then saturated with sodium chloride and cooled to 5 °C. This obtained precipitate was centrifuged (5000 rpm), dissolved in 50 ml DMSO, and precipitated with a 300 ml water and centrifuged. The final obtained product was dried in a vacuum for 12 h at 50^0 C [180].

4.2.4. b-LMS synthesis optimization from reactive precursor

The suspension-emulsion copolymerization inverse technique optimized by Podkocielna et al. is used for synthesis b-LMS. Disodium laureth sulfosuccinate was agitated for 30 minutes at 80 °C in a water. Then, the mass of 11. 6 g TMPTA, 4.3 g KfL-AA and the initiator (1 wt.% AIBN) were added. The combination of pore-forming solvents (20 g mixture of 1:1 triacetin:ethyl levulinate) was followed and shaked at 80 °C for 18 hours. After centrifugation, the lignin microspheres (b-LMS) were extracted by Soxhlet apparature with acetone and washed with ethanol. The 2 g of b-LMS was dried for 24 hours at 40^0C and characterized. The rest of the b-LMS was rinsed with water many times, and wet b-LMS (56 to 58 % moisture) was used in the adsorption experiment [180].

4.2.5. Sulfonation with sulfate group and formation b-LMS-OSO_3H

Synthesis of b-LMS-OSO_3H was performed by modification of b-LMS microspheres with chlorosulfonic acid. The 5 g of synthesized and dry b-LMS was dispersed for 2 minutes in 100 ml of chloroform using a vacuum, and then cooled to -1 °C. After cooling the dispersion, 7.5 ml of HSO_3Cl in chloroform (100 ml) was added drop-wisely, and the obtained solution was agitated throughout 3 minutes. Obtained sulfated microspheres (b-LMS-OSO_3H) were poured in 200 ml ice-cold deionized water with mixing. Then, the b-LMS-OSO_3H microspheres were decanted, washed with deionized water, and saved at 55 - 57% moisture content [180].

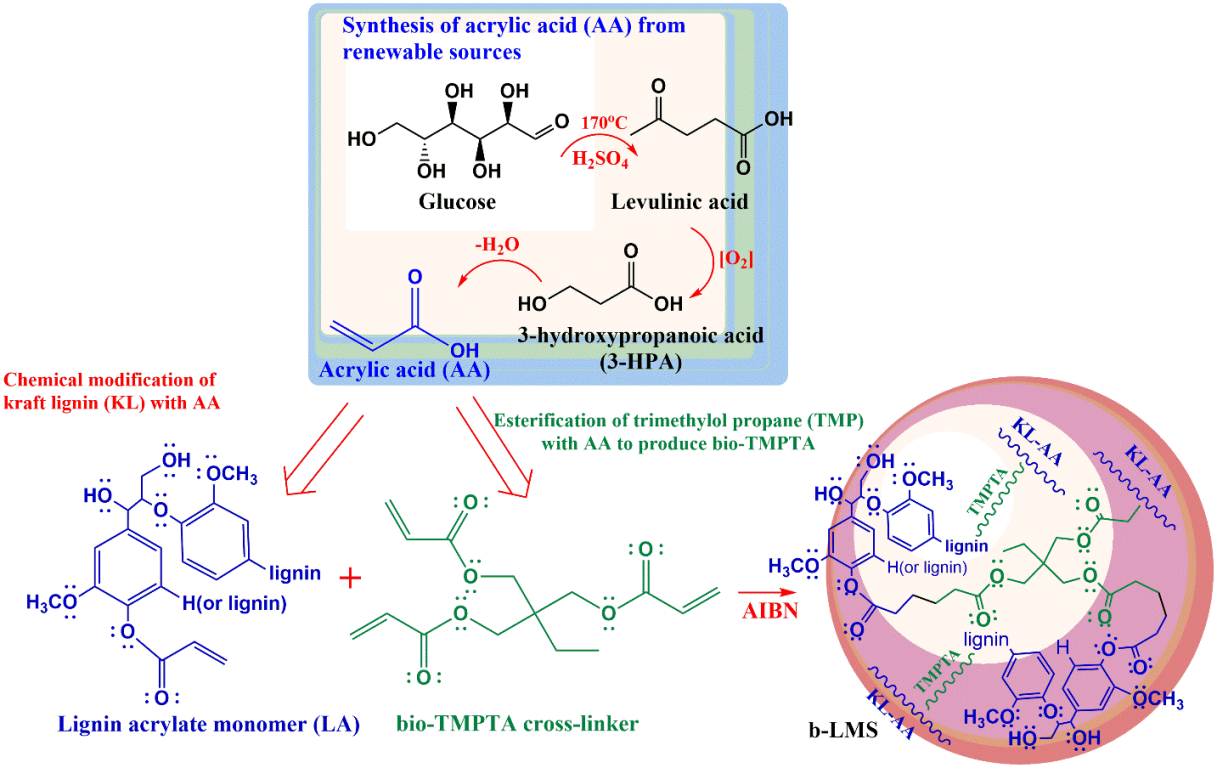

Figure 10: Synthesis of b-LMS microspheres [180]

4.2.6. b-LMS synthesis optimization-RSM design

Figure 11 graphic shows the developed technique for b-LMS synthesis, followed by an optimizing method, with changeable goal parameters such as a capacity for Malachite green adsorption against the bio-reactants ratio (bio-TMPTA; KfL-AA) vinyl bio-reactants and porogen content. The red region on the contour diagram corresponds to the greatest value of goal attributes. Table 2 provides the values range for chosen variables and experimental design, which consists of sixteen experimental runs with five repeats. Due of the large region with ideal qualities, point prediction using RSM software was used to identify optimal circumstances carefully. For experimental data fitting, a second-order equation was utilized. Table 3 provides the findings from statistical analysis and experimental design.[180].

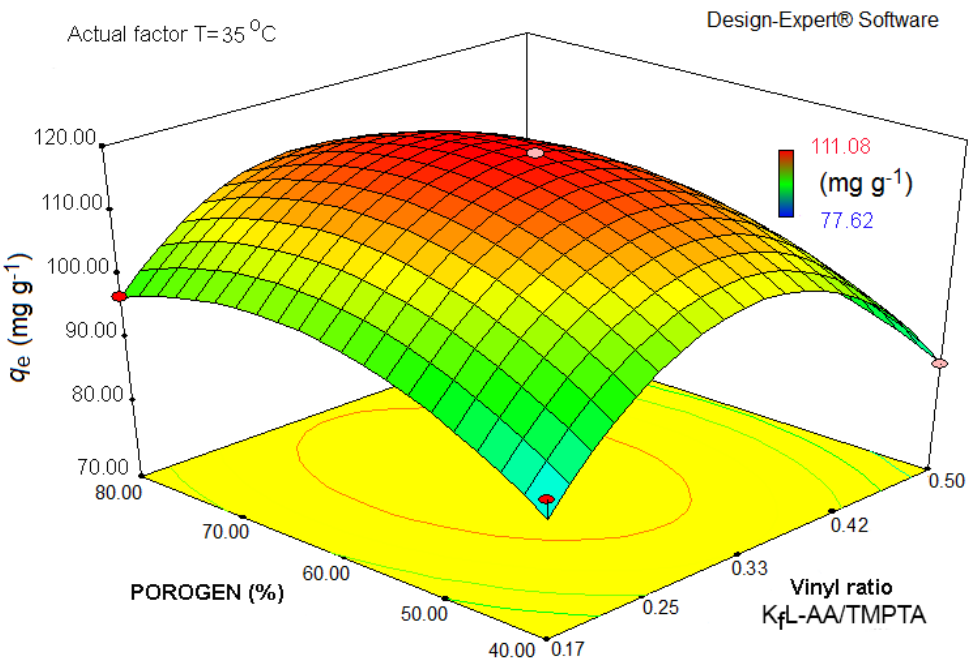

Figure 11. Diagrams for q_e of Malachite Green versus ratio of bio-TMPTA/KfL-AA content of porogen (1:1-2-ethylhexyl levulinate: triacetin ww%) [180]

Table 2. Box-Behnken design-RSM optimization model to optimize adsorbent synthesis with three numerical factors, three value levels, and five repetitions in the center point.

Run	A, POROGEN (%)	B, Ratio of KfL-AA/TMPTA	C, T (°C)	Response, MG removal capacity q_e (mg g^{-1})
1	60	0.33	35	110.92
2	60	0.33	35	111.08
3	80	0.33	25	95.13
4	60	0.5	25	85.13
5	60	0.33	35	110.82
6	60	0.17	45	83.96
7	60	0.5	45	77.61
8	40	0.5	35	86.49
9	40	0.33	25	87.58
10	40	0.17	35	89.49
11	80	0.17	35	95.26
12	80	0.33	45	92.70
13	60	0.33	35	111.02
14	40	0.33	45	89.65
15	60	0.17	25	84.75
16	60	0.33	35	110.66
17	80	0.5	35	83.22

Table 3. ANOVA results for Box-Behnken RSM design for adsorbent synthesis optimization

Source	Sum of Squares	df	Mean Square	F value	p-value	
					Prob > F	Significance
Model	**2192.447**	**9**	**243.6053**	**64.61967**	**< 0.0001**	**significant**
A – ratio of KfL-AA/TMPTA	55.1658	1	55.1658	14.63349	0.0065	
B – porogen (%)	21.42309	1	21.42309	5.682772	0.0486	
C - T	9.386513	1	9.386513	2.489902	0.1586	
AB	20.43718	1	20.43718	5.421245	0.0527	
AC	11.31808	1	11.31808	3.002277	0.1267	
BC	5.064975	1	5.064975	1.343555	0.2844	
A^2	992.2219	1	992.2219	263.2006	< 0.0001	
B^2	203.5101	1	203.5101	53.98388	0.0002	
C^2	679.3494	1	679.3494	180.2068	< 0.0001	
Residual	26.38882	7	3.769832			
Lack of Fit	26.38882	3	8.796274			
Pure Error	0	4	0			
Cor Total	2218.836	16				

**The F-value of 64.62 confirms the model's significance. If a ,,Prob>F'' values <0.05 model are significant (A, B, A2, B2, C2). Model is insignificant when,,Prob>F'' higher than 0.1000.*

Step-by-step achievement of desired function, such as the b-LMS maximum capacity, have a balance against materials geometry, porosity, and dimensional/mechanical stability to determine operational capability. It is necessary to achieve these qualities for a high-loading system to use b-LMS to achieve optimal adsorption performance. Table 4 showed some parameters such as porosity, hydroxyl, phenol group contents, and surface parameters, such as the pH_{pzc} of b-LMS produced using best method [180].

Table 4. Phenol, porosity and ^{-}OH content, pH_{pzc} of KfL, b-LMS, b-LMS-OSO_3H

Material/properties	Porosity	Phenol group mmol/g	Hydroxyl group mmol/g	pH_{PZC}	
Lignin (KfL)	-	3.8±0.12	3.2±0.13	6.23 [191]	
b-LMS	59	1.8±0.08	1.9±0.07	6.42	6.14
b-LMS-SO_3H	56	0.5±0.02	0.3±0.01[5]	1.28	

The concentration trend of hydroxyl and phenols groups, KfL vs b-LMS indicates the adsorbent production success with phenol and hydroxyl groups losings. The adsorption properties of b-LMS were affected by the consumption of these specific phenolic groups throughout the transition to acrylate ester. The precursors of vinyl reactivity when used as cross-linking reactants in the synthesis of b-LMS, offer a sufficient amount of surface aromatic groups for efficient dye adsorption. Values for the iodine number of bio-TMPTA and KfL-AA (146 and 98, respectively) before and after synthesis of b-LMS demonstrated effective computation of system reactivity and b-LMS synthesis optimization method. In addition, porosity measurement and image analysis suggest that the synthesized b-LMS spheres have a high porosity, with pore sizes ranged from sub-micrometer to nanoscale size [180]. Figure 10 depicts the comprehensive procedure for b-LMS synthesis. The obtained

b-LMS sample was used to compare sorption performance properties, with quantum chemical computations providing support. According to the pKa, the lowest pKa value is 9.10 for a phenolic group from lignin, meaning that at pH 7 or below, the adsorbent surface will be neutral. Distribution of microspecies diagrams reveals that at pH 7, Malachite Green is present as the cation (+1 charge), while Tartrazine is predominantly in tri-anion and Methyl Red is predominantly in mono-anion form. These different charges form were used in the theoretical modeling of adsorbent/dye interaction to investigate the adsorptive process [180].

4.3. Characterization of prepared adsorbents

4.3.1. BET analysis

Barret-Joyner-Halenda (BJH) models analyzed the textural properties of b-LMS and LMS-DEGDMA samples. The well-developed distribution of pores gives the large surfece area required to achieve a high dye adsorption rate. The results are given in Table 5. The adsorption/desorption isotherm is dictated by significant capillary-condensation hysteresis and may belong to the type III mesoporous materials class. The BET analysis showed that the S_{bet} for b-LMS is 69.4 m^2/g, with S_{meso} being 69.7. m^2/g, which means that the sample is mesoporous. [180].

The BET results for LMS-DEGDMA microspheres showed that they have S_{bet} of 39 m^2/g; with ε_p=62 porosity; D_m is 12 nm, and the V_{total} of 0.14 cm^3/g. Due to their extensively cross-linked structure, DEGDMA-modified lignin microspheres don't dissolve in water and are suitable, hard, and robust [181].

Table 5: Textural properties of b-LMS and LMS-DEGDMA

Samples	S_{bet} m^2/g	S_{meso} m^2/g	V_{total}, cm^3/g	$V_{micro,}$ cm^3/g	D_m, nm
b-LMS	69.4	69.7	0.1392	0.0015	9.83
LMS-DEGDMA	36.9	-	0.1431	0.1386	12.11

4.3.2. NMR analysis

Results of the NMR analysis are showed in Figures 12 and 13-1. Observed signals in the range δH 0.80 - 1.83 for non-acrylate kraft lignin were ascribed to aliphatic methylene and methyl protons (Figure 12a). Further, signals in the range δH 3.24 - 4.02 can ascribe to heterogenous methoxyl ($^-OCH_3$) overlapping with aliphatic hydroxyl groups [192]. Also, in this area, several peaks at δH 3.45 can be ascribed to (Hα)-α protons in - aryl ethers (β-O-*4*) (substructure (II)) (Figure 14), whereas signals ranged from δH 3.55 to 3.85 may attribute to (Hγ)-γ protons in α-O-γ linkage which containing β-β resinol substructure [192–194]. In some regions of the KfL-AA spectrum presented in Figure 13a, the intensity, shape and position of peaks obtained from those spectra of kraft lignin show some difference [180]. Firstly, evaluating signals at δH 1.10, 1.25, and 1.83, several aliphatic group signals are weakened/disappeared and somewhat shifted relative to lignin's NMR spectrum. Secondly, the chemical shift of aliphatic ^-OH and oxygenated methyl groups is moved to the area between δH 3.16 and 3.84. The intensity of the singlet at δH 3.26 has diminished, and an upfield shift to δH 3.16 has

been observed. In addition, the strength of signal at δH 3.56 in the lignin spectrum decreases dramatically (Figure 12a), resulting in the appearance of a new doublet at δH 3.47 (Figure 13a). Two strong signals in Kf spectra at δH 3.85 and 3.72 disappeared simultaneously with wide signals at δH 3.67. During the acrylation process, a probable alternative mode of hydrogen/interaction bonding between various -OH and -OCH_3 monomer units, which were coupled in a complex lignin structure, may account for this alteration [180]. Thirdly, the extra wide signal at δH 4.70 in the spectra of KfL-AA might be attributed to H of the resinol substructure of lignin and δH in -arylethers (*β-O-4*) [193]. Three doublets of doublets at δH 5.44 (J_1 = 10.3, J_2 = 1.8 Hz), 5.84 (J_1 =17.1, J_2 = 1.8 Hz), and δH 5.95 (J_1 =17.1, J_2 = 10.3 Hz) correspond to vinyl-acryloyl moieties groups connected with aliphatic -OH and phenyl groups in kraft lignin. (Figure 13a) [180]. In addition, the acrylation of kraft lignin broadens the signals from lignin aromatic protons in region δH 6.50-7.40 (Figures 1a and 13-1a). The protons of phennolic groups intensity in KfL, found at δH 8.37 in lignin decreased and moved upfield to δH 8.28 following acrylation (Figure 12a) [180] .These fundings validated the optimization of aliphatic -OH and phenolic groups to obtain the capability of residual groups (Table 4) for application in the removal of dyes [180].

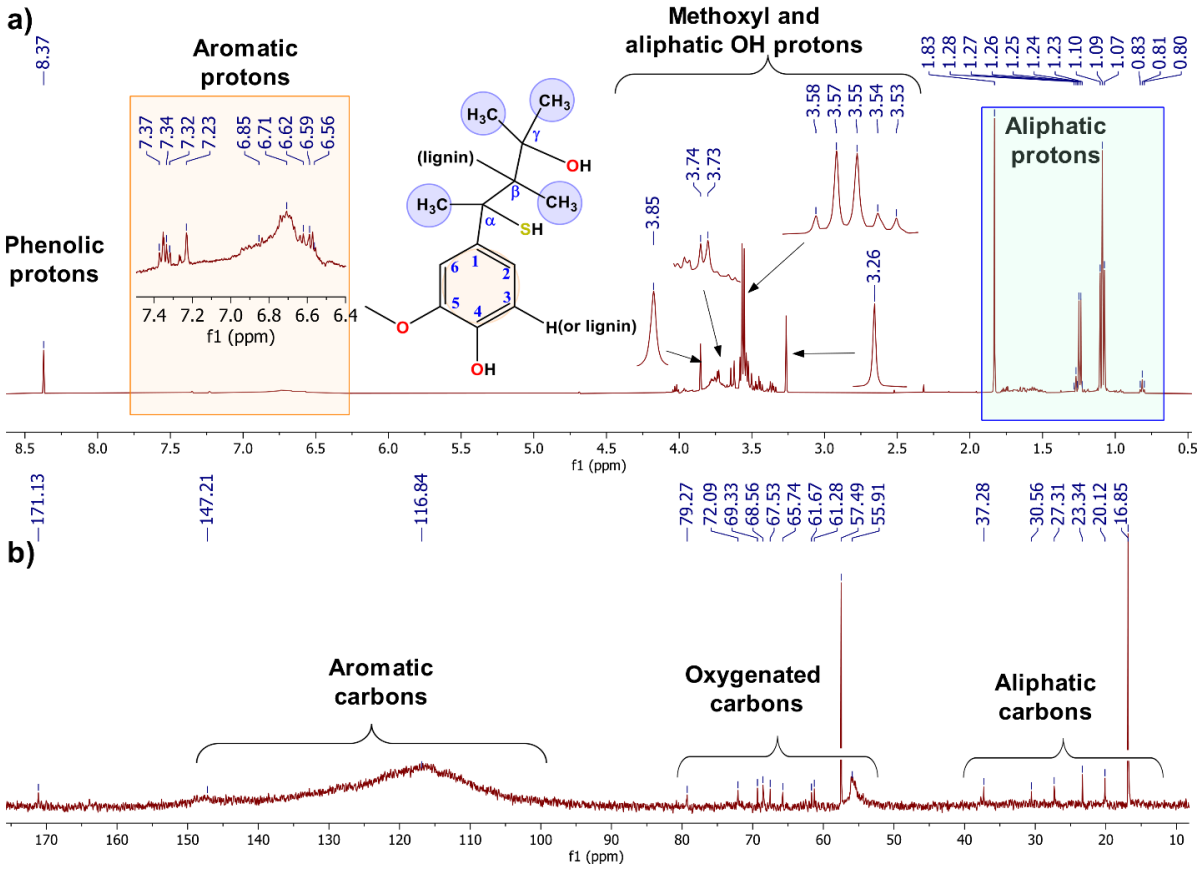

Figure 12. a) ^{1}H NMR, b) ^{13}C NMR spectra of KfL [180]

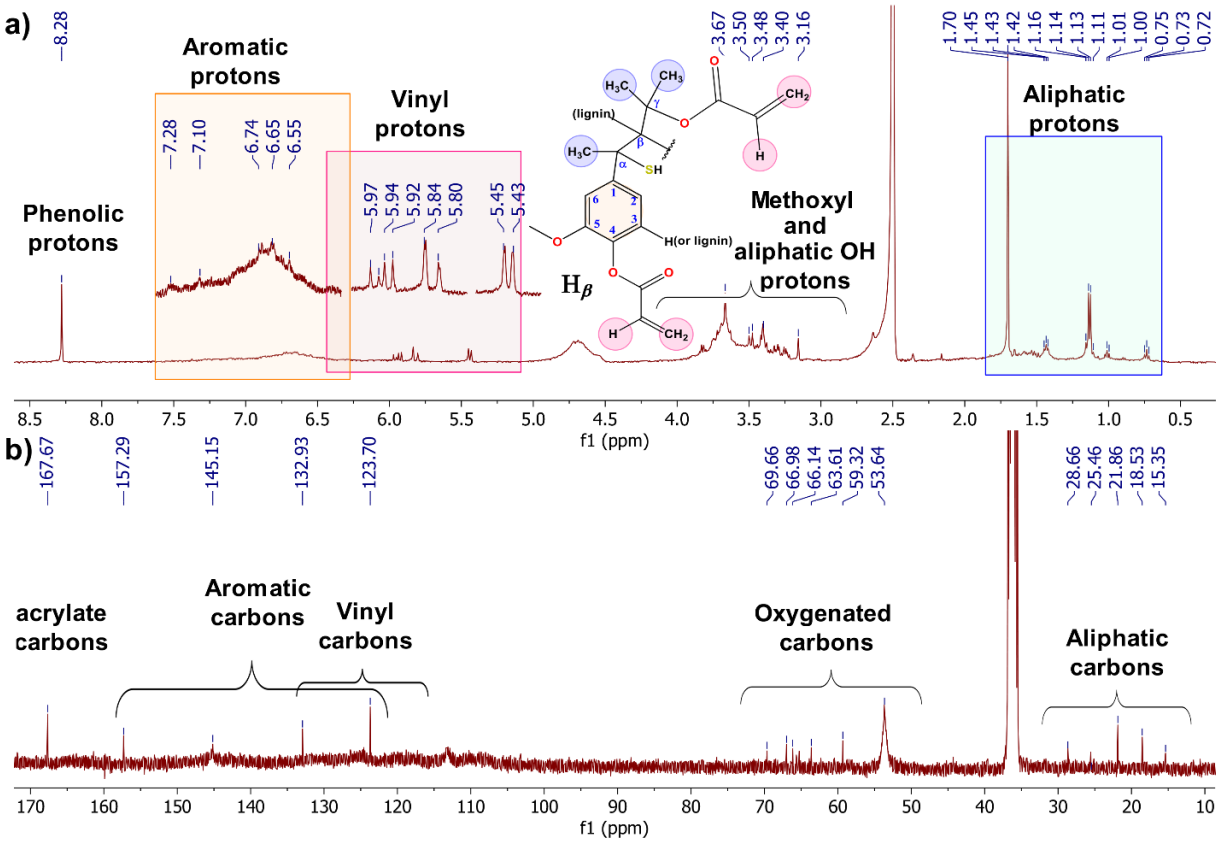

Figure 13: a) ^{1}H NMR b) ^{13}C NMR spectra of KfL-AA [180]

Figure 12b presents results of the ^{13}C NMR spectra of kraft lignin. Spectrum displays signals at δ_C 16.8, 20.1, 23.3, 27.3, 30.6, and 37.3 that correspond to C_α, C_β, and C_γ carbons present in sideways chains *β-O-4* and/or, *β- β* of an structural aliphatic part. Signal at δ_C 20.1 seems to be assigned to the acetate methyl group in the lignin structure [192]. After acrylation, the strength of signals from aliphatic cabons, δ_C 15.4 to δ_C 28.3 decreased and shifted upfield (Figure 13b). At δ_C 55.9 and 57.5, two signals in this area are from aromatic and aliphatic methoxy groups, respectively. In addition, γ_C carbons were found between δ_C 61.3-61.7 in *β-O-4*, as well as non-oxygenated β_C and γ_C cabons in KfL between δ_C 65.7 and 67.5. Figure 12b present the signals from Cα-OH, C_β, and C_γ carbons in the *β-O-4*, *α-O-γ*, *β-β* substructures and resinol[192,195,196] [180]. In acrylated lignin, methoxy group signals, δ_C 63.6-69.7 and δ_C 53.5-59.3, were shifted up and decreased. The weak signal of aromatic hydrocarbons at δ_C 147.2 are assigned to C_3 and C_3/C_5 etherified carbons in S and G units, linked by *β-O-4*. As illustrated in Figure 13b, acrylation product reflects novel signals for vinyl carbons at δ_C 123.7 and 132.9, which overlapped with C1/C4 and C2 carbons of H, S, and G phenyl rings. Signals at δ_C 113.1, 145.2, and 157.3 are from the phenyl ring C6, the C_3 and C_3/C_5 etherified phenyl carbons. According to the intensities of signals at δ_C 163.9 and 171.1, conjugated ester groups are present in non-acrylated lignin [180].

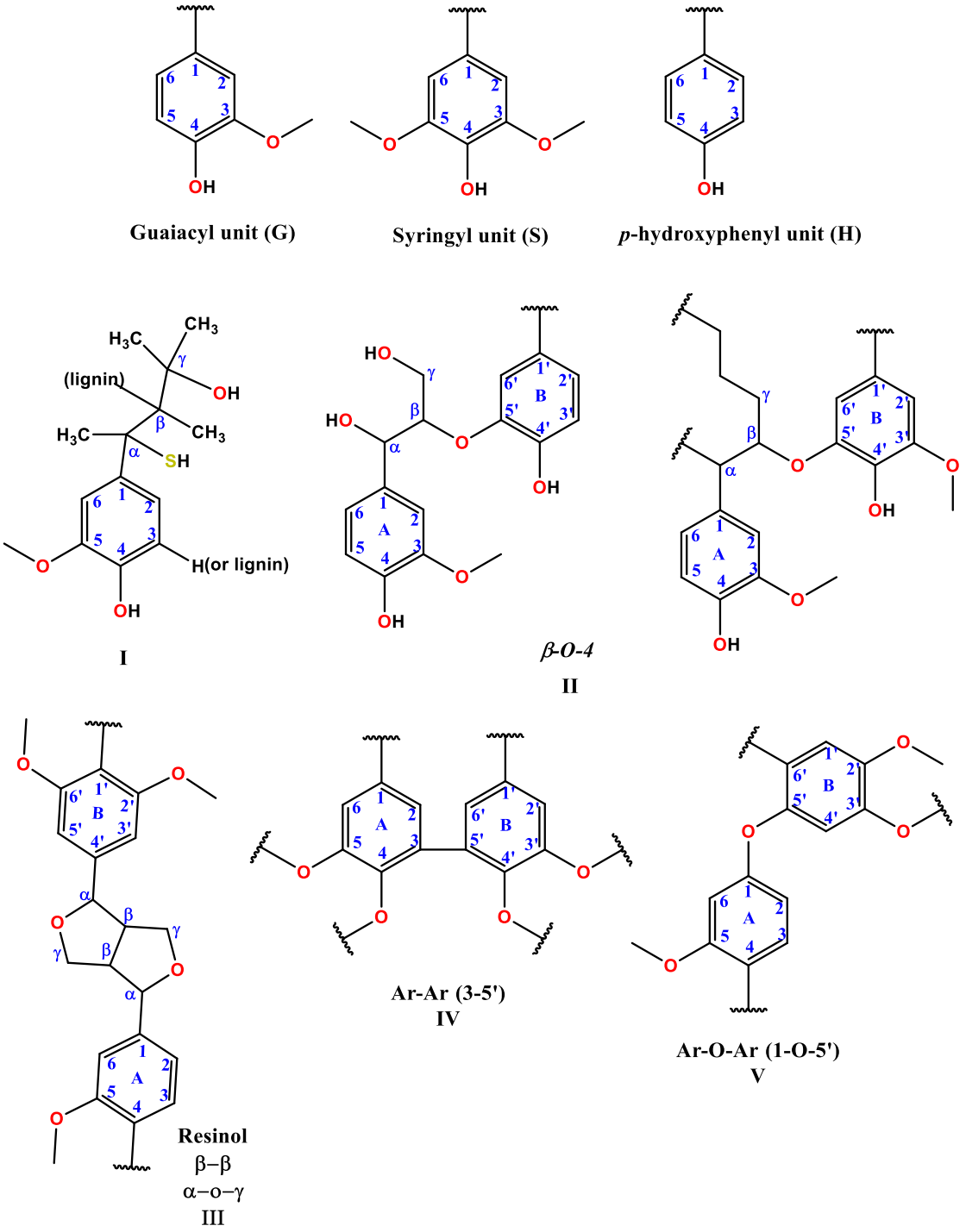

Figure 14. Kraft lignin substructures used in NMR

4.3.3. Thermogravimetric analysis

Figure 15 presents the dTG and TGA curves of KfL-AA, lignin, b-LMS, while Table 6 displays the thermal stability data (5% and 50% loss of mass). All samples lose moisture and absorb gases at temperatures below 200 ^{0}C (stage I - endothermic reaction) [197]. Due to its hydrophobic character, the b-LMS sample exhibits loss of lowest mass and maximum thermal stability during the initial phase of disintegration [180].The KfL sample exhibits the greatest weight loss due to its abundance of aliphatic, phenolic, or -OH groups and strong moisture removal affinity, and results presents in Table 6. Kraft lignin acrylication results in decreasing hydroxyl functionality and a decrease its ability to absorb moisture. Moreover, lignin pyrolysis occurs at greater temperatures, which marks the 2nd phase and tracked two exothermic reaction processes, resulting in two signals on the DTG curve; firstl at 263 °C and the second at 349 °C. At 263 °C, lignin surface starts to carbonize and the aliphatic lignin groups begin to separate, while the aromatic lignin structure separates and carbonizes at 349 °C. If observing the b-LMS sample, this peak moves to a higher temperature. Copolymerization of lignin with bio-TMPTA results in the greatest weight reduction at 700°C [180].

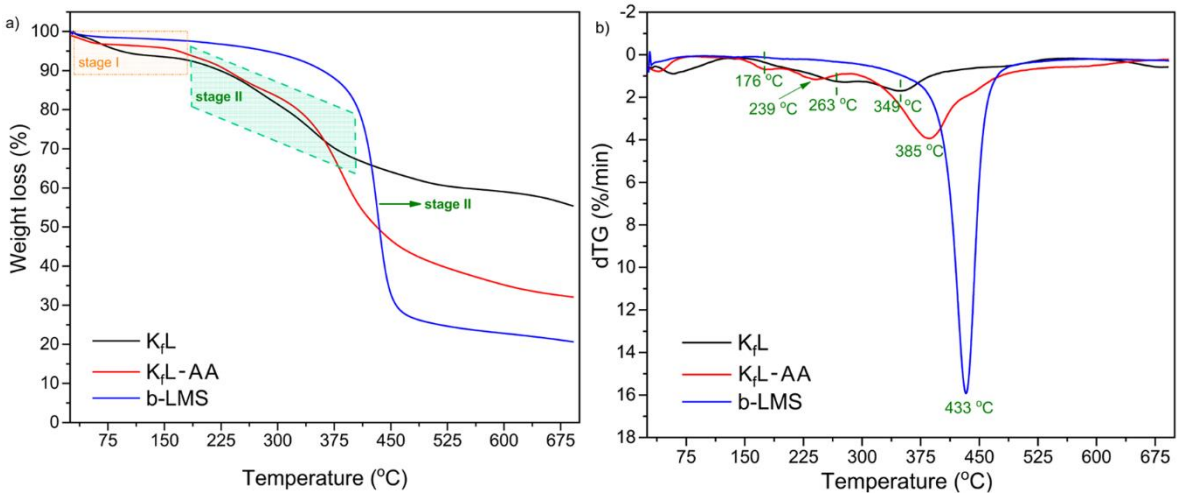

Figure 15: TGA and dTG of KfL-AA, KfL, b-LMS [180]

Table 6: Temperatures of 5% and 50 % of weight loss of l KfL, KfL-AA and b-LMS

Sample	$T_{5\%}$, °C	$T_{50\%}$, °C	Residue at 700 °C, %
KfL	92.1	-	58.36
KfL-AA	168.1	434.8	32.09
b-LMS	285.0	434.8	20.62

TGA analysis of LMS-DEGDMA also confirmed its production success. TGA and dTG curves of LMS-DEGDMA and KfL are shown in Figure 15. Results of temperatures 5 % and 50 % loss of mass are reported in Table 6. All samples lose weight at temperatures below 200 °C due to water's evaporation and the gas absorption (stage I - endothermic reaction). The lignin sample shows the hogher weight loss during the initial stage of decomposition, which may be attributed to its strong tendency for absorbing moisture (Table 7) [181]. In addition, lignin pyrolysis takes place at higher temperatures (phase II - exothermic processes) and follows two pathways that result in the production of two signals on the dTG curve; first at 263 °C and second at 349 °C. At 263 °C, aliphatic groups from lignin begin to separate, and the lignin surface starts it to carbonized, while the aromatic lignin

structure begins to separate and carbonize at 349 °C. After lignin copolymerization with DEGDMA, less thermally stable structures with more weight loss at 700^0C are produced (Table 7) [181].

Table 7. Temperatures of 5 % and 50 % of weight loss of lignin, LMS-DEGDMA and LMS-DEGDMA with immobilized laccase.

Sample	$T_{5\%,}$ °C	$T_{50\%,}$ °C	Residue at 700 °C, %
Kraft-lignin (KfL)	84.5	-	58.36
LMS-DEGDMA	255.4	430.6	14.36
LMS-DEGDMA-laccase	202.0	409.3	20.67

4.3.4. Point of zero charge analysis (pH_{pzc}), porosity, phenol and hydroxyl groups content

Results for pH_{PZC} analysis, porosity, phenol, and hydroxyl group content are presented in Table 8. The obtained results revealed a very similar pH_{pzc} value for all tested samples. Hydroxyl group content ranges from 1.9 for LMS-DEGDMA to 3.2 for KfL. The amount of phenol group ranges from 2.0 for LMS-DEGDMA to 3.8 for KfL [180,181].

Table 8. Porosity and quantification values for certain organic groups from analyzed samples

Material/properties	Porosity	Phenol group mmol g^{-1} of support	Hydroxyl group mmol/g of support	pH_{PZC}
Lignin (KfL)	-	3.8	3.2	6.3
LMS-DEGDMA	62	2.0	1.9	6.2
b-LMS	-	-	-	6.23

4.3.5. FT-IR and Raman analysis

Figure 16a showed the FTIR of the bio-TMPTA and KfL-AA sample used in the copolymerization procedure to make extremely porous b-LMS microspheres. The peak at 2937, 2969, and 2887 cm^{-1} of KfL-AA, bio-TMPTA, and copolymerized microspheres are attributed to stretching asymmetric vibrations of methylene and methyl groups. Signal at 1720 cm^{-1} from bio-TMPTA is attributed to the stretching vibration of the carbonyl groups formed during the esterification process of bio-AA with TMPTA. All lignin-based samples (KfL, KfL-AA, and b-LMS) have the following phenolic/aromatic bonds: the peaks between 1390-1461 cm^{-1} appear as a increment of aromatic skeletal multiple vibrations of syringyl and guaiacyl units, with highest intensity signal at 1418 cm^{-1} [198]; the aliphatic C-H deformation vibration at 1460 cm^{-1}; the O-H signal from phenol near 1398 cm^{-1} which is overlapped with aliphatic C–H signal; and the signal at 1590 cm^{-1} are assigned to vinyl and aromatic skeletal vibration. However, the signals at 3431 and 3468 cm^{-1} are ascribed to phenolic and hydroxyl group. Signals at 1185, 1142/1152, and 1029/1057 cm^{-1} are assigned to the asymetric stretcching vibrations of C-O bonds and C-O-C rings from alcohols or phenols. The peak of the carbonyl ester group at 1733 cm^{-1} confirms the presence of lignin treated groups with bio-acrylic acid. The signal at 1728 cm^{-1} are attributed to carbonyl stretching vibrations [181] in the b-LMS. The strong band at 807

cm^{-1} in the bio-based TMPTA and KfL-AA spectra indicates the precence of vinyl acrylate =C-H deformation vibration [180].

Raman spectra of investigated samples are presented in Figure 16b. By the literature searching, Raman bands of kraft lignin have been assigned, and here we are validated aromatic/phenolic structure in all lignin-containing samples [180]. Aromatic C-H deformation vibrations are detected at lower Raman shift levels, between 750 and 900 cm^{-1}, while C-H deformation vibrations in-plane are observed at 976 cm^{-1}. The signal at 1092 cm^{-1} is attributed to C-O bonds. The large signal at 1210 cm^{-1} originates from C-C, C-O, and C=O vibrations bonds. In the region between 1340 and 1575 cm^{-1}, symmetric and asymmetric aryl ring vibrations are detected. The signal at 1407 cm^{-1} can assigned to kraft lignin aromatic skeleton bending vibration of the CH_3O^- group. Lower intensity of C=O and C=C stretching vibrations of sinapyl and coniferyl aromatic rings in the structure of lignin detected at 1640 and 1663 cm^{-1} as Raman signals. The chemical modification of lignin with bio-AA and the copolymerization of KfL-AA with bio-TMPTA leads to a lower intensity of signals. In acrylate system, the signals detected at 1644 cm^{-1} and 1730 cm^{-1} in the spectra of bio-TMPTA, KfL, and KfL-AA are attributed to vinyl C=C deformation and ester carbonyl stretching vibrations. However, observed Raman and FTIR spectra verified the correct copolymerisation of acryl-functionalized lignin with bio-TMPTA, allowing synthesis of b-LMS and conversion of phenolic -OH groups to acrylate esters [180].

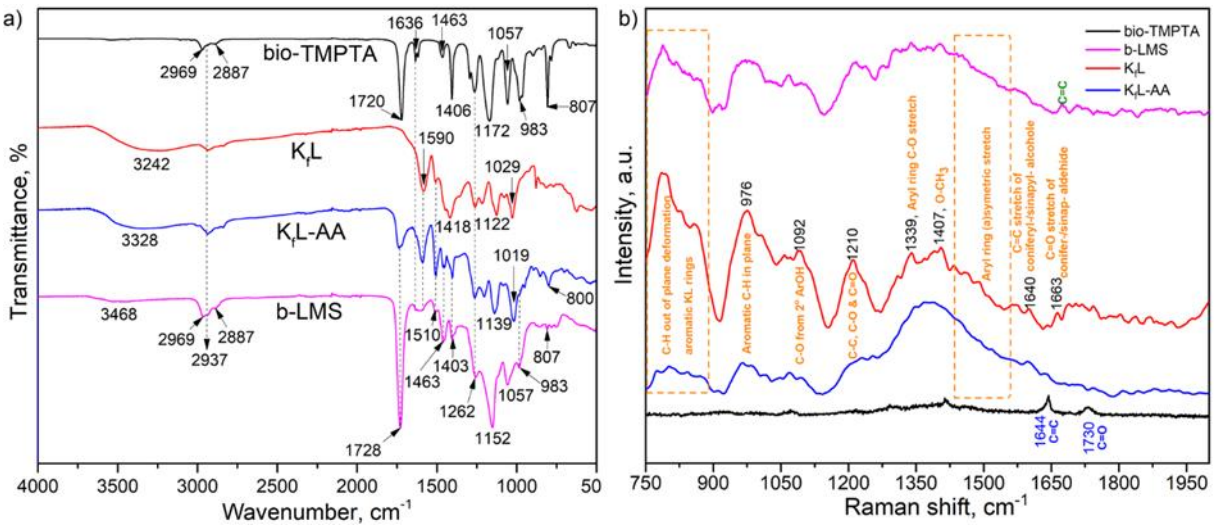

Figure 16: a) FT-IR b) Raman spectra of Lignin, TMPTA KfL-AA, KfL, and b-LMS [180]

Figure 17 showed the FTIR spectra of KfL, KfL-AA, LMS-DEGDMA, Laccase and Laccase-LMS-DEGDMA to confirm formation of acrylic modified kraft lignin (KfL-AA) and success of polymerization process between diethylene glycol dimethacrylate (DEGDMA) and the surface of KfL-AA. The peaks at 2969, 2937 and 2887 cm^{-1}, of all samples derived from the methylene or methyl group's symmetric and asymmetric stretching vibration (Figure 17a) [199]. The bonds at 1728 and 1732 cm^{-1}, from spectra of LMS-DEGDMA and KfL-AA before and after laccase immobilization, derived from carbonyl group stretching vibration. Phenolic and aromatic bands vibrations are present in the spectra of all samples which contain lignin [181]. Skeletal multiple vibrations of syringyl and guaiacyl units are present to contribute to the band between 1395 and 1457 cm^{-1} [199]. The phenolic O-H peak occurs at around 1395 cm^{-1}. Signal at 1257 cm^{-1} results from the in-plane vibration in guaiacyl rings. The lower wavelength bands detected between 750 and 985 cm^{-1} are acribed to aromatic C-H bond deformation vibrations into rings [181]. In addition, a wide band

between 3250 and 3450 cm^{-1} was assigned to phenolic and/or hydroxyl -OH vibrations. [25] At 1626 cm^{-1}, the -OH bending vibration is present. The signals at 1152 or 1135 cm^{-1} correspond to C-O-C ring asymmetric stretching vibrations and C-O bonds in phenols or alcohols, as well as =C-H deformation vibrations in vinyl acrylate system [181].

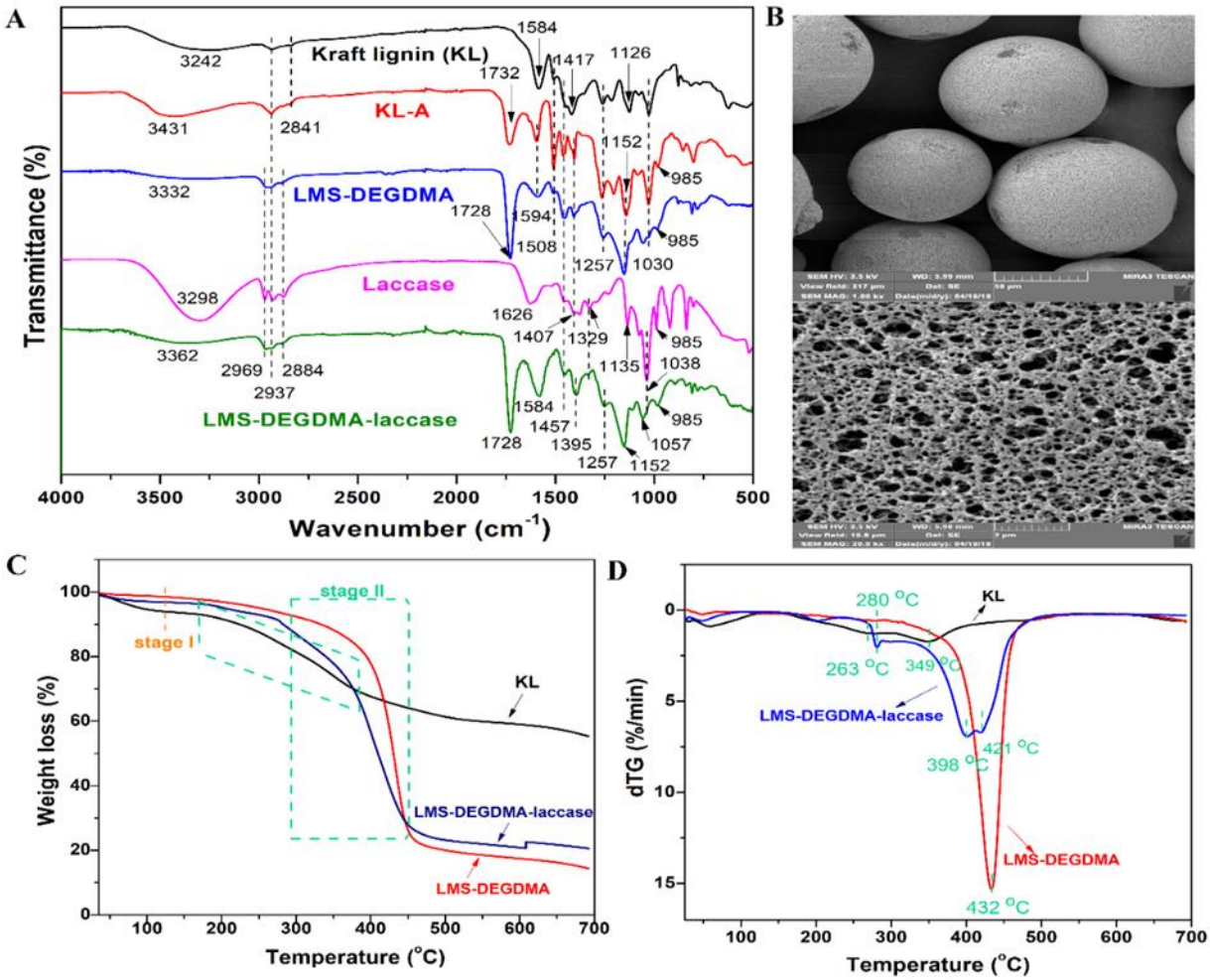

Figure 17. (A) FT-IR spectra and (B) FE-SEM images of lignin-based microspheres (C) TGA and (D) dTG curves of KfL, LMS-DEGDMA and LMS-DEGDMA-laccase [181]

4.3.6. X-ray photoelectron spectroscopy study

Figure 18 showed the XPS survey spectra of investigated samples (KfL, KfL-AA and b-LMS) while Table 9 showed the elemental composition of samples. After chemical modification of KfL with AA, the amount of Na and S decreases, however Na 1s is detected in b-LMS. The modified KfL has a higher C/O ratio than the raw KfL and KfL-AA copolymerized with TMPTA. The XPS study verifies structural alterations, the successful modification of KfL, and the copolymerization of KfL-AA with bio-TMPTA. Figure 18 shows the XPS spectra of C 1s and O 1s, of KfL, KfL-AA and b-LMS. [180].

The signal at 284.8 eV found in all samples (Figure 19a) is assigned to carbon in C-H and C-C bonds of bio-TMPTA and lignin. The signal at 286.2 eV corresponds to C-O bond or a carbon atom bonded with oxygen atom that is not carbonyl through σ bonds. This is verified by the O 1s spectra (Figure 19b), where the O-C signal is more prominent in the identical analyzed samples than in raw KfL[180]. Signals derived from 288.2-288.9 eV region are predominantly from the carbon from inside the O=C-

OH, Ph-C=O, and Ph=O groups. The acquired spectra reveal the fraction of C=O and C-O bonds rises following KfL modification, validating the efficacy of the functionalization approach. In addition, the peak corresponding to C=O group is notably apparent in the b-LMS sample because copolymerization of KfL-AA and bio-TMPTA. The O 1s spectra deconvolution showed two peaks, one corresponding to the oxygen atom, first in C-O and second at C=O bonds [180].

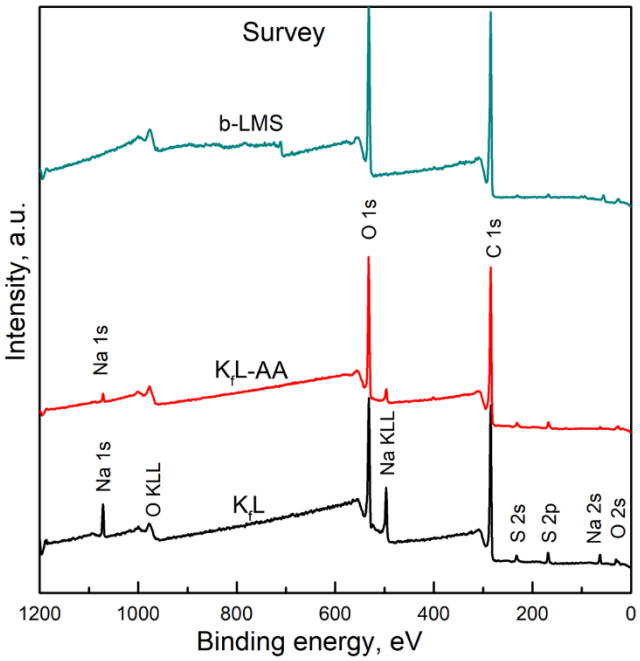

Figure 18. The survey XPS spectra of the raw KfL, KfL-AA, and b-LMS

Table 9. Elemental composition calculated from the XPS survey spectra

Element/sample	KfL	KfL-AA	b-LMS
C (at%)	73.27	77.11	77.12
O (at%)	20.71	19.96	22.50
Na (at%)	3.69	0.70	-
S (at%)	2.33	1.78	0.38
Si (at%)	-	0.45	-
C/O	3.54	3.86	3.43

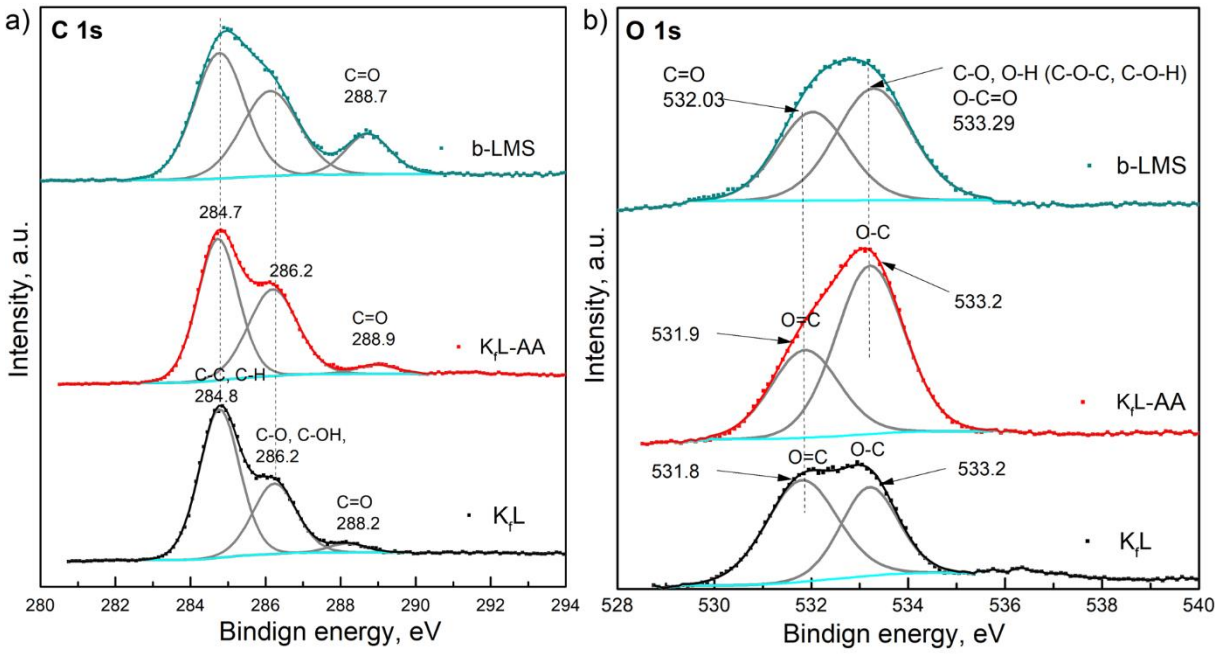

Figure 19. The XPS s spectra of: a) C 1s; b) O1s of raw KfL-AA, KfL, and b-LMS [180]

4.3.7. Scaning Electron Microscopy (SEM) analysis

Figure 20 represents the copolymerization of KfL-AA and bio-TMPTA, which produces an adsorbent with a spherical shape; its pore diameter is 253±42 μm, and they have a very porous interior and surface. The surface of b-LMS has linked open pores, making it more conducive to the diffusional transport of dye to adsorption site. This fact showed good agreement with Image analysis [180].

The SEM analysis was also used to investigate LMS-DEGDMA microsphere surface morphology because the morphological and physical features of the support have directly impact the enzymatic properties after immobilization. As shown in FE-SEM photos, the LMS-DEGDMA has a spherical shape, homogenous morphology, and a high count of pores. With pore dimensions ranging from 4-20 nm and a limited pore size distribution, LMS-DEGDMA microspheres might be regarded as highly organized [181].

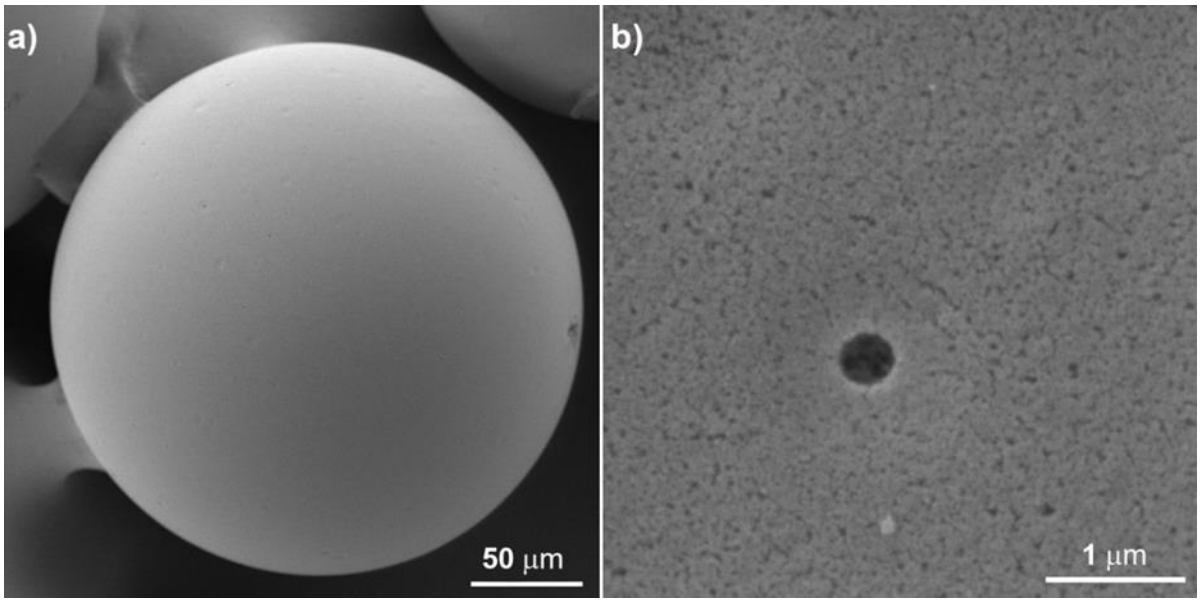

Figure 20. FE-SEM photographs b-LMS with magnification: a) 800x b) 50.000x [180]

4.4. Laccase Novozyme® 51003 immobilization on produced LMS-DEGDMA

In this work, after the successful synthesis of LMS-DEGDMA microspheres, it has been decided to examine the possibility of these microspheres being used as support for the immobilization of laccase produced by *Myceliophthora thermophila* stain and then expressed in *Aspergillus oryzae*. Structure of laccase Novozym 51003® is shown on Scheme 2. It should be noted that he pH optima for this laccase used in this study was around pH 6.8 determined in reaction with commercial substrate ABTS. Isoelectric point of Novozym 51003® laccase has the value of pI 4.0. Although, several studies was published on immobilization of laccases [200], the combination of this specific commercial laccase preparation (Novozym 51003®) and lignin based microspheres, as far as we know, has never before been investigated for possible application for wastewater treatment.

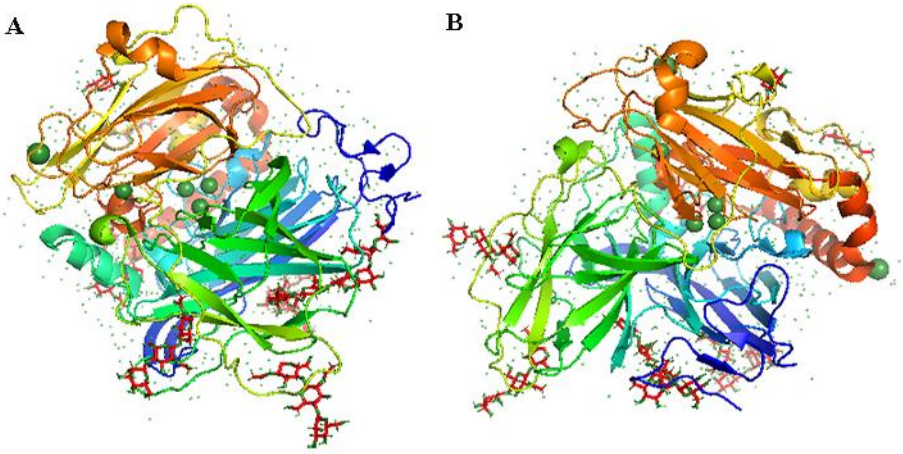

Scheme 2: The 3D structure of laccase Novozym 51003® (PDB number 6F5K) obtained through PyMOL

The LMS-DEGDMA preliminary screening for possible use as support for imobilization of enzyme was performed based on parameters that describe the immobilization process effectiveness: the protein immobilization yield (%), protein loading (mg g^{-1}), activity immobilization yield (%) and the catalytic activity of immobilisation enzyme (IU g^{-1}). As part of the screening process, the immobilization is carried out at a pH of 4.0-7.5 (Figure 21). It may be expected that laccase attachement on LMS-DEGDMA happens through physisorption *via* hydrogen bonding, electrostatic interaction, Van der Waals interaction, whereas determined the concentration of total and phenolic -OH groups on support surface, it has been between 2 and 1.9 mmol g^{-1} (Table 8) [181].

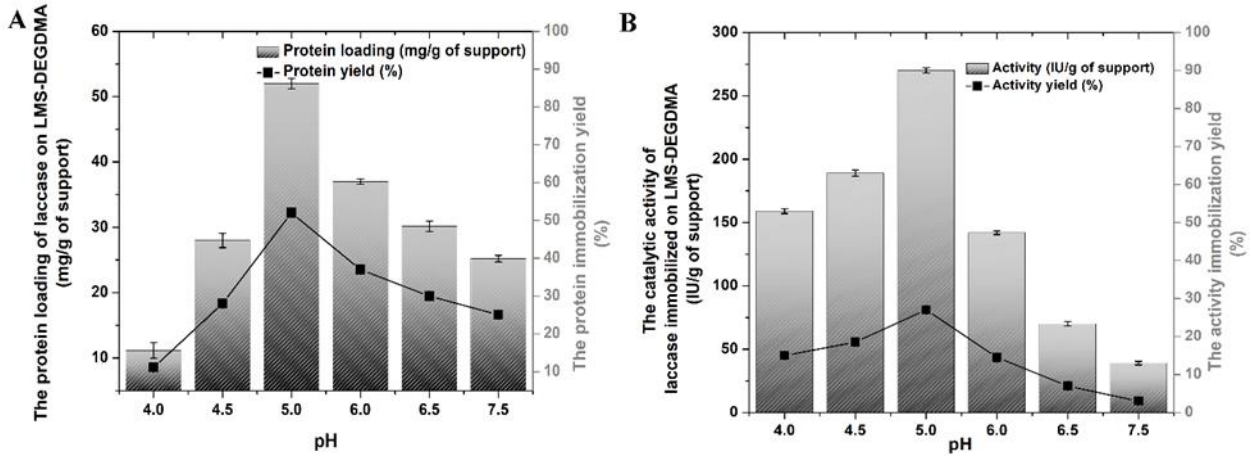

Figure 21. Determination of optimal pH for laccase imobilization on LMS-DEGDMA Experimental conditions are: C_i for enzyme 100 mg g^{-1}; time 2 h [181]

The total charge on the enzyme surface and created lignin-based microspheres surface may change when the pH value of buffer are varied, affecting the immobilization process's effectiveness. The maximum protein yield (52 %) and loading (52 mg g^{-1}) are obtained when immobilization is conducted at pH 5.0 (Figure 21). However, even a minor drop or rise in pH results in a significant decrease in these two parameters. The attractive forces between enzyme and microspheres emerge when their net charges are in opposition, which occurs at pH value between the pH_{pzc} of LMS-DEGDMA (6.2) and the laccase isoelectric point of (pI=4.0) leading to ideal pH for immobilization of 5.0. The reduction in the immobilization efficacy on LMS-DEGDMA over pH 5.0 is related to the creation of repulsive forces between support and enzyme as a consequence of their equal net charges [181].

With respect to the obtained results for catalytic activity and activity immobilization yield, it can be concluded whether or not the enzyme is bound in an active shape. The maximum activity yield (27 %) and catalytic activity (265 IU g^{-1}) of immobilized preparation were accomplished at pH 5.0, showed that the bonded enzyme onto LMS-DEGDMA in an active conformation, and that the quantity of attached enzyme per g of support was appropriate (52 mg g^{-1} of support). In summary a pH value of 5.0 is ideal for laccase immobilization onto LMS-DEGDMA [181].

4.5. Laccase immobilization on LMS-DEGDMA and its catalytic properties

The immobilized laccase activity on LMS-DEGDMA reaches a maximum (283 IU/g) as the initial enzyme concentration (C_i) rises to 200 mg g^{-1} (Figure 22). The catalytic activity reduced 2-times when the offered enzyme concentration (C_i) was 1000 mg g^{-1} of support (Figure 22A). LMS-DEGDMA-laccase displayed the lower activity of 104 IU g^{-1} at the highest offered enzyme concentration. Despite the fact that the maximal protein loading was acquired at all tested C_i within 30 minutes, the peak of catalytic activity was not reached for 1-2 hours. However, the specific activity and immobilization yield (%) of immobilized laccase (Figure 22B) revealed the maximal specific activity of 6.42 IU mg^{-1} of proteins, and it was derived when immobilization is carried out at C_i of the enzyme was 55 mg g^{-1} of support. This obtained value indicates that a high yield of attached enzymes occupies an active conformation, resulting in a 45 % activity yield (Figure 22B). The specific activity and lowest activity immobilization yield were reached at maximal C_i (1000 mg g^{-1}). The specific activity of lignin-based microspheres whose laccase loading was increased 28 - 424 mg/g decreased by around 95%. Inconsistency between catalytic activity of immobilized enzyme (Figure 22A) and protein loading (Figure 22B) at protein loadings greater than 200 mg g^{-1} may be due to enzyme allocation on a support surface; orientation of occupied enzyme after immobilization, enzyme structural changes, and a various microenvironment within the pores compared to bulk.[201,202] [181].

According to all of the findings, it was determined that laccase immobilization onto LMS-DEGDMA exposed the best features when immobilization process is conducted at pH 5.0 and the initial enzyme concentration of 100 mg g^{-1} for 1h (protein and activity immobilization yield of 70% and 27% respectively, and specific activity of 4.9 IU mg^{-1}) [181].

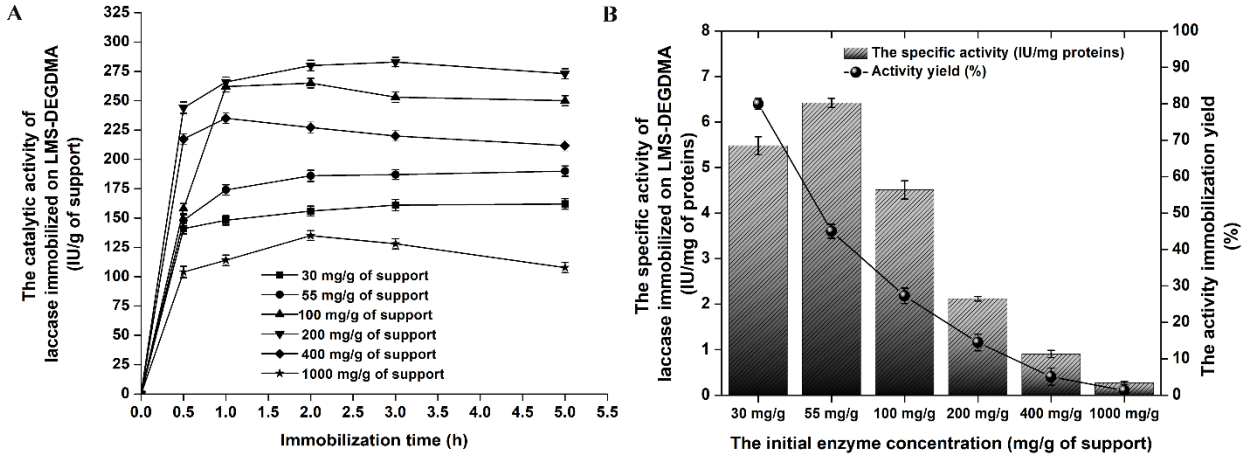

Figure 22**:** (A) Changes in the catalytic activity of LMS-DEGDMA-laccase during the time (B) The activity immobilization yields and specific activity (IU mg^{-1} proteins) for different offered protein concentration (in %, and for immobilization time 1h) [181]

4.6. Degradation of dye with LMS-DEGDMA-laccase

Dye effluent from the plastic, printing, pharmaceuticals, textile, paper, and sectors is one of the hardest to treat among industrial wastewaters. By releasing dyes into the environment, thus staying in the soil and water for an extended period of time, posing a threat to plant and human life. A low quantity of dye in water (10-50 mg L^{-1}) is very toxic and noticeable. Laccase's ability for degradation of phenolic compounds makes it a suitable enzyme for dye decolorization in wastewater treatment. In addition, using immobilized laccase preparations in the dye decolorization may be more beneficial

to wastewater treatment since treatment with immobilized enzyme will be environmentally friendly, cost-effective, and generate fewer sludge [181].

After optimizing the immobilization method, the LMS-DEGDMA-laccase preparation was used for the degradation of a commercially important anthraquinone textile dyes Lanaset® violet B (C.I. Acid Violet 109 (AV 109)), Acid Green 40, Ciba® and Lanaset® blue 2R and C.I. dye. It should be noted that because of their high toxicity anthraquinonic synthetic dyes are environmental contaminats. Additionally, up to 770 000 tons of dyes are generated annualy meaning that dyes cause up to 20% of industrial pollution of water. The optimal conditions chosen for degradation of these tree dyes are: temperature 37^{o}C, pH 5.0, and incubation time of up to 72 hours. Notably, the sorption dye from wastewater utilizing immobilized enzymes is a result of support adsorption, enzymatic degradation, and their synergistic action. During the early phase of removal, molecules of dye diffuse from the bulk to the support surface, where they are subsequently adsorbed by the support and brought close to laccase activity sites. Following adsorption, dye molecules are degraded enzymatically. Under the optimal conditions, the synergistic impact of enzymatic degradation and adsorption for dye removal may be achieved. In first set of experiments Lanaset® violet B dye solution was treated individually with the produced LMS-DEGDMA and LMS-DEGDMA-laccase (Figure 23). This mixture combining a solution of dye and created lignin-based support should provide information about the role of dye sorption on the support surface to decolorization of dye [181]. For evaluation of the decolorization capabilities of the immobilized laccase preparation, Lanaset® violet B dye was additionally decolored using free laccase (Figure 23A). The 90 % decolorization of Lanaset® violet B was achieved in 24 hours using an immobilized laccase preparation. After 2 hours of treatment with free laccase, decolorization, efficiency was 45%, while only applying LMS-DEGDMA on Lanaset® violet B decolorization was solely 42%, despite incubation in dye solution for 24 hours (Figure 23A). This finding suggests that in addition to dye adsorption, the LMS-DEGDMA-laccase was accountable for the extra dyes degradation and therefore the efficiency of decolorization was two times over in the case of LMS-DEGDMA-laccase compared to only LMS-DEGDMA (without enzyme). The difference in the findings obtained for the free and immobilized enzymes demonstrates that immobilization had a favorable effect on laccase affinity for decolorization of this dye [181].

Furthermore, the efficiency of LMS-DEGDMA-laccase decolorization was examined with two more anthraquinone dyes Lanaset® blue 2R, Ciba® and Acid Green 40, (Figure 24A). Both dyes showed efficiency of decolorization reached 85 %. The Acid Green 40 was deccolorized after 45 min by laccase immobilized preparation, while for Lanaset® blue 2R it was necessary 2 h.

With respect to all present results for anthraquinone dyes decolorizytion with laccase immobilized preparation, it could be stated that the factors on which decolorization depended were incubation time and molecular structure of the dye. The molecular structure of used dyes are presented on Scheme 3, all three dyes have similar molecular weight approximately 800 g/mol.

The incubation period and dye molecular structure were the main determinants of decolorizaton process, according to all of the present results for antraquinone dyes decolorization with laccase immobilized preparation. The molecular structure of used dyes are presented in Scheme 3, all three dyes have similar molecular weight, approximately 800 g/mol.

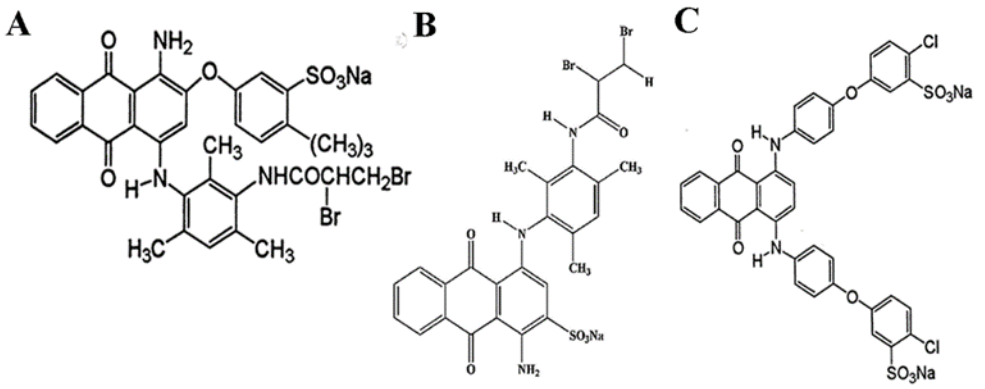

Scheme 3: Molecular structure of used dyes: (A) Lanaset® violet B, (B) Lanaset® blue 2R and (C) Acid Green 40, Ciba®.

In addition to increasing its catalytic activity in the decolorization procedure, the benefit of immobilized laccase is that it is reusable. The economic value of immobilized enzymes' reusability is enormous for a variety of industrial applications. Therefore, the degree of LMS-DEGDMA-laccase reusability was also assessed (Figure 23B and 24B). If it is observed Lanaset® violet B, each reaction cycle lasted 3 hours. The findings suggested that the LMS-DEGDMA-laccase may be reused to seven times while maintaining a decolorization yield up to 63 %. (Figure 23B) [181]. The decrease in activity is seen in between the 3th and 7th cycle (from 84% to 63%) may be mostly attributable to activity lost or inhibition by products since enzyme leakage from the microspheres during reuse was not detected. Considering the 5 % adsorbed dye on LMS-DEGDMA after the zero cycle, the decolorization impact between the 1st and 7th cycle can be ascribed nearly completely to enzymatic degradation (Figure 23B). On the other hand, in case of Lanaset® blue 2R and Acid Green 40, the LMS-DEGDMA-laccase may be used up to 5 cycles with decolorization efficiency decrease from 90% in 1st cycle to 70 % in 5th cycle (Figure 24B). The reaction cycle lasted 45 min and 2 h for Acid Green 40 and Lanaset® blue 2R, respectively [181].

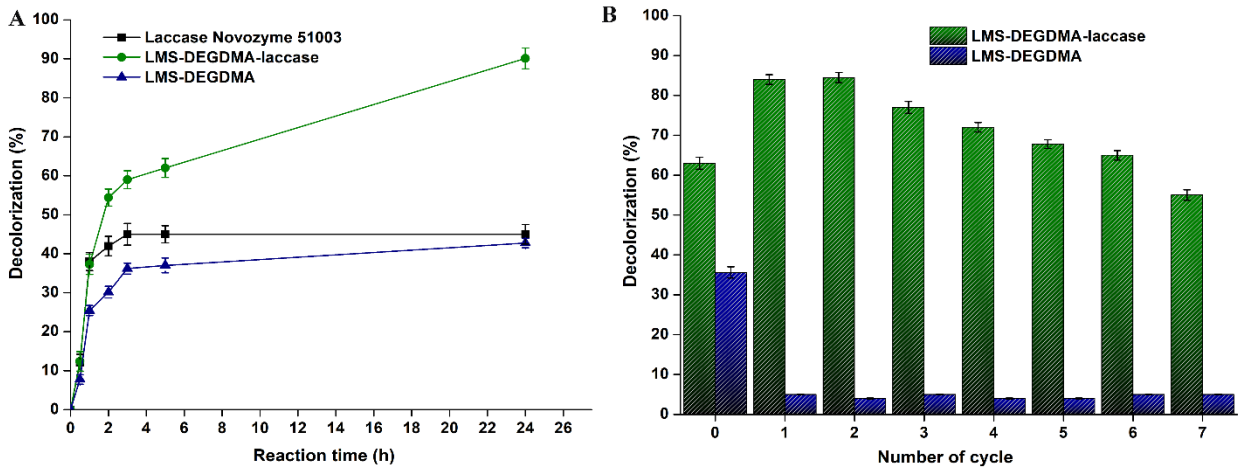

Figure 23: (A) The Lanaset® violet B decolorization. (B) Reusability of LMS-DEGDMA-laccase in decolorization of Laet® violet B [181]

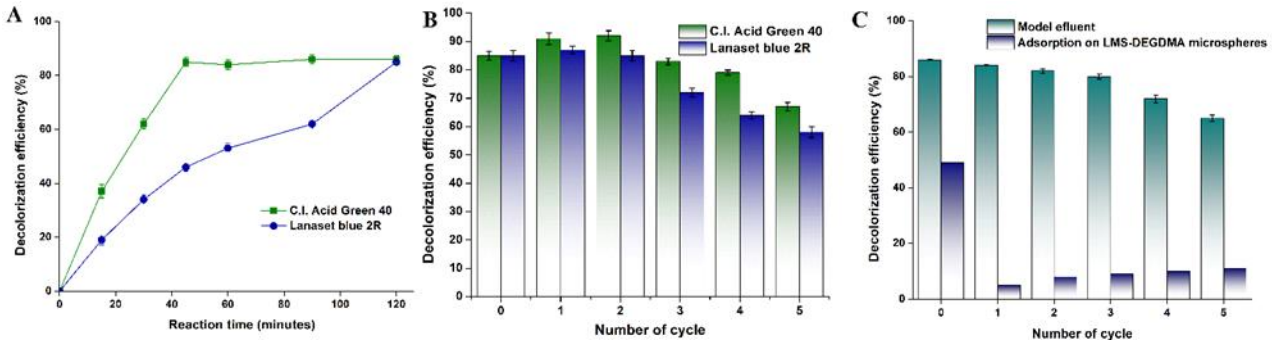

Figure 24: (A) Utilization of LMS-DEGDMA-laccase and LMS-DEGDMA in decolorization of Lanaset® blue 2R and C.I. Acid Greeen 40. (B) Reusability of LMS-DEGDMA-laccase in decolorization of Lanaset® blue 2R and Acid Green 40. (C) Utilization of LMS-DEGDMA-laccase and LMS-DEGDMA in decolorization of model effluent.

Additionally, a more realistic approach was applied by expanding research on real effluents or mixtures of dyes (Scheme 4). The possibility of LMS-DEGDMA-laccase utilization in decolorization of three dyes mixture (Lanaset® violet B, Lanaset® blue 2R, and Acid Green 40, Ciba®) was validated (Figure 22 and 23C). The mixture of dye contained an equal quantity of each dye (20 mg/L). It has been proven that LMS-DEGDMA-laccase was capable to decolorize a dyes mixture up to 86 % into 3 hours (Figure 24C). Moreover, LMS-DEGDMA removed 49 % of the dyes present in mixture. As presented on Figure 23C, LMS-DEGDMA-laccase demonstrate stability during 5 cycles in the decolorization of a three dyes mixture with yield of 86 % in the 1th down to 65 % in the 5th cycle. HPLC analysis of reaction mixture confirmed the great decolorization efficiency of LMS-DEGDMA-laccase during reaction with dye mixture (Figure 25).

Scheme 4: Application of LMS-DEGDMA-laccase in dyes decolorization

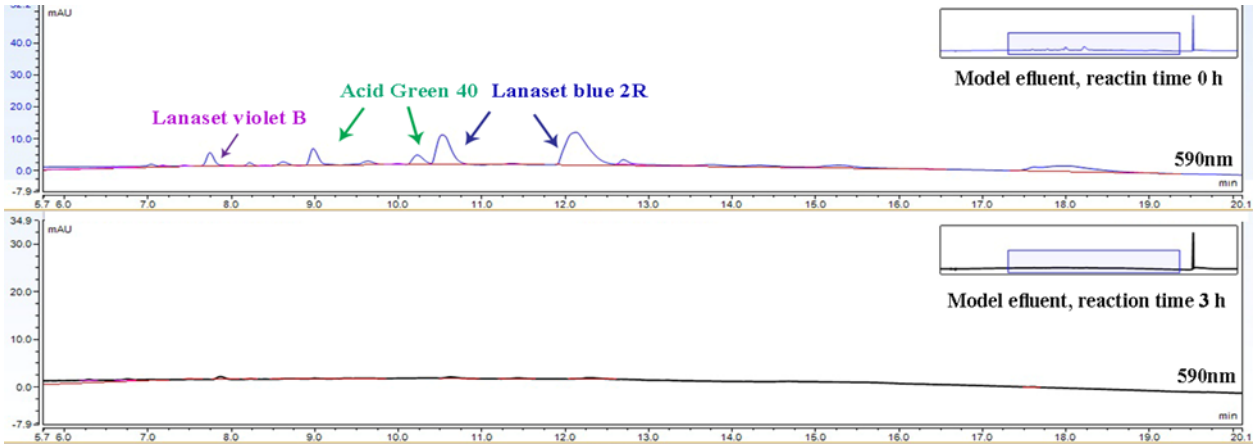

Figure 25: (A) HPLC analysis of model effluent sample. (B) HPLC analysis of model effluent sample after decolorization by LMS-DEGDMA-laccase. Reaction time 3 h

4.7. Adsorption studies

4.7.1. Laccase adsorption kinetic study on LMS-DEGDMA

The adsorption study was examined in conditions of loading of protein during the incubation period from 0 to 300 min. Results are presented in Figure 26. Initial enzyme concentrations was varied from 30 mg g^{-1} of support to 1000 mg g^{-1} of support. These findings demonstrated that rapid adsorption of enzyme on LMS-DEGDMA surface happened within the first 5 minutes of incubation and the equilibrium was reached after 30 minutes. Stated fact may be explained that the enzyme bind easily on vacant binding sites on the LMS-DEGDMA surface when the adsorption begins. Because of the significant difference in the concentration of enzyme between the support surface and the bulk solution, the adsorption rates are higher. As more and more enzyme accumulated on LMS-accesible DEGDMA surface (36 m^2 g^{-1}) the surface binding sites became occupied thus the rate of adsorption slowed down. Maximum protein loading (424 mg g^{-1}) was accomplished after 30 minutes of incubation at C_i of1000 mg g^{-1}. Figure 26A depicts the curves that represent the protein attachement against time for pseudo-first-order immobilization of laccase on LMS-DEGDMA at various initial enzyme concentrations (C_i) [181]. Equilibrium constants rate of pseudo-first-order (k_1) were 0.77 1/min at C_i of 30 mg g^{-1} and 0.58 1/min at C_i of 1000 mg g^{-1}, presented in Table 10. The experimental results fitted well with a pseudo-first-order kinetics (R^2 near to 1 (Table 10), indicating that molecules of laccase adsorb on LMS-DEGDMA according to first-order adsorption kinetics. Also, the Langmuir isotherm model exhibited good fitting with the experimental results (Figure 26B). The Langmuir isotherm constants, q_m and b, have physical implications that accurately characterize the support's maximum adsorption capacity and surface properties. Based on results shown in Figure 26B, could be concluded that the Langmuir adsorption model offered a satisfactory fit to the equilibrium data (R^2=0.96) showing that adsorption follows according to this mechanism. The adsorption capacity (q_m) for LMS-DEGDMA and Langmuir constant b were determined and their values are 547 mg g^{-1} and 0.43 mL g^{-1}, respectively [181].

As it is shown in the Figure 26C, the protein loading rises from 30 to 1000 mg g^{-1} as C_i increases, while the protein yield decreases from 93% at the lowest C_i down to 42% at the highest C_i. This demonstrated that the enzyme molecule completely filled all accessible binding sites on lignin-based microspheres surfaces at a protein loading level of 424 mg g^{-1} [181].

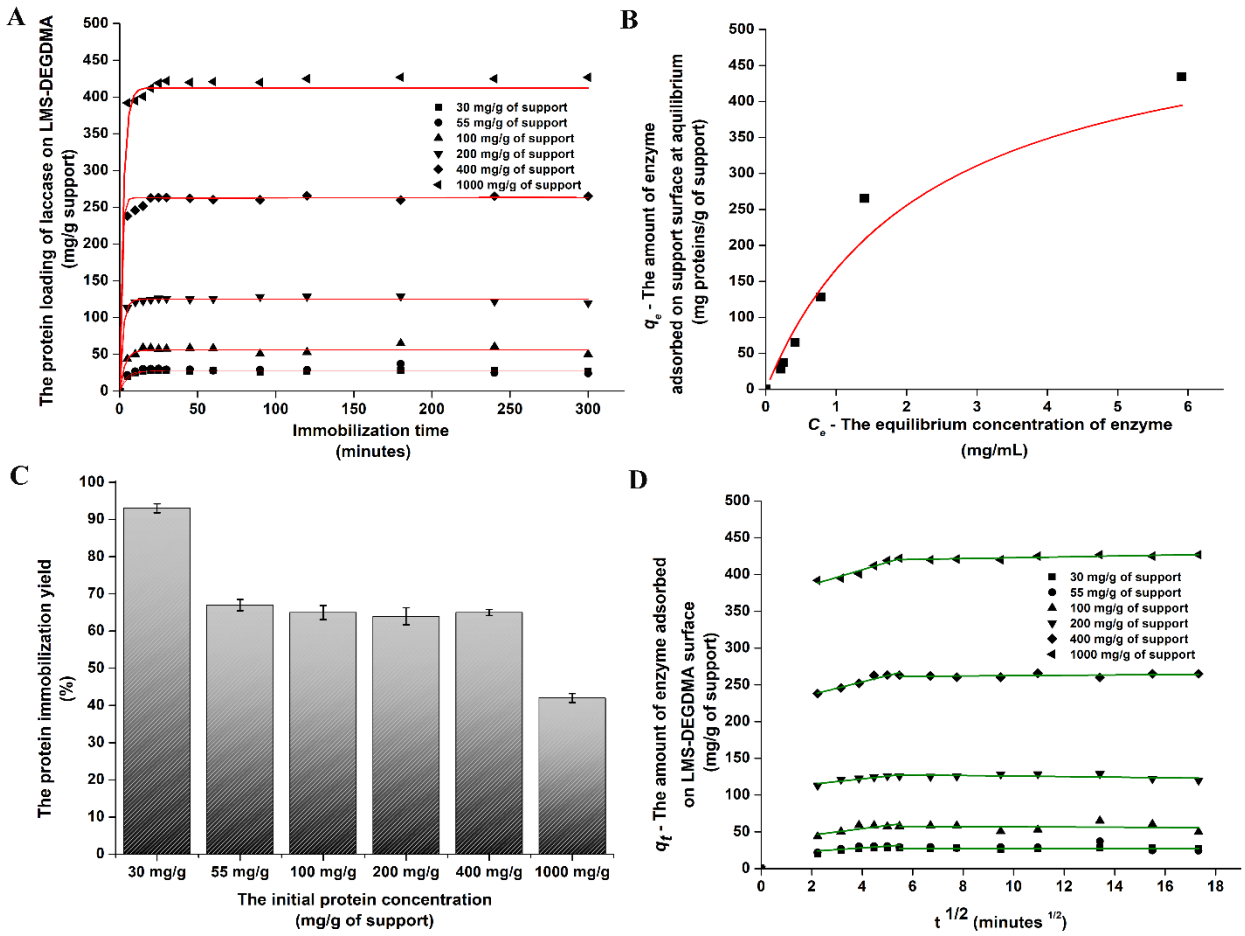

Figure 26: (A) Pseudo-first-order kinetic model of laccase. (B) Langmuir adsorption isotherm (C) The effect of initial concentration of protein on the protein immobilization yield. (D) Weber and Morris plot of q_t against $t^{1/2}$ at different C_i of enzyme [181]

Table 10. Pseudo-first-order kinetics parameters for laccase adsorption onto LMS-DEGDMA surface at different C_i of enzyme

C_i of enzyme (mg/g of support)	k_1 (1/min)	q_e (mg/g of support)	R^2
30	0.77±0.01	27.21±0.52	0.99
55	0.75±0.06	29.31±0.94	0.95
100	0.67±0.10	57.07±0.28	0.94
200	0.63±0.02	125.05±0.78	0.99
400	0.62±0.02	260.06±0.57	0.99
1000	0.58±0.04	418.29±0.50	0.99

Whereas the laccase Novozyme® 51003 dimensions are 6.74 nm x 12.84 nm x 16.36 nm and the as stated average and maximum pore diameters of LMS-DEGDMA were determined to be 23 nm and 12 nm, respectively. With pores that have openings similar to or somewhat larger than the enzyme, it may be predicted that laccase will diffuse further into the pores (17 to 23 nm). Through pore holes smaller than the laccase molecule, enzyme will be adsorb on microspheres surfaces (17 nm). High protein loading may be possible if the pore opening are much greater than enzyme, albeit enzyme leakage may be an issue. Therefore, it is generally acknowledged that the ratio of pore size which directly affects on the enzyme conformational stability, determines the efficiacy of enzyme immobilization on porous support [181].

To get more insight into these observations, the intra-particle diffusion process (Weber–Morris model) was used to the analyzing obtained experimental data (Figure 26D). The Weber and Morris plots of q_t against $t^{1/2}$ of adsorption results on LMS-DEGDMA laccase immobilization at various starting enzyme concentrations exhibit 2-linear sections, indicating that the adsorption comprises two steps. The estimated parameters for every step are presented in Table 11 [181] .

While stage II, concomitant with the ongoing stage of adsorption, is the enzyme diffusion inside the pores of LMS-DEGDMA microspheres phase I is the enzyme diffusion throughout the solution to the outer LMS-DEGDMA surface. As a result, the adsorption rate-limiting step is either the bulk or diffusion od pore and its resistance. Constant rate parameters (k_{id1} and k_{id2}) were used to establish diffusion rate throughout stage I and II (Table 11). Since the value of k_{id1} was much greater than k_{id2} it can be conclude that laccase is extremely quickly adsorbed on the LMS-DEGDMA surface as opposed to very slowly diffusing into its pores as a results of a drop in enzyme concentration in the solution. In addition, the depicted straight lines on Figure 26D do not pass throughout zero, showing that pore and bulk diffusion both regulate the adsorption rate simultaneously.[181]

Table 11: Intra-particle diffusion model parameters for laccase adsorption onto LMS-DEGDMA

C_i enzyme (mg g^{-1})	k_{id1} (mg/(g $min^{-1/2}$))	C_{i1} (mg/g of support)	k_{id2} (mg/(g $min^{-1/2}$))	C_{i2} (mg g^{-1})	(R^2)
400	8.59±0.12	219.51±1.57	0.23±0.02	260.18±1.2	0.99
1000	10.21±0.4	365.59±1.50	0.57±0.04	417.10±1.8	0.99

The laccase adsorption success on LMS-DEGDMA was validated using TGA and FT-IR analysis. FTIR and TGA analyses give further information by functional and structural properties of obtained immobilised preparation. Peaks identified the laccase molecules at 3229, 1626, 1135 and 1407 cm^{-1}, which are assignated to the carboxyl and amine groups of their amino acids. On FT-IR spectra of immobilized laccase, the presence of Amide I (1600–1750 cm^{-1}) and Amide II (1480–1584 cm^{-1}) for -NH and -CO stretches was found and confirms the effective immobilization of laccase molecules onto LMS-DEGDMA surface. TGA analysis showed that the immobilization of the laccase support shifts the onset of thermal degradation to lower temperatures than LMS-DEGDMA. The loss of mass from 200 °C to 300 °C in the LMS-DEGDMA-laccase TGA curve, was ascribed to the degradation of the protein backbone of immobilized laccase molecules [181]. The adsorption kinetics analysis revealed that acryl-modified lignin-based microspheres could be used as a support for immobilization of laccase. The TGA and FTIR analyses corroborated this finding. [181].

4.7.2. Adsorption kinetic study of removal Malachite green (MG), Tartrazine (T) and Methyl Red (MR)

Adsorption kinetic removal of dyes, by b-LMS sample was performed in a batch mode to define the overall kinetics. The obtained kinetic results was analyzed using pseudo-first, pseudo-second-order, Second-order, Elovich model, Weber-Morris, Dunwald-Wagner model and Homogenous Solid Diffusion model, Urano-Tashikawa and Bangham models. Results from adsorption experiments confirms that the pseudo-second-order model best fitted with the experimental data of all investigated samples. The fitting results of this model are given in Table 12 [180]. The other results from kinetic data are presented in Table 13. In table 14 are presented statistical analysis of the used model for adsorption data. For Malachite Green adsorption on b-LMS, the temperature-dependent kinetic data (Table 12, PSO model) indicate a greater rise in k_2 with increasing temperature. These findings demonstrate that diffusional mechanisms are more effective at high temperatures. Lower E_a for Tartrazine adsorption, 7.01 kJ mol^{-1}, is indicative of advantageous diffusional processes and surface interactions [180]. Physisorption and diffusion-controlled processes are characterized by an adsorption activation energy (40 kJ/mol) [203]. Activation energies given in Table 12 reveal that transport within a porous system (film diffusion; Fickian) is the primary component that affects the rate of adsoption inside the pore, but only under conditions of lower diffusional resistance. The small activation energies for all dyes point out a moderate effect of temperature on the pollutants diffusivity inside the pore, and after 10 minutes, adsorption is controlled by intra-particle diffusion [180]. The observed data indicate a significant disparity between adsorption capacity and affinity. The modeling of kinetic data contributed to a thorough knowledge of adsorbent/adsorbate interaction processes, as the limiting step: diffusional transport (external, surface, internal), desolvation, and adsorption at the specific site. All of these processes are significantly impacted by pollutant characteristics and surface functions. The interaction phenomena between dyes and surface functionalities were studied using quantum chemical computations model [180].

Table 12: Kinetic parameters for MG, T and MR adsorption onto b-LMS at 25^0C (C_i for all three dyes were 20 mg l^{-1})

Pollutant	Parameter	Pseudo-first-order	Pseudo-second-order	Second-order	E_a (KJ mol^{-1})
MG	q_e	48.904	86.4026	86.4026	10.21
	k (k_1, k_2)	0.0531	0.00211	0.003	
	R^2	0.914	0.994	0.968	
T	q_e	84.408	73.291	73.291	7.01
	k (k_1, k_2)	0.08935	0.00139	0.00026	
	R^2	0.885	0.997	0.935	
MR	q_e	55.815	63.117	63.117	8.33
	k (k_1, k_2)	0.1002	0.0016	0.0002	
	R^2	0.944	0.992	0.788	

Table 13: Kinetic parameters of the D-W, Elovich, HSDM, Urano-Tashikawa and Bangham models for dyes adsorption onto b-LMS at 25^0C (C_i for all three dyes were 20 mg l^{-1}) [180]

Model	Parameters	MG	T	MR
Dunwald-Wagner	$K^a \times 10^{-2}$	3.033	2.283	2.145
	R^2	0.967	0.998	0.841
Elovich	α^b(mg g^{-1} min^{-1})	29.7558	3.9384	13.146
	β^{**}(mg g^{-1})	0.08252	0.06836	0.0715
	R^2	0.981	0.998	0.950
Homogenous Solid Diffusion	$Ds^c \times 10^{-11}$	3.41	2.82	2.71
	R^2	0.974	0.989	0.831
Urano and Tachikawa	$Di^d \times 10^{-4}$	3.594	6.072	6.823
	q_e	82.8	64.00	53.00
	R^2	0.898	0.861	0.944
Bangham	k_o^e	4.018	2.538	2.145
	q_e	3.872	3.39	3.253
	R^2	0.989	0.993	0.942

Table 14: Analysis of variance and statistical significance for the best adsorption models for the removal of pollutants onto b-LMS adsorbent[180]

Pollutant	Adsorption model	ANOVA					Statistics	
		Df	Sum of squares	Mean square	F value	Prob>F	χ_r^2	R^2
MG	Langmuir	2	13428.28	6714.14	2590.59	5.53^x10^{-8}	2.592	0.995
	Freundlich	2	13372.74	6686.37	488.09	3.53^x10^{-6}	13.699	0.976
	Bohart Adams	2	9.714	4.857	10623.94	1^x10^{-9}	4.57^x10^{-4}	0.997
	PSO	2	12626.13	6313.06	1079.76	4.90^x10^{-7}	5.846	0.962
T	Langmuir	2	8251.38	4125.69	350.91	7.98^x10^{-6}	11.757	0.961
	Freundlich	2	7657.13	3828.56	789.71	1.07^x10^{-6}	4.848	0.982
	Bohart Adams	2	10.11	5.05	26542.21	1^x10^{-10}	1.90^x10^{-4}	0.999
	PSO	2	16843.98	8421.99	2472.17	6.22^x10^{-8}	3.41	0.979
MR	Langmuir	2	6246.94	3123.47	1151.10	4.18^x10^{-7}	2.713	0.986
	Freundlich	2	6246.69	3123.34	1130.3	4.37^x10^{-7}	2.763	0.986
	Bohart Adams	2	9.714	4.857	10623.93	1^x10^{-9}	4.57^x10^{-4}	0.997
	PSO	2	31064.96	15532.48	1039.68	5.39^x10^{-7}	14.939	0.867

4.7.3. Effect of pH

The effect of pH is valuable parameter for adsorption and adsorbent/pollutant interaction. The large pH_{PZC} difference between b-LMS and b-LMS-OSO_3H shows great potential for their application in pollutant removal. However, the rule that positive species have a stronger adsorptive capacity at $pH<pH_{PZC}$ or $pH>pH_{PZC}$ for negative species was one of the factors for the pH selection. Calculating microspecies distribution based on expected pKa values and carrying out pH effect, adsorption removal of T and MG in pH ranged from 2 to 12 was the first step in understanding to define working conditions better results are given in Figures 27-29 [180]. In the pH ranging pH 4 - 6, there are no major pH effect on MR removal efficiency (Figure 29), however T and MG removal efficiencies exhibit a sharp rise and a reduction in the pH range from 4 to 9. (Figures 27 and 28). A thorough examination of the obtained data (Figures 26-28) demonstrated that high pH, i.e. pH>8, significantly reduces the adsorption efficiacy of T and MR, but it was seen the other way around for MG. It suggests that the pH effect of charged species is essential for achieving high removal efficiency. Furthermore, the adsorption performance of MG improves by 7.8% at pH 8, indicating that the usefulness of b-LMS depends on the pH of the water. Consequently, based on these findings pH value 7 for MG and pH value 6 for T and MR were selected as the operating pH values [180]. Long-term exposure to pH values below 4 or above 9 may damage the hydrolytically unstable ester bond in the b-LMS structure. Thus, extraordinarily high usable of b-LMS may be achieved without adjusting the pH of natural water (usually between 5 and 9). Positively and negatively charged pollutant removal at operational pH demonstrates the adaptability of b-LMS. Additionally, b-LMS-OSO_3H may be used in the lower pH range (from 4 to 6), which is advantageous for water purification. In conclusion, the best pH would satisfy the following characteristics for achieving excellent results from described adsorption process: capacity, adsorbent lifetime and regeneration, and using a broad range of natural water with no pH regulation [180].

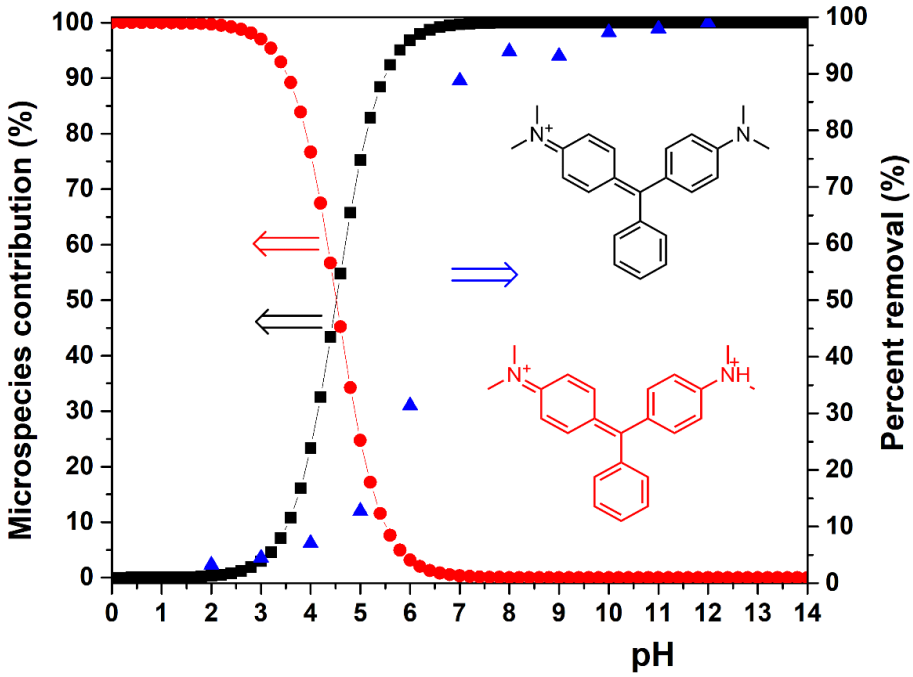

Figure 27. Microspecies distribution and pH effect for MG ($C_{i[MG]}$ = 10 mg dm^{-3}; m/V=1000 mg dm^{-3}, T=25^{0}C) [180]

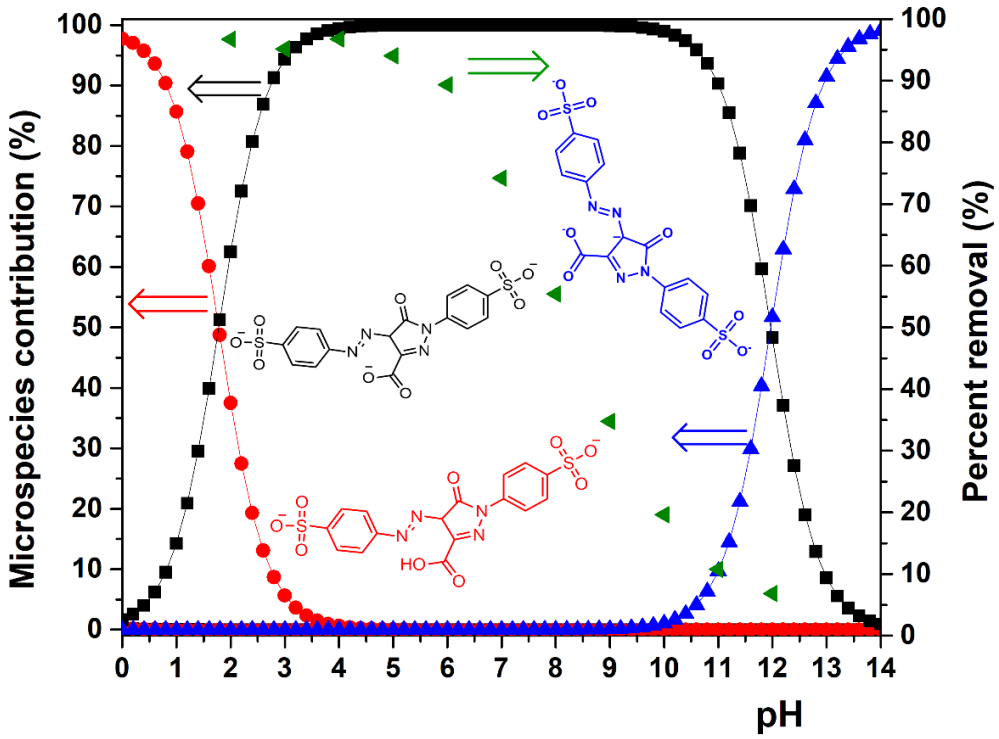

Figure 28. Microspecies distribution anf pH effect for T ($C_{i[T]}$ = 10.0 mg dm^{-3}; m/V=1000 mg dm^{-3}, T=25^{0}C) [180]

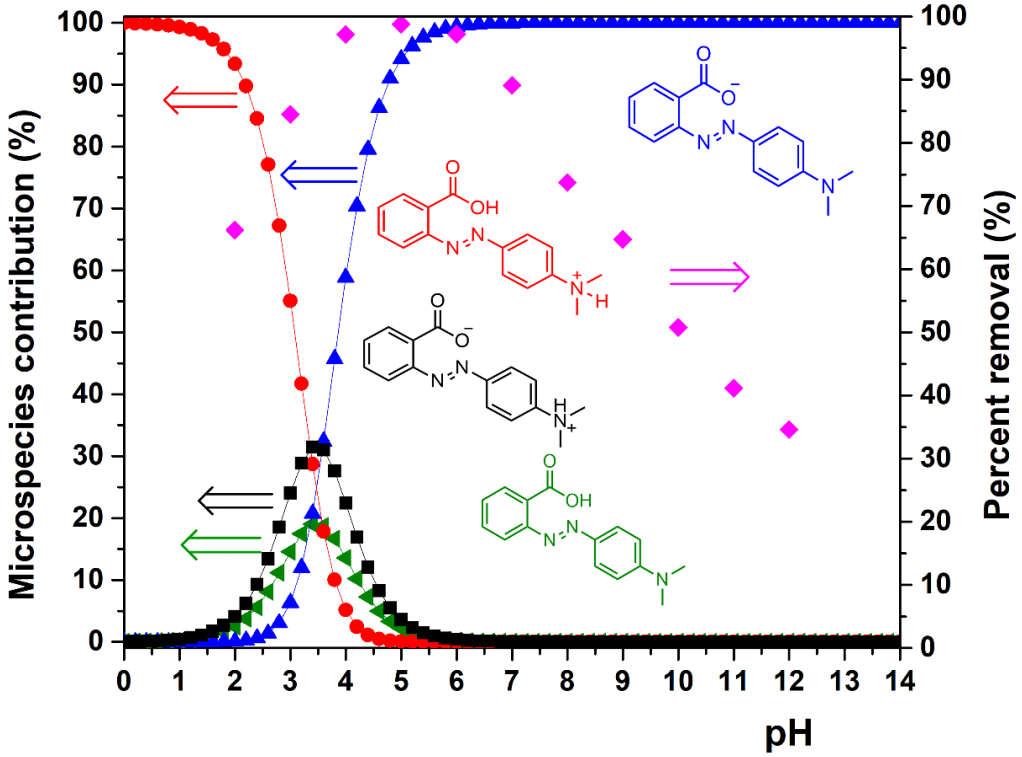

Figure 29. Microspecies distribution and pH effect chart for MR ($C_{i[MR]}$ = 10.0 mg dm^{-3}; m/V=1000 mg dm^{-3}, T=25^{0}C) [180]

4.7.4. Adsorption isotherms studies

The adsorption isotherms have aplication to examine adsorptive potential of investigated samples. Pb, Ni, MG, As(V), and MR, such as pH-dependant emerging pollutants, are used for that purpose. The adsorption experiments results fit the appropriate isotherm model (Langmuir Freundlich, Temkin, Dubinin-Radushkevich (D-R)). The following results showed low to middle removal capacities: 28.9 and 15.4 mg g^{-1} for Pb^{2+} and $Ni^{2+,}$ 12.1 mg g^{-1} for As(V), and 81.4 and 62.6 mg g^{-1} for MG and MR, confirming the satisfactory adsorption potential of KfL. Lengthy approach to the filtering was available at the laboratory level (sometimes more than 10h). Due to the limited manipulation capability of the original KfL, the major objective of this research was to construct customized modifications. In accordance with this concept, the acryloyl modification of KfL, i.e. the formation of KfL-AA, provides suitable vinyl functionality into KfL that participates in the synthesis of b-LMS. The results of adsorption MG, T and MR, derived from Langmuir isotherm model, are present in Table 15. Also, the non-linear fitting the experimental data results using the other isotherm model are given in Tables 15-18 [180].

Table 15. Langmuir isotherm model for adsorption T, MG, and MR onto b-LMS (C_i for all three dyes were 20 mg l^{-1})

	T (K)	q_m (mg g^{-1})	K_L (dm^3 g^{-1})	K_L (dm^3 mol^{-1})	R^2	χ_r^2	F value
	298	116.8	0.19669	71774.34	0.995	2.49	2590
MG	308	113.5	0.19671	71781.64	0.996	2.34	2757
	318	110.1	0.19706	71909.36	0.995	2.22	2790
	298	86.8	0.17765	105091.47	0.961	11.757	351
T	308	83.6	0.18306	105102.15	0.972	7.781	515
	318	80.6	0.188	105289.16	0.981	4.848	789
	298	68.6	0.20271	54590.61	0.986	2.713	1151
MR	308	69.1	0.21238	57194.78	0.982	3.797	858
	318	70.1	0.22064	59419.23	0.967	7.162	476

The obtained results showed the high removal capacities were observed for all analyzed dyes (Table 15), but the maximum adsorption capacity decreased somewhat with temperature enhancement, except for MR. Given the Langmuir constant K_L, a high adsorption affinity suggests many adsorption sites with low binding energy. The Freundlich constant value K_F verifies the excellent absorption of b-LMS. In addition, a good fit with Freundlich isotherm was observed (Tables 16-18), and parameter n shows that adsorption sites are very reactive. The A_T parameter of the Temkin isotherm indicates the bond constant seen in the maximum binding energy (L/g). As an analog to adsorption energy, the mean B index value shows that physisorption predominates for all dyes. The average free energy derived from the D-R isotherm indicates that physical interactions are primary adsorption process [180]. Using b-LMS in severely polluted water, defined as water with a chemical oxygen demand more than 1000 mg O^2 dm^{-3}, demonstrated its broad applicability. As shown in Table 15, the acquired findings indicated a 7 to 8-fold increase in the expected Langmuir values. It indicates that b-LMS might be used effectively across a broad range of pollution concentrations. In addition, experiments of applicability b-LMS for removal of cation revealed a moderate adsorption capacity: 34.4 mg g^{-1} for Pb^{2+} and 22.6 mg g^{-1} for $Ni^{2+.}$ It was known that the sulfate group has a high tendency for cations as

well as a high capacity for regeneration, the next step was to introduce sulfate to form b-LMS-OSO_3H, where adsorption findings were validated [180].

Table 16. Non-linear parameters of selected isotherm model for MG adsorption onto b-LMS

	Parameters	25 ºC	35 ºC	45 ºC
Freundlich isotherm	K_F (mg g^{-1}) (dm^3 mg^{-1})$^{1/n}$	22.11	21.56	21.04
	$1/n$	0.540	0.538	0.534
	R^2	0.976	0.973	0.971
Temkin isotherm	A_T (dm^3 g^{-1})	2.375	2.314	2.260
	b_T	106.48	111.87	117.60
	B (J mol^{-1})	23.281	22.900	22.491
	R^2	0.965	0.970	0.974
Dubinin-Radushkevich isotherm	q_m (mg g^{-1})	52.95	52.62	52.21
	K_{ad} (mol^2 KJ^{-2})	8.84	8.84	8.85
	E_a (KJmol^{-1})	7.521	7.518	7.515
	R^2	0.820	0.834	0.847

Table 17. Non-linear parameters of selected isotherm model for T adsorption onto b-LMS

	Parameters	25 ºC	35 ºC	45 ºC
Freundlich isotherm	K_F (mg g^{-1})(dm^3 mg^{-1})$^{1/n}$	16.28	15.98	15.69
	$1/n$	0.521	0.517	0.512
	R^2	0.998	0.998	0.996
Temkin isotherm	A_T (dm^3 g^{-1})	2.56	2.383	2.243
	b_T	154.25	158.24	162.9
	B (J mol^{-1})	16.070	16.189	16.228
	R^2	0.918	0.922	0.964
Dubinin-Radushkevich isotherm	q_m (mg g^{-1})	38.14	38.87	39.57
	K_{ad} (mol^2 KJ^{-2})	9.55	9.53	9.51
	E_a (KJmol^{-1})	7.236	7.243	7.251
	R^2	0.701	0.762	0.816

Table 18. Non-linear parameters of selected isotherm model for MR adsorption onto b-LMS

	Parameters	25 ºC	35 ºC	45 ºC
Freundlich isotherm	K_F (mg g^{-1})(dm^3 mg^{-1})$^{1/n}$	14.34	14.98	15.72
	$1/n$	0.490	0.483	0.474
	R^2	0.986	0.993	0.998
Temkin isotherm	A_T (dm^3 g^{-1})	2.151	2.381	2.774
	b_T	170.5	178.9	190.8
	B (J mol^{-1})	14.54	14.32	13.86
	R^2	0.986	0.978	0.958
Dubinin-Radushkevich isotherm	q_m (mg g^{-1})	36.87	36.68	35.55
	K_{ad} (mol^2 KJ^{-2})	8.896	8.901	8.933
	E_a (KJmol^{-1})	7.497	7.495	7.482
	R^2	0.859	0.826	0.739

4.7.5. Adsorption thermodynamics

Using Van't Hoff equations, the findings of Gibbs free energy (ΔG), entropy (ΔS) and enthalpy (ΔH), and calculations offer some insight of the thermodynamic component of dyes removal. The parameters of thermodynamics are determined at three different temperatures from isothermes (Table 19). Negative levels of ΔG constitute spontaneous, effective adsorption. According to the literature, ΔG is more than the specified boundary value of -42 kJ mol-1, indicating physical adsorption [167,180].

The total energy impact exhibited a little endothermic component and a minor ΔH difference. The near-zero values of ΔH for MG imply that temperature has little influence on the equilibrium state. How to precisely identify the contribution of the fundamental stage in adsorption while accurately determining the total thermodynamic data is often disputable. The primary contributing aspects to using energy during adsorption are the dye's hydration capacities, diffusional transport (external/internal), and energy impact at the surface of the adsorbent. The most significant elements of ΔH change are endothermic dehydration and adsorbate/adsorbent interactions. Interestingly, the transition to an exothermic process (ΔH = 2.96 kJ/mol) for the MG/b-LMS system at pH = 9.6 indicates a high strength of phenoxide/MG electrostatic interactions than phenol/MG at pH 6. However, it has been shown that physisorption predominates when the energy is lower than 80 kJ mol^{-1}) [204 180]

When ΔS>0 represents the unpredictability of the equilibrium state. Numerous variables impact system disorder throughout adsorption and contribute varying degrees to the transition of S from the initial state to the equilibrium stage with more randomness. Hydration shell surrounding pollutant (dispersive, hydrogen-bonding, electrostatic interactions) and adsorbent surface hydration leads to negative entropy. The ΔS>0 changed state from the development of pollutant/surface functions contacts with a surrounding water and water displacement from the sorbent surface (increased rotational and translational motion higher orderliness). Following these principles, this work used geometrical characteristics of investigated dyes and molecule electrostatic potential to better comprehend the dyes surfaces' behavior. A greater ΔS of the system indicates a greater affinity of the dyes for the adsorbent surface. At higher dye concentrations, thermodynamic characteristics for adsorption showed a similar trend. The results are presented in Table 20. These findings indicate that the energy effects and adsorption mechanisms with varied concentration ranges of analyzed dyes are comparable [180].

Table 19: The thermodynamic parameters of dyes adsorption onto b-LMS ($C_{i[MG]} = C_{i[T]} = C_{i[MR]}$ = 20.0 mg dm^{-3}; m/V= 100-1000 mg l^{-3})

Dye	ΔG^{Θ} (kJ mol^{-1})			ΔH^{Θ} (kJ mol^{-1})	ΔS^{Θ} (J mol^{-1} K^{-1})	R^2
	298 K	308 K	318 K			
Malachite Green	-36.92	-38.16	-39.40	0.07	124.08	0.991
Tartrazine	-36.67	-37.97	-39.28	2.23	130.47	0.999
Methyl Red	-36.99	-38.35	-39.70	3.34	135.30	0.998

Table 20: The values of ΔG^{Θ}, ΔH^{Θ} and ΔS^{Θ} thermodynamic descriptor dyes adsorption onto b-LMS ($C_{i[MG]}$ =120 mg dm^{-3}; $C_{i[T]}$ = 160 mg dm^{-3};$C_{i[MR]}$ = 140.0 mg dm^{-3}; m/V= 100-1000 mg l^{-3})

Dye	ΔG^{Θ} (kJ mol^{-1})			ΔH^{Θ} (kJ mol^{-1})	ΔS^{Θ} (J mol^{-1} K^{-1})	R^2
	298 K	308 K	318 K			
Malachite Green	-32.41	-33.47	-34.52	-0.93	105.58	0.999
Tartrazine	-33.21	-34.40	-35.59	2.29	118,86	0.999
Methyl Red	-31.61	-33.08	-34.55	12.17	146.86	0.999

4.7.6. External and internal mass-transfer

This research was valuable for analyzing the role of external/internal mass transfer in overall processes, and the adsorption kinetics study analyzes the overall mass transfer in the examined system. Varying mixing speeds bring about changes in adsorption's diffusional regime. As shear rate increases, the resistance of the boundary layer decreases, i.e. diffusion through the liquid film is accelerated.[205 180]. The kind of flow pattern was identified based on the dimensionlss Reynolds (*Re*) parameter and, also, the results for other criteria: Sherwood (Sh) and Schmidt (Sc) number. The values of this parameter are given in Table 21. Increasing the speed mixing 100 - 400 rpm causes a small k_f rise from 1.39 to 2.55 for MG and from 2.14 to 3.80 for MR. Sample T had a substantial increase from 1.59 to 7.45. The observed changeable trend of k_f reveals the contributon of increasing transfer of mass (in boundary layer diffusivity and bulk), resulting from a reduction in boundary layer thickness and the impact of dye structural effects. Presented is the inverse relationship between mass transfer increases and film thickness. Thus, even the moderate influence the rate of mixing for MR and MG on the k_f value changes does not imply a greater fluid film effect external resistance; rather, it is likely that the structural properties of these dyes contributed more to reducing their diffusivity. In contrast, the greatest increases in k_f values for T imply efficient diffusion from bulk to pore interior or surface as a result of enhanced hydration of one carboxylic groups and two sulfonic[180].

Many parameters, including dye geometry/structure, polarizability, electronic structure, mixing speed, hydration capacity, and adsorbent surface properties such as affinity, porosity, contribute to dye transport rate to varying degrees, as shown by the obtained findings. In addition, bonding mechanism and dye affinity to surface functions substantially influence diffusional transport inside

the adsorbent. Contradictory movement of desorbed dye from the surface of adsorbent influences a little changes in parameter B for T and MG dye (Table 6) [206]. The identical values of the B and k_{fa} parameters (Table 21) indicate that the external/internal mass transfer played a significant role in the early period (10 min) but intra-particle pore diffusion governed the subsequent time. This result was supported by the fact that the computed B_{iot} numbers in the range of 71.5 to 139.9 are more than 100, indicating that the process is controlled by intraparticle diffusion. Briefly, the total internal process was governed mostly by Fickian and less by diffusion on surface, with Fickian dominating the overall flow as the concentration gradient decreased [180].

Table 21**:** Calculated mass-transfer parameters

Dye	N (rpm)	$k_f a$	*Re*	*Sc* × 10	*Sh*	$k_f \times 10^{-2}$	$D_{eff} \times 10^{-9}$ (cm^2/s)	*B*	$D_e \times 10^{-8}$	$D_p \times 10^{-8}$	$D_s \times 10^{-11,*}$	$D_s \times 10^{-11,**}$
MG	100	0.048	18.37	8.34	12.51	3.02	4.58	0.029	3.59	10.70	3.41	1.52
	250	0.047	45.920	8.34	18.62	4.49	4.53	0.028	3.50	10.70	3.35	1.53
	400	0.046	73.47	8.34	23.03	5.55	4.47	0.028	3.41	10.70	3.91	1.54
T	100	0.037	18.37	8.03	12.38	3.10	3.24	0.020	2.64	11.10	3.37	1.50
	250	0.035	45.92	8.03	18.42	4.61	3.12	0.019	2.59	11.10	3.28	1.51
	400	0.034	73.47	8.03	22.76	5.70	3.00	0.019	2.55	11.10	3.20	1.52
MR	100	0.033	18.37	10.2	13.25	2.61	3.33	0.021	2.33	8.72	3.30	1.51
	250	0.032	45.92	10.2	19.78	3.90	2.85	0.018	2.43	8.72	3.17	1.52
	400	0.030	73.47	10.2	24.49	4.82	2.32	0.015	2.55	8.72	3.00	1.53

Where **b-LMS** radius is 0.0001265 m; peripheral speed (N - *v*): 100 rpm – 1; 250 rpm – 2.5 and 400 – 4; [1] D_{eff} – effective intraparticle diffusion coefficient [51] (* homogeneous diffusion model; ** shell progressive model) [208].

4.7.7. Adsorption mechanism

As shown in Figure 30, possible molecular routes for the multifunctionality of lignin-based (b-LMS) adsorbent include an interaction of phenol, $^{-}$OH and aromatic group with pollutants. Consideration was given to pollutant and surface of adsorbent attributes such as electrostatic potential, structure, charges, adsorbent/optimized dye electronic geometry, proton donating/accepting capabilities, and interaction at operational pH. Electrostatic interactions may dominate in intermolecular interactions, which follow by hydrogen bonding and least by hydrophobic interactions. In addition, certain dye/adsorbent interactions were compared [180]:

- positively charged Malachite Green as compared to the negative end of dipole electronic density,
- negatively charged sulfonic group in Tartrazine compared to positive pole of dipole and proton donating site at b-LMS surface (HBD effect)
- Theoretical estimate of pH ionizable HBD site carboxylic and, dimethyl amino group, in MR vs all interactions for Malachite green and Tartrazine are described. Due to the high geometric need for achieving aromatic interaction, it would be anticipated that their contribution would be reduced. Due to the above hypotheses, theoretical investigation was employed to incorporate the electronic structure as an essential characteristic of the equilibrium system [180].

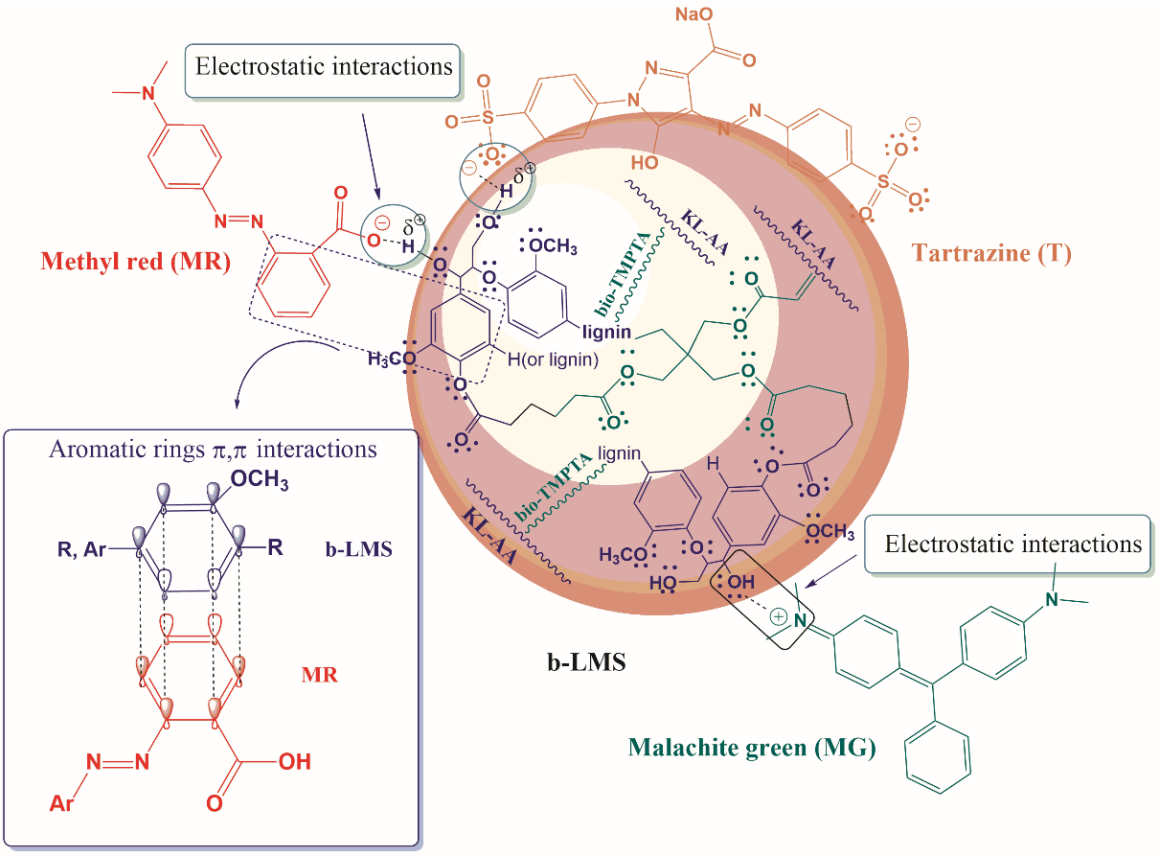

Figure 30. Possible dyes/adsorbent interaction [180]

The significance deprotonation of phenolic was shown by the capacity measurements of Malachite Green and Methylene blue (both positive-charged dyes): MG had a 23.6 % higher value at pH 9.0 (144.4 mg g^{-1}) compared at pH 7 (116.8 mg g^{-1}) The value of pH 9 produces similar outcomes of Methylene blue (166.1 mg g^{-1}) and pH 6 (124.1 mg g^{-1}) [180]. This type of finding indicates the notability of pH adjustment to suitability $^{-}$OH groups on molecule surface, which supply the enhanced attraction of oppositely charged places. Tartrazine showed the opposite pattern, decreasing from 86.8 mg g^{-1} on pH 7 to 17.4 mg g^{-1} on pH 9.0. Because of repulsion with protons and positive surface charged $ROH^{2+/}ArOH^{2+}$ groups about cation, MG exhibited a considerable decrease in adsorption efficiency at pH 4 compared to MR [180].

The adsorption of cations occurs through a proton exchange process or electrostatic interactions with phenolic -OH groups. Also, coordination complexes on surface may form. Lignin phenol and hydroxyl groups behaving are as Lewis acids, and at higher pH, i.e. pH > pH_{PZC}, deprotonation occurs, yielding phenoxide groups with greater electrostatic interaction potential with positively charged groups, such as cations or cationic dye. The -OH group has a role as both acceptor and donor (HBA and HBD). In conclusion, the surface interaction, where S is marked as the lignin surface, displays various interactions schematically present in Eq. 43-47. This electronic arrangement of the -OH group allows for several mechanisms with the HBA/HBD centers in dye [180].

$$\equiv S - OH \rightleftharpoons \equiv S - O^- + H^+ \quad \text{(Eq.43)}$$

$$\equiv S - OH + M^{2+} \rightleftharpoons (\equiv S - O^-)M^{2+} + H^+ \quad \text{(Eq.44)}$$

$$2(\equiv S - OH) + M^{2+} \rightleftharpoons (\equiv S - O^-)_2M^{2+} + 2H^+ \quad \text{(Eq.45)}$$

$$\equiv S - O^- + M^{2+} \rightleftharpoons \equiv S - O^-M^{2+} \quad \text{(Eq.46)}$$

$$2(\equiv S - O^-) + M^{2+} \rightleftharpoons (\equiv S - O^-)_2M^{2+} \quad \text{(Eq.47)}$$

At pH < pH_{PZC}, processes (Eq. 43–46) insignificantly contribute to adsorption mechanism, however at pH > 9, process (Eq. 47 and 48), do make a significant impact [180]. The surface sites with low-energy, deprotonated phenol and -OH group forms at pH > 8 participate through an ion exchange mechanism (Eq. 46 and 47). Adsorption of cation was followed by pH decrease due to proton release (Eq. 43-45) [180]. At equilibrium, FTIR spectroscopy is a valuable tool for analyzing an investigated system. Because of the strong dyes' dipolarity, matching linkages produce peaks with high-intensity absorption that may be used to follow of b-LMS adsorption sites saturation. In the spectra shown in Figure 31, obvious changes in peak location, intensity, and development of additional peaks are noticeable. The most significant changes in absorbance bands after dye adsorption were seen in two regions: 900-500 cm^{-1} and 1650-1400 cm^{-1}. Signals in the FTIR spectra between 1636 and 1550 cm^{-1} are due to variations in the vibrational constamts of dyes aromatic skeletal vibrations at 1578, 1550, and 1592 cm^{-1}, imino group in Tartrazine present stretching asymmetric vibration of O-C=O ion. Changes were also found in the range 1390-1461 cm^{-1}, originating from several skeletal aromatic vibrations of syringyl and guaiacyl units. Also, the O-H phenolic peak at 1398 cm^{-1} and C-H deformation vibration at 1460 cm^{-1} overlapped with an aliphatic C–H vibration. In addition, variations observed between 900 and 500 cm^{-1} correspond to deformation vibrations of aliphatic and aromatic groups, which confirms adsorption of dye [180].

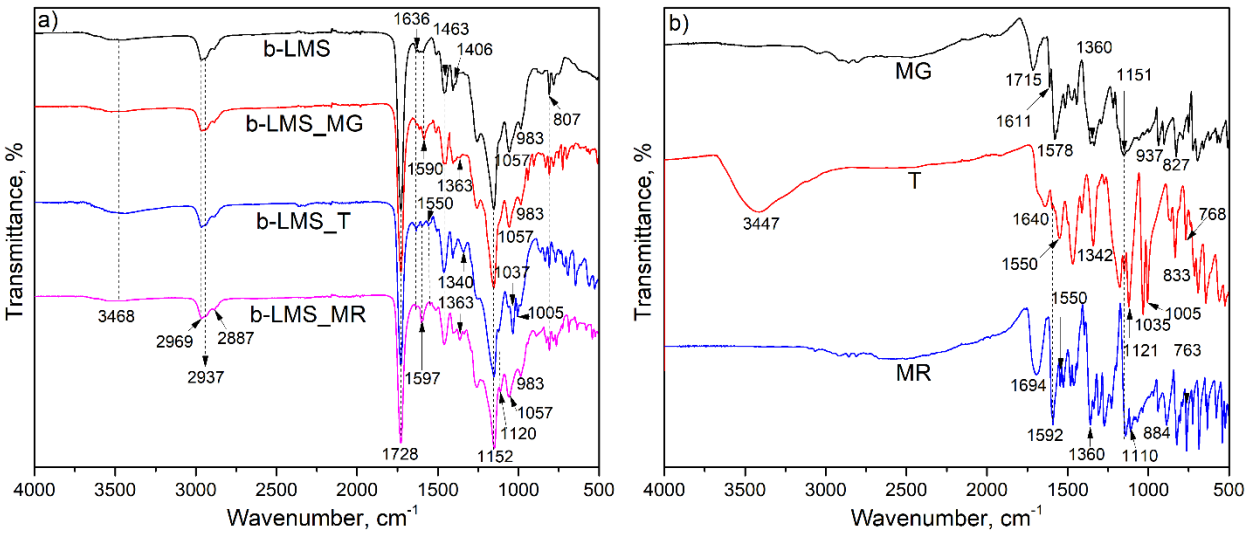

Figure 31: a) FT-IR spectra of dyes**)** b) b-LMS and adsorbent after dyes adsorption [180]

As the last phase in the adsorption mechanism investigation, quantum chemical calculations were performed. The creation of intermolecular bonds among lone electron pairs from hydroxyl and phenolic groups, and electron-deficiency sites in the dye structure is an effective method for binding harmful pollutants. Deformation of the dye's electron density in the surface functional group region, both adopted in response to a global change in the dispersion interaction. As a result, a quantum chemical computation was utilized to identify particular interactions that contribute significantly to adsorption process. Application of dispersion-corrected semiempirical quantum chemical techniques was used to describe the dispersion and electrostatic interactions, i.e. the binding energy owing to interactions, as the main objective of present work [180].

The analyzed dyes binding enthalpies are determined by optimizing the dye/lignin complex geometry used of the semi-empirical PM7 approach, which includes equations for hydrogen bonds and dispersion forces. According to the formula $H_{bind} = H_{complex} - (H_{dye} + H_{lignin})$, the binding enthalpies were computed and presented in Table 22, which indicates that the cationic MG dye exhibits the higher interactions with lignin. This emphasizes the significance of Malachite green aromaticity, charge distribution, and interactions with lignin's phenolic groups. Figure 32a depicts the geometry of the complex MG/lignin. MG forms advantageous hydrophobic interactions by stacking between two aromatic rings of lignin (Figure 32b and 32c). The findings indicate hydrophobic interctions as the primary initiate mechanism for Malachite green-lignin bonding [180].

Table 22: Binding enthalpies of dyes-b LMS

	Binding enthalpy, kJ/mol
Malachite Green	-238.4
Tartrazine	-147.7
Methyl Red	-106.0

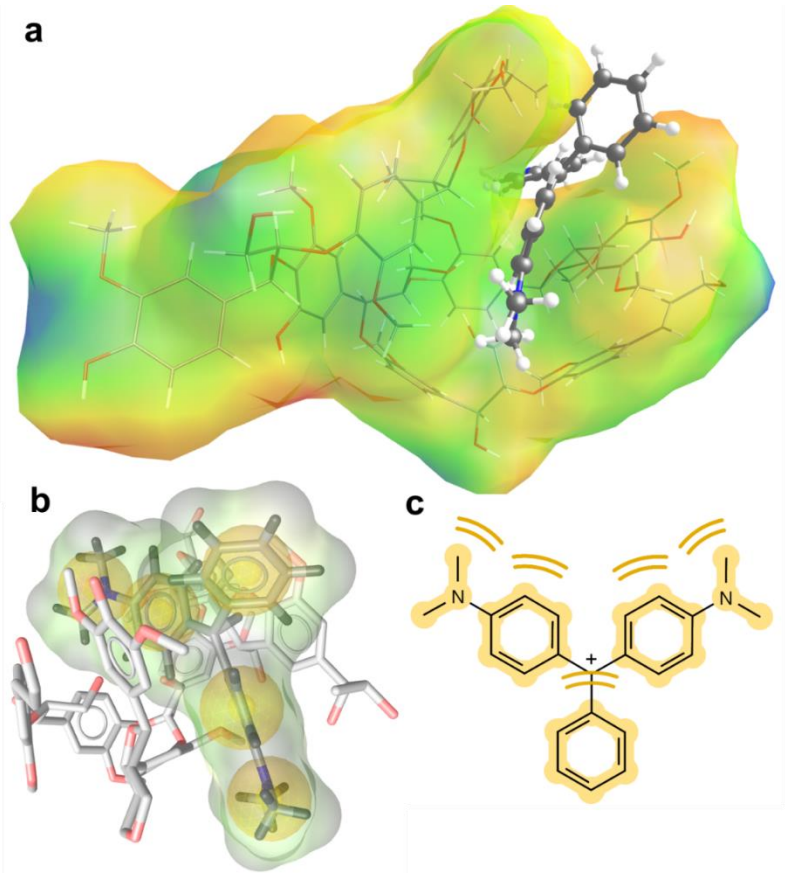

Figure 32: a) The lowest-energy complex between MG and lignin. The adsorbent MEP surface. Blue regions have negative potential; red regions have positive potential; b) MG/lignin complex investigated with pharmacophore approach. Yellow spheres indicate hydrophobic interactions of MG with the environment and the surface is dyed by tendency contribution of atom binding; c) 2D displays of ligand pharmacophores [180]

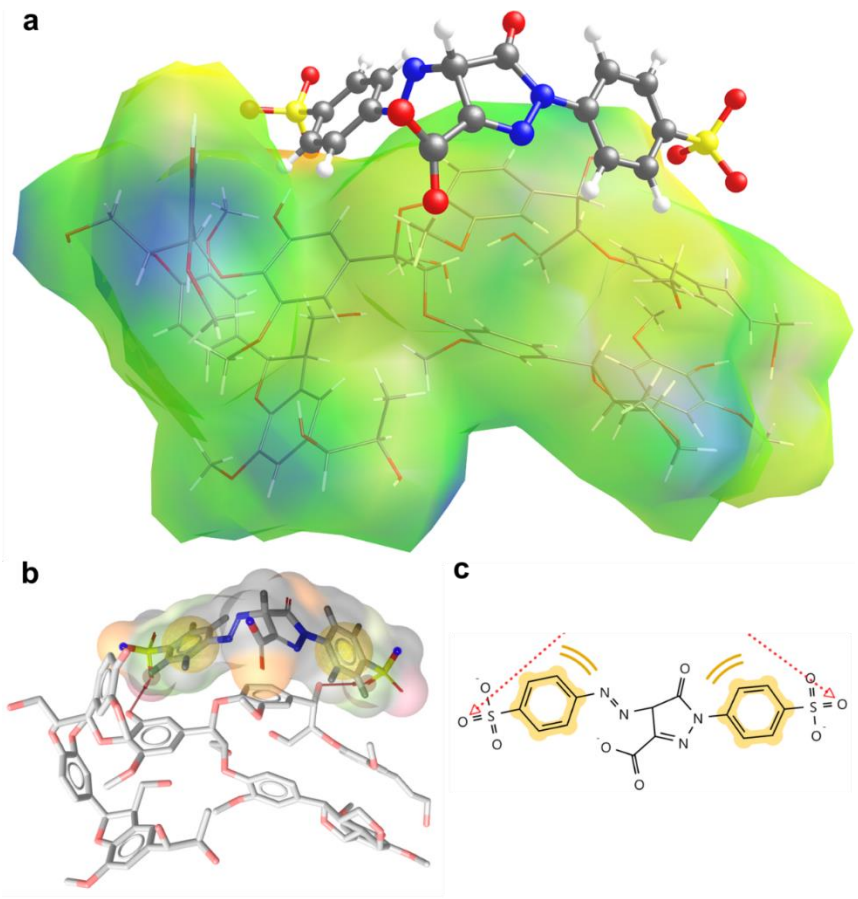

Figure 33: a) The lowest-energy complex between T and lignin. The adsorbent MEP surface. Marked blue present regions with negative potential and red marked present regions with positive potential; b) T/lignin complex investigated with pharmacophore approach. Marked yellow spheres present MG's hydrophobic interactions and red arrows show HBA interactons with environment c) 2D displays of ligand pharmacophores [180].

At the sample T, both sulfonate groups create HBA interaction with arylglycerol-aryl ether groups or phenolic with positive region of lignin MEP. Additionally, aromatic rings of Tartrazine form hydrophobic interactons with lignin (Figure 33). Nonetheless, the greater binding enthalpy of the polyaromatic and cationic MG dye suggests that low hydrophobic interactions have an important role in the dye removal process. The optimal binding mode of MR based on negatively charged carboxylic group according to the positively charged portion of lignin, whereas the fragment of N,N-dimethyl is positioned close to positively charged MEP segments (Figure 34a). The aliphatic $^{-}$OH (HBA interactions) and hydrophobic groups between two aromatic rings are the primary interactions for the binding of MR. This dye exhibits the weakest interactions concerning the relative binding enthalpies of analyzed dyes with lignin [180].

Based on these results, the whole process comprises various cooperating processes, i.e. a low degree of chemical sorption and a predominance of physisorption, such as hydrogen bonding, electrostatic, and van der Waals interactions. Experimentally confirmed that the estimated bnding enthalpies accurately mirrored adsorption capabilities. In addition, theoretical studies demonstrated the significance of hydrophobic interactions in MG adsorption process. Considering that the entropy governs by the hydrophobic effects, these findings validate the parameters of thermodynamics obtained from the Van't Hoff equation [180].

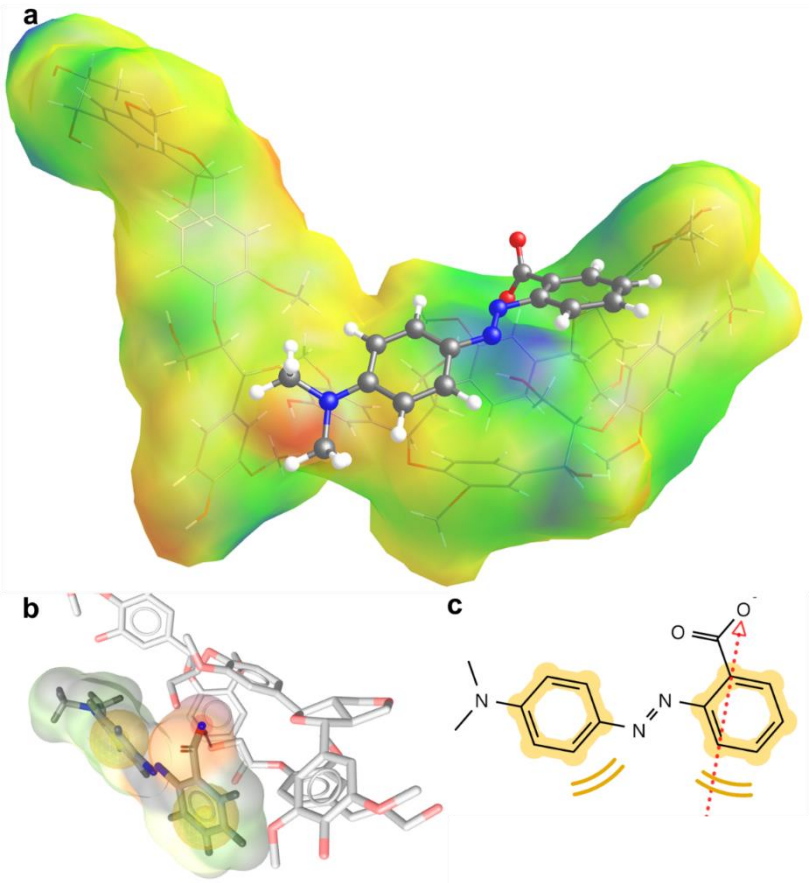

Figure 34: a) The lowest-energy complex between lignin and Malachite Red. The adsorbent MEP surface. Blue marked presents regions with negative potential while red marked regions with positive potential; b) methyl red/lignin complex investigated with pharmacophore approach. Yellow spheres marked hydrophobic interactions of MG and red arrows marked HBA interactions with the environment. The ligand surface is dyed by atom bindng tendency contribution; c) 2D displays of ligand pharmacophores[180].

4.7.8. PSDM modeling and Bed Column study (BCS)

A Bed Column study was conducted using b-LMS to expand the batch system's results and assess the utilization of the prepared adsorbent. The alternate method for determining adsorption capacity was based on the breakthrough curve area multiplied by the number of bed volumes until the effluent concentration met the regulatory minimum. The breakthrough point analysis was defined and standardized by a legislative document: ,,Decree on limit values for the emission of pollutants into water and deadlines for their achievement'' Sl. RS Gazette, no. 67/2011, 48/2012 and 1/2016. This document defined the maximum values of some parameters: Chemical oxygen demand = 200 mg O_2 dm^{-3}; Biochemical oxygen demand = 30 mg O_2 dm^{-3} and Total organic carbon = 60 mg dm^{-3}. The flow rates (Q) of 0.5, 1.0, and 1.5 cm^3 min^{-1} were used to collect a predetermined volume of effluent

model water. The fitting data results for Bohart-Adams (B-A), Yoon-Nelson (Y-N), and Thomas models are shown in Tables 23 and 24. The B-A model applies to one-component systems in which kinetics of adsorption dominate the whole process, i.e. other process parameters have minor influence. All models were fitted using a non-linear function with the goal of obtaining equation parameters with a minimum sum of squares (Table 28) [46,180].

Table 23. Yoon-Nelson, Thomas and Bohart-Adams model fitting for MG and T

			Malachite green			Tartrazine		
Model	Q	$cm^3\ min^{-1}$	0.5	1	1.5	0.5	1	1.5
B-A	k_{BA}	$dm^3\ mg^{-1}\ min^{-1}$	0.030	0.054	0.075	0.039	0.067	0.892
	q_o	$mg\ g^{-1}$	98.10	89.87	81.38	76.06	71.35	65.49
	R^2		0.997	0.996	0.996	0.994	0.997	0.998
Y-N	k_{YN}	min^{-1}	0.059	0,054	0,050	0.077	0.067	0.069
	θ	min	129.46	118.63	107.42	100.401	94.186	86.458
	R^2		0.997	0.996	0.996	0.994	0.997	0.998
Thomas	k_{Th}	$cm^3\ min^{-1}\ mg^{-1}$	0,059	0,054	0,049	0.077	0.067	0.056
	q_o	$mg\ g^{-1}$	98.08	90.77	82.19	76.06	71.35	65.59
	R^2		0.997	0.996	0.996	0.994	0.997	0.998

Table 24. Yoon-Nelson, Thomas and Bohart-Adams model fitting for MR

Model	Q	$cm^3\ min^{-1}$	0.5	1	1.5
B-A	k_{BA}	$dm^3\ mg^{-1}\ min^{-1}$	0.035	0.069	0.101
	q_o	$mg\ g^{-1}$	62.62	57.19	52.08
	R^2		0.998	0.997	0.998
Y-N	k_{YN}	min^{-1}	0.070	0.070	0.067
	θ	min	81.11	74.741	68.740
	R^2		0.998	0.997	0.998
Thomas	k_{Th}	$cm^3\ min^{-1}\ mg^{-1}$	0.070	0.069	0.067
	q_o	$mg\ g^{-1}$	46.08	42.47	39.06
	R^2		0.998	0.997	0.998

This investigation also demonstrated the well-known fact that an increase in flow rate results in a large reduction in adsorption capacity. Increasing flow rate or reducing EBCT decreases capacity of adsorption proportionally: 81.38, 65.49, and 52.08 $mg\ g^{-1}$ za for MG, T, and MR, respectively (Tables 28 and 29).

PSDM modeling was used for a small bed column study packed with b-LMS to derived realistic results without leading pilot experiments. Obtained results are presented in Figure 35. The boundary conditions are determined by Gnielinski equation: $Re \times Sc > 500$; $0.6 \leq Sc \leq 104$; $1 \leq Re < 100$; $0.26 < \varepsilon < 0.935$ [209]. Fitting results, from Freundlich model are K: K_f = 22.1, 14.34 and 16.28 $(mol^{1-n})(L^n\ g^{-1})$ and $n^{-1} \approx 0.540$, 0.490 and 0.521 for MG, MR and T, respectively. Determined porosity is 3.37,

and coefficient pore diffusion (D_p) of 10.7, $8.72 \cdot 10^{-8}$ and 11.1 $m^2\ s^{-1}$ for MG, MR and T as well as Biot number (*Bi*) of 71.5 – 131.6, 75.7 – 139.9 and 70.7 – 130.2 for MG, MR and T, respectively, which indicated that the domination of resistance in internal mass transport. According to this findings, It was defined that when Bi > 20, the intra-particle diffusion controlled for overall mass transport. [209], [180]

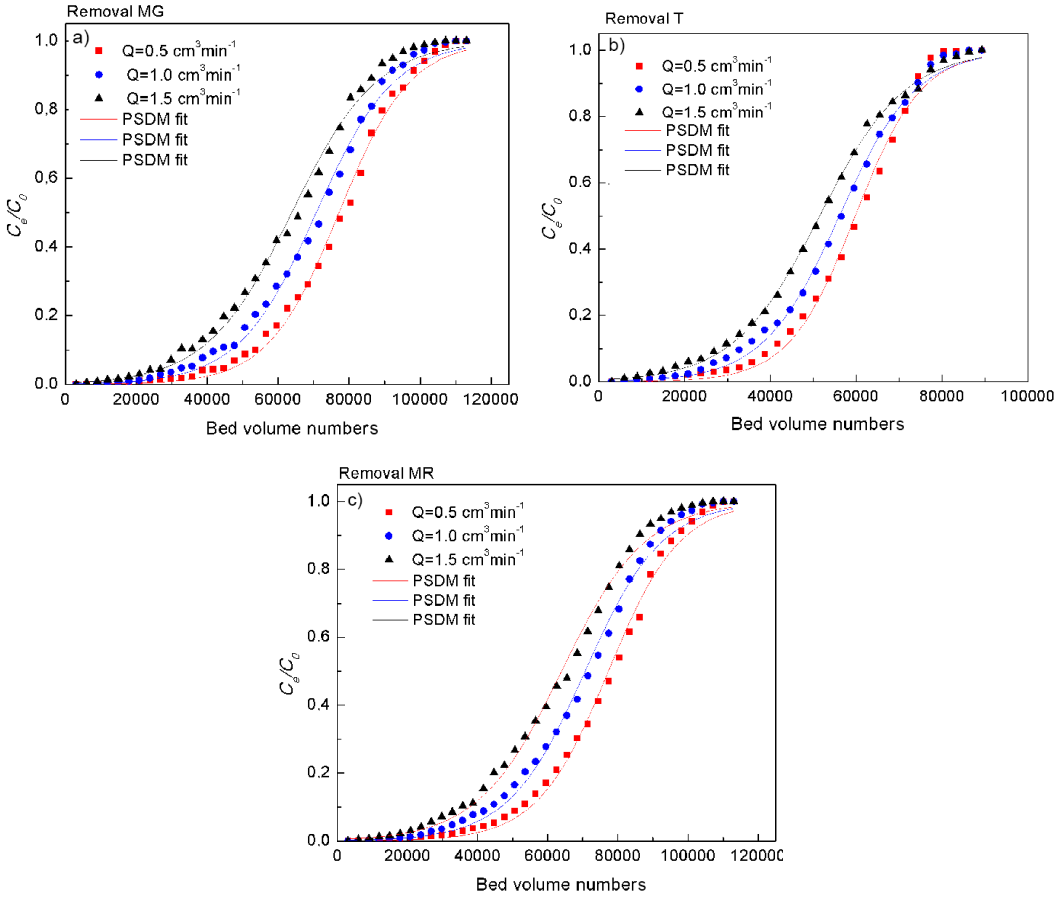

Figure 35. Breakthrough curve for a) MG, b) T, c) MR obtained using PSDM modeling [180]

4.7.9. b-LMS sample regeneration in a flow system

The application of synthesized b-LMS was assessed based on the following output parameters: kinetics, selectivity, uptake of adsorption, integrity/stability, and duration of use. Usage is the effective operating time, i.e. the number of successive adsorption/desorption cycles, after which the utilization of the sorbent is no longer economically feasible. The utilized material might be recycled or disposed of in a landfill (non-hazardous material). A desorption investigation was conducted to determine whether the requirements for achieving a low degree of adsorbent degradation were met throughout successive adsorption/desorption cycles. The selection of the desorption agent is controlled by several factors such as adsorption mechanism, pollutant chemistry (geometrical and electronic features) and surface properties. The choice of operating factors – concentration, pH, regenerator, flow rate, and desorption time - determines a practically relevant procedure. An upward flow fixed-bed column desorption investigation was chosen as a more practical technique [180].

Typically, acid or base substances were used in regeneration process. The most effective desorption substances were determined to be 0.2 mol dm^{-3} HCl for MG and MR and 2 wt. % of NaOH/2 wt. % NaCl for T. The findings of adsorption and desorption are presented in Table 9. Also, sodium acetate and trisodium citrate were shown as excellent desorbents, but their impact on increased COD in effluent water led to their exclusion from future investigation [180].

Decreasing trend efficiency of desorption was obtained and presented at Table 25: from 95.0% to 94.1% for T dye (82.8%) and 94.2 % to 93.2% for MG (overall 80.3%) from 1th to 5th desorption cycle. Also, a similar investigation was conducted for MR, where the desorption efficiacy decrease from 93.8 % (1st) to 92.9 % (5th) for MR dye (overall 79.8 %). Because adsorbate/adsorbent surface intearction are weak, regeneration is a possible procedure. Due to electrostatic repulsion, the anionic regenerator displaces the loosely attached T dye with prominent anionic characteristics (resulting from carboxylate anion and two sulfonic groups). For both MG and MR, similar process is at work: electrostatic repulsion with positive surface of adsorbent, and for the latter, in addition owing to protonation of the dimethylamino group. It is implies that labile bonds are a primary need for desorption capability. After the 10th cycle, there is a comparable decline in desorption efficiency: 92.5% for T, 91.7% for MG and 91.2 % for MR. In contrast to hydrolytically aggressive desorbents, which likely exert a limited amount of ester bond hydrolysis, the regeneration of b-LMS would be more favorable with 4% NaCl to use a mild-medium. As a consequence of applying a moderate nucleophile and using 4% NaCl, the desorption efficiency of T (after 5th cycle) was reduced to 74.6 %. Also, a greater flow rate effect on the desorption efficiacy decrease was observed (1th cycles): 86.8% and 94.3% for MG. In a future investigation, the cost-effective vs regeneration efficiacy will be evaluated. In summary, the suggested optimum approach for b-LMS synthesis resulted in porous material with surface functionalities capable of forming weak bindings with dye, readily breaking by the used desorbent [180].

Table 25: The five adsorption/desorption cycles of the MG and T using b-LMS at following desorption condition: (Q = 3.0 cm^3 min^{-1}; m_{ads} = 1.32 g (MG) and 1.28 g (T); C_i(MG) = C_i(T) = 20 mg dm^{-3}) using 0.2 mol dm^{-3} HCl and 2% NaOH/2% NaCl for MG and T, respectively (V = 150 cm^3)

Adsorbate	MG				T			
	I	III	V	Σ[4]	I	III	V	Σ
Adsorption (mg g^{-1})[1]	98.10	91.32	84.49		76.06	71.68	66.92	
Volume of feed water[2] (L)	6.47	6.03	5.58		4.87	4.59	4.28	
Desorption (mg g^{-1})[1]	92.42	85.66	78.74		72.26	67.67	62.97	
C (ppm) [3]	813.3	753.9	692.9		616.6	577.5	537.3	
Δq (mg g^{-1}) [4]	5.68	5.76	5.75	17.2	3.8	4.0	3.95	11.8

[1] quantity of desorbed pollutants; [2] feed water volume to attain breakthrough point (dm^3); [3] pollutant concentration in effluent water; [4] quantity of the bonded pollutants after nth cycle and overall amount after five cycles. [180]

In order to prevent the formation of waste, the following experiments were performed (as example MG is used): [180]

a) adsorption (flow system, C_i = 0.5 mg l^{-1}, Q = 1 cm^3 min^{-1} V = 5 dm^3, q_e = 4 mg $g^{-1,}$ m = 0.6 g,);

b) desorption (regenerator 0.3 mol dm^{-3} HCl, , Q = 3 cm^3 min^{-1}, V = 0.1 dm^{-3})

c) photocatalytic degradation [210], i.e. photo-Fenton: m(TiO_2 – Degussa P25

It indicates that implementing the 3-step method might be acquired quality of water ready to be released into the water pathway. Because of produced nitrate ion, a shortfall in water quality was remedied by application of Amberlite IRA 900-Cl to achieve >90% removal. In this manner, the water purification loop was completed without negative environmental influence, while adhering to sustainable development ideals and actual requirements [180].

4.8. Cation and cationic dye removal by b-LMS-OSO_3H

In order to increase time of b-LMS application or to overcome its limited adsorption capacity for cations, b-LMS was changed using chlorosulfonic acid to add a sulfate group. It is well-known that these groups may coordinate cationic contaminants [211]. In addition, Pb^{2+} and Ni^{2+} removal utilizing b-LMS-OSO_3H was investigated. Tables 26 and 27 and Figure 36 showed the adsorption data and those obtained at three different temperatures utilized for computation of thermodynamic parameters. Even at lower initial pollutant concentrations, high adsorption capabilities with regard to both cations were found. Using a larger C_i for Pb^{2+} (100 mg dm^{-3}) results in greater adsorption capacity: 310 mg/g, which is close to the saturation threshold based on the concentration of sulfonic groups in b-LMS-OSO_3H. Also found was a high q_e for MG (364 mg/g; C_i = 20 ppm) [180].

Table 26. Adsorption isotherms non-linear parameters for Ni^{2+} and Pb^{2+} removal on b-LMS-OSO_3H ($C_{i[Ni^{2+}]}$ = $C_{i[Pb^{2+}]}$ = 10.0 mg dm^{-3}; m/V= 100-1000 mg dm^{-3})

Isotherm model	Ion	Ni^{2+}			Pb^{2+}		
	Temperature	25 °C	35 °C	45 °C	25 °C	35 °C	45 °C
Langmuir	q_m (mg g^{-1})	52.8	51.1	49.3	137.1	126.3	117.3
	K_L (dm^3 mg^{-1})	1.543	1.526	1.515	1.082	1.068	1.060
	K_L (dm^3 mol^{-1})	90558.7	89560.9	88915.3	224190.4	221289.6	219632
	χ^2	4.446	4.275	4.096	8.452	11.504	14.808
	F Value	301.1	302.5	304.2	670.2	470.5	349.0
	R^2	0.969	0.968	0.970	0.988	0.982	0.976
Freundlich	K_F (mg g^{-1})(dm^3 mg^{-}	29.6	28.4	27.1	67.4	60.6	55.3
	n	1.926	1.948	1.974	1.621	1.676	1.729
	χ^2	0.0117	0.0197	0.03097	0.144	0.643	1.841
	F Value	115571	66061	40557	39414	8455	2825
	R^2	0.999	0.999	0.999	0.999	0.999	0.997

Table 27. The thermodynamic parameters of Ni^{2+} and Pb^{2+} adsorption on b-LMS-OSO_3H ($C_{i[Ni^{2+}]}$ = $C_{i[Pb^{2+}]}$ = 10.0 mg dm^{-3}; m/V= 100-1000 mg dm^{-3})

Ion	ΔG^{Θ} (kJ mol^{-1})			ΔH^{Θ} (kJ mol^{-1})	ΔS^{Θ} (J mol^{-1} K^{-1})	R^2
	298 K	308 K	318 K			
Ni^{2+}	-38.85	-40.13	-41.41	-0.73	127.87	0.989
Pb^{2+}	-37.97	-39.21	-40.47	-0.79	124.72	0.979

Contrary to b-LMS, the thermodynamic characteristics reported for b-LMS-OSO3H showed mostly physical interactions between both cations. It seems that ion exchange predominates in removing Ni^{2+} and Pb^{2+} using b-LMS-OSO_3H, as stated for commercial cation exchange resin (https://lenntech.com/). In contrast to the cooperative process, i.e. the involvement of electrostatic attraction, hydrogen bonding interaction, and π-π interactions, which applies to b-LMS adsorption b-LMS-OSO_3H removes cations largely by ion exchange. The bonding of Pb^{2+} and MG to b-LMS-OSO_3H was shown by FTIR analysis: the primary change in peak intensities occurred at 1059 and 984 cm^{-1}, corresponding to *ν*S=O and *ν*S–O, respectively. In addition, the presence of substantial peaks in the regions 1585-1366 and 833-750 cm^{-1} verifies the attachment of MG to b-LMS-OSO_3H. (Figure 37) [180].

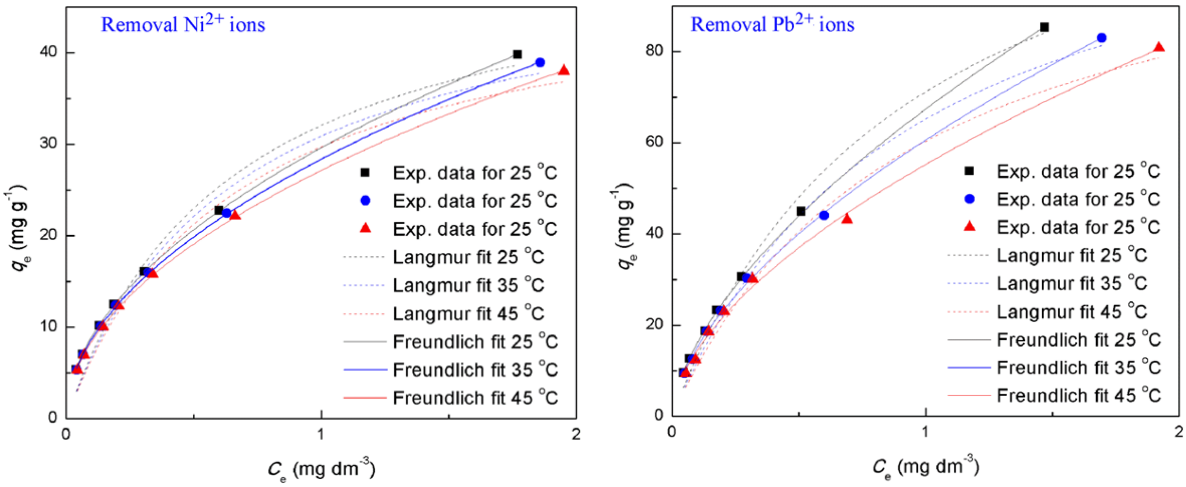

Figure 36: Langmuir model plots of adsorption of Ni^{2+} and Pb^{2+} ions obtained at 298, 308 and 318 K using b-LMS-OSO_3H adsorbent [180]

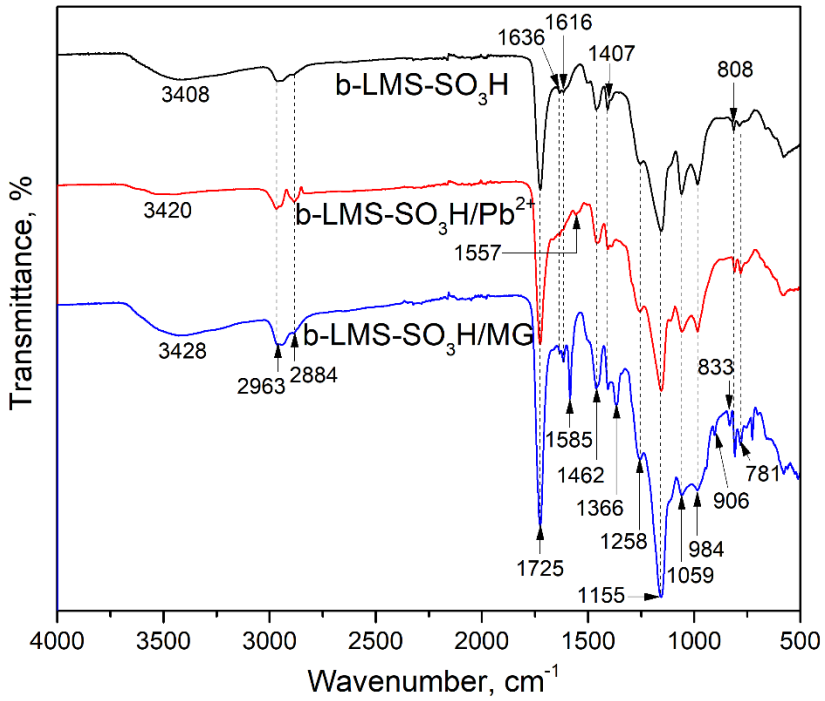

Figure 37. FTIR spectra of b-LMS-OSO_3H**,** b-LMS-OSO_3H/Pb^{2+} and b-LMS-OSO_3H/MG [180]

4.9. Applicability of b-LMS and b-LMS-OSO_3H in multi-component model of water

Competing ions considerably reduce the adsorption process efficiency, i.e. selective sorption of the target ion is diminished. Thus, competitive adsorption was carried out to determine the tendency of b-LMS and b-LMS-OSO_3H for various water contaminants relative to the applied dyes. Multiple-component water media, including molecules, organic colloids, ions, and inorganic particles, significantly increase the likelihood of system fouling due to the interference of competing ions. Conceptually, it was required to incorporate a variety of pollutants with diverse properties (structure, electronic properties, geometry, radius/charge ratio) to establish the correct relationship between adsorption efficiency of pollutant and pollutant/adsorbent bonding processes. Existing contaminants with particular electronic characteristics, i.e. affinity to b-LMS and b-LMS-OSO_3H, may form interactions of varying strengths with surface functions. Consequently, their involvement and existence in the entire competitive system were investigated [180].

In this work we used the model water sample to achieve the most applicable adsorption findings for real-world wastewater. In this instance, a simulation of mine effluent containing organic dyes was used in this investigation [180,212]. All collected effluent water samples was analyzed by atomic absorption spectrometry (AAS) using Perkin Elmer PinAAcle 900T instrument. The findings of the competitive dye removal in a column system are shown in Table 28.

Table 28. The competitive dyes removal from model wastewater (flow rate of 1.0 cm^3 min^{-1} and m_{ads} of 1.88 g)

Before wastewater treatment		After wastewater treatment			
		b-LMS		b-LMS-OSO_3H	
Ions	C_i, mg dm^{-3}	C_e, mg dm^{-3}	Removal %	C_e, mg dm^{-3}	Removal %
Pb^{2+}	16.4	11.1	32.3	3.1	81
Cu^{2+}	122.1	108.4	11.2	88.2	27.8
Ca^{2+}	254	223.5	12	189	25.6
Mn^{2+}	14.8	11.5	22.3	6.2	58.1
Cd^{2+}	9.6	6.9	28.1	1.8	81.3
Ni^{2+}	17.9	14.8	17.3	3.1	82.7
Zn^{2+}	44.6	38.5	13.7	22.7	49.1
Cr(VI)	0.56	0	100	0.53	5.3
As(V)	11.5	8.2	28.7	11.4	0.86
Cl^-	138	132	3.6	138	0
MG	20	5.2	74	0.4	98
T	20	7.1	64.5	19.9	0.5

(pH was set to 6.3; model water solution was 6 L)

Due to its functionality, the b-LMS demonstrated adequate nonselective capability for the removal of contaminants under competitive settings. b-LMS has a greater affinity for organic contaminants, while b-LMS-OSO_3H mostly removes cations or positive dyes. In the context of textile industry effluent, it is intriguing to examine selectivity towards another structurally similar compounds. Changes in selectivity caused by the sulfonation of b-LMS to produce b-LMS-OSO_3H may represent an interesting phenomenon. We have noticed two major trends:

a) poor selectivity of b-LMS concerning cations, oxyanions, and positively or negatively charged dye molecules; and

b) good selectivity of b-LMS-OSO_3H about cations and positively charged dyes.

Results showed the excellent applicability of both b-LMS and b-LMS-OSO_3H in actual water purification procedures. The results of an adsorption analysis of chosen dyes provided further evidence of the flexibility of b-LMS. Using b-LMS-OSO_3H for Methylene blue removal resulted in 188.4 mg/g capacity (initial concentration - 20 ppm at pH 6). Generally, an abundance of surface functional groups leads to strong adsorption capacities about certain pollutant attributes. Therefore, the b-LMS and b-LMS-OSO_3H may be extensively used in a flow system for wastewater treatment or production of drinking water, especially in the pesticide and textile industries, attaining water quality in compliance with current regulations [180]

5. CONCLUSION

This doctoral dissertation examined the possibility of applying lignin-based microspheres to remove dyes from water by the adsorption process. Firstly, procedure for synthesis of lignin microspheres modified with acrylic acid was applied, and then synthesis with acrylic crosslinkers from natural sources, trimethylpropane triacrylate (TMPTA), was optimized. Acrylic kraft lignin (KfL-AA) synthesized from kraft lignin by modification with acrylic acid was further modified with diethyleneglycol dimethacrylate (DEGDMA) acrylic crosslinker. On obtained lignin microspheres (LMS-DEGDMA) laccase Novozyme® 51003 was immobilized, and then used to remove textile dyes. Porous microspheres (b-LMS) were obtained by reacting of acrylic modified kraft lignin (Kf-AA) with acrylic reactant TMPTA. By reacting of b-LMS with chlorosulfonic acid b-LMS-OSO_3H microspheres are produced. b-LMS and b-LMS-OSO_3H were tested for the water adsorption of cations and cationic dyes. All produced b-LMS samples were structurally and morphologically characterized by instrumental characterization techniques.

The scientific contribution of this dissertation is in the following:

- The synthesized samples are based on raw materials from renewable sources, which resulted in ecological samples which are economically acceptable.
- Lignin microspheres were modified with diethyleneglycol dimethacrylate and trimethylpropanetriacrylate to obtain adsorbents with improved characteristics. Adsorption studies showed higher adsorptive performance, improved stability, and better regeneration performance compared to unmodified lignin. The introduction of a sulfate group into the structure of the microspheres resulted in higher sensitivity and better selectivity for cations and cationic dyes.
- After adsorption of textile dyes from water with b-LMS-OSO_3H, the success of the adsorption of pollutants was checked by FTIR spectroscopy. Change signal intensity at 1059 and 984 cm^{-1}, formation of additional peaks in the region 1585-1366 and 833-750 cm^{-1} was observed, which confirmed that binding of dyes had occurred.
- Experimental data from adsorption studies were fitted using kinetic, adsorption models, and thermodynamic adsorption parameters were also calculated. Results showed that the pseudo-second-order model best fits with the experimental data of all investigated systems. Positive values of ΔS for all samples represent the equilibrium state of the system's unpredictability. Negative levels of ΔG for all samples constitute spontaneous, effective adsorption
- The mechanism of adsorption was observed from a theoretical aspect and it can be concluded that the adsorption mechanism is affected by the charge of the analyte, i.e. if the analyte is protonated, positively charged will have a higher binding affinity.
- Applied quantum-mechanical calculations showed that their hydrophobic interaction is the main driving force behind binding malachite green and lignin.
- Bed column study shows that the experimental data fitted well with a non-linear function, which is the goal of obtaining equation parameters with a minimum sum of squares.
- PSDM modeling point out the dominance of resistance internal mass transport.
- The optimal conditions for laccase immobilization on the lignin microspheres-DEGDMA are determined: immobilization buffer pH 5.0, the initial enzyme concentration 100 mg/g, immobilization time is 1 h.

- Kinetics of laccase binding to lignin microspheres were investigated. Results showed that the activity of LMS-DEGDMA-laccase reaches a maximum of 283 IU/g of support as the initial enzyme concentration rises to 200 mg/g support. The maximum protein loading was obtained within 30 minutes, while the maximum activity was achieved after 2 h. The maximum specific activity of 6.42 IU/mg of bonded proteins and activity immobilization yield of 45 % was acquired when immobilization is carried out at initial enzyme concentrations of 55 mg/g of support, indicating that a high yield of attached enzyme molecules on LMS-DEGDMA occupy an active conformation.
- Degradation of Lanaset® violet B dye with LMS-DEGDMA-laccase showed efficiency of 90 % in 24 hours. Free laccase exhibited maximum efficiency of 45 %, while LMS-DEGDMA microspheres without enzyme adsorbed 42 % of dye for 24 h. So, it can be concluded that the laccase immobilization have a favorable effect on affinity of laccase for the decolorization of dye.
- Similar results (85 % decolorization efficiency) were obtained when LMS-DEGDMA-laccase was used to decolorize two more dyes Lanaset® blue 2R and C.I. Acid Green 40. One difference was observed during the decolorization process of these three dyes, namely in the duration of the decolorization process. The maximum decolorization efficiency was achieved for the decolorization of Acid Green 40 for only 45 minutes while in the case of Lanaset® violet B and blue 2R reaction times were 3 and 2 h, respectively. With respect to all present results for anthraquinone dyes decolorization with laccase immobilized preparation, it could be stated that the factors on which decolorization depended were incubation time and molecular structure of the dye.
- LMS-DEGDMA-laccase expressed good stability in the decolorization reaction since it may be applied for five repeated cycles in the decolorization of a mixture of three anthraquinone dyes with an efficiacy of 86 % in the 1^{th} to 65 % in the 5^{th} cycle.
- Desorption and reusability studies showed good regeneration ability. Decreasing trend of desorption efficiency was observed: from 95.0% to 94.1% for Tartrazine (82.8%) and 94.2 % to 93.2% for Malachite Green (overall 80.3%) from 1^{th} to 5^{th} desorption cycle. Also, a similar investigation was conducted for Methyl Red, where the efficiecy of desorption decreased from 93.8 % (1^{st}) to 92.9 % (5^{th}) for Methyl Red dye (overall 79.8 %).

Based on the above results, it can be concluded that the synthesized samples are ecological, biodegradable, and economically acceptable, per the principles of circular economy and sustainable development. In addition, they have proven to be effective and stable dye adsorbents, which can be a potential solution for water purification as a necessary tool for environmental protection.

6. REFERENCES

1. G. Sandin, G. M. Peters, *J Clean Prod* **184** (2018).
2. K. Roa, E. Oyarce, A. Boulett, M. ALSamman, D. Oyarzún, G. D. C. Pizarro, J. Sánchez, *Sustainable Materials and Technologies* **29** (2021).
3. A. L. Popovic, J. D. Rusmirovic, Z. Velickovic, Z. Radovanovic, M. Ristic, V. P. Pavlovic, A. D. Marinkovic, *Int J Biol Macromol* **156** (2020).
4. G. Z. Kyzas, D. N. Bikiaris, A. C. Mitropoulos, *Polym Int* **66** (2017).
5. D. N. Tran, K. J. Balkus, *ACS Catal* **1** (2011).
6. P. G. Wang, *Q Rev Biol* **73** (1998).
7. A. M. Girelli, M. L. Astolfi, F. R. Scuto, *Chemosphere* **244** (2020).
8. L. Alvarado-Ramírez, M. Rostro-Alanis, J. Rodríguez-Rodríguez, C. Castillo-Zacarías, J. E. Sosa-Hernández, D. Barceló, H. M. N. Iqbal, R. Parra-Saldívar, *Int J Biol Macromol* **181** (2021).
9. M. Chen, G. Zeng, C. Lai, J. Li, P. Xu, H. Wu, *RSC Adv* **5** (2015).
10. M. Culebras, H. Geaney, A. Beaucamp, P. Upadhyaya, E. Dalton, K. M. Ryan, M. N. Collins, *ChemSusChem* **12** (2019).
11. X. Guo, S. Zhang, X. quan Shan, *J Hazard Mater* **151** (2008).
12. S. Gillet, M. Aguedo, L. Petitjean, A. R. C. Morais, A. M. Da Costa Lopes, R. M. Łukasik, P. T. Anastas, *Green Chemistry* **19** (2017).
13. E. Adler, *Wood Sci Technol* **11** (1977).
14. H. Harmita, K. G. Karthikeyan, X. J. Pan, *Bioresour Technol* **100** (2009).
15. S. Laurichesse, L. Avérous, *Prog Polym Sci* **39** (2014).
16. F. G. Calvo-Flores, J. A. Dobado, *ChemSusChem* **3** (2010).
17. J. Andraos, *ACS Sustain Chem Eng* **6** (2018).
18. M. N. Collins, M. Nechifor, F. Tanasă, M. Zănoagă, A. McLoughlin, M. A. Stróżyk, M. Culebras, C. A. Teacă, *Int J Biol Macromol* **131** (2019).
19. G. Panzarasa, A. Osypova, J. Ribera, F. W. M. R. Schwarze, F. Quasso, G. Consolati, *J Polym Environ* **26** (2018).
20. A. J. Ragauskas, G. T. Beckham, M. J. Biddy, R. Chandra, F. Chen, M. F. Davis, B. H. Davison, R. A. Dixon, P. Gilna, M. Keller, P. Langan, A. K. Naskar, J. N. Saddler, T. J. Tschaplinski, G. A. Tuskan, C. E. Wyman, *Science (1979)* **344** (2014).
21. M. H. Sipponen, H. Lange, C. Crestini, A. Henn, M. Österberg, *ChemSusChem* **12** (2019).
22. B. Podkościelna, M. Goliszek, O. Sevastyanova, *New approach in the application of lignin for the synthesis of hybrid materials*, in *Pure and Applied Chemistry*, 2017.
23. A. Grossman, V. Wilfred, *Curr Opin Biotechnol* **56** (2019).
24. Y. Ge, L. Qin, Z. Li, *Mater Des* **95** (2016).

25. A. Duval, M. Lawoko, *React Funct Polym* **85** (2014).

26. D. Schorr, P. N. Diouf, T. Stevanovic, *Ind Crops Prod* **52** (2014).

27. N. E. El Mansouri, J. Salvadó, *Ind Crops Prod* **26** (2007).

28. L. Ramrakhiani, A. Halder, A. Majumder, A. K. Mandal, S. Majumdar, S. Ghosh, *Chemical Engineering Journal* **308** (2017).

29. S. Meseldzija, J. Petrovic, A. Onjia, T. Volkov-Husovic, A. Nesic, N. Vukelic, *Journal of Industrial and Engineering Chemistry* **75** (2019).

30. Y. Ge, Z. Li, *ACS Sustain Chem Eng* **6** (2018).

31. K. A. Taleb, J. D. Rusmirović, M. P. Rančić, J. B. Nikolić, S. Drmanić, Z. S. Veličković, A. D. Marinković, *Journal of the Serbian Chemical Society* **81** (2016).

32. M. Šciban, M. Brdar, *Kraft lignin as an adsorbent to remove heavy metal ions from water*, in *Lignin: Structural Analysis, Applications in Biomaterials and Ecological Significance*, 2014.

33. S. Babel, T. A. Kurniawan, *J Hazard Mater* **97** (2003).

34. Z. Song, W. Li, W. Liu, Y. Yang, N. Wang, H. Wang, H. Gao, *RSC Adv* **5** (2015).

35. Y. Li, M. Wu, B. Wang, Y. Wu, M. Ma, X. Zhang, *ACS Sustain Chem Eng* **4** (2016).

36. W. Zhan, L. Gao, X. Fu, S. H. Siyal, G. Sui, X. Yang, *Appl Surf Sci* **467–468** (2019).

37. J. D. Rusmirovic, N. Obradovic, J. Perendija, A. Umicevic, A. Kapidžic, B. Vlahovic, V. Pavlovic, A. D. Marinkovic, V. B. Pavlovic, *Environmental Science and Pollution Research* **26** (2019).

38. M. Kumari, C. U. Pittman, D. Mohan, *J Colloid Interface Sci* **442** (2015).

39. Q. Chen, J. Zheng, L. Zheng, Z. Dang, L. Zhang, *Chemical Engineering Journal* **350** (2018).

40. T. Malutan, R. Nicu, V. I. Popa, *Bioresources* **3** (2008).

41. Y. Zhang, S. Ni, X. Wang, W. Zhang, L. Lagerquist, M. Qin, S. Willför, C. Xu, P. Fatehi, *Chemical Engineering Journal* **372** (2019).

42. E. Larrañeta, M. Imízcoz, J. X. Toh, N. J. Irwin, A. Ripolin, A. Perminova, J. Domínguez-Robles, A. Rodríguez, R. F. Donnelly, *ACS Sustain Chem Eng* **6** (2018).

43. R. Saravanan, S. Karthikeyan, V. K. Gupta, G. Sekaran, V. Narayanan, A. Stephen, *Materials Science and Engineering C* **33** (2013).

44. O. Sevastyanova, B. Podkościelna, B. Gawdzik, M. Sobiesiak, A. Bartnicki, O. I. Poddubnaya, M. E. Lindström, A. M. Puziy, *Sorbents from kraft lignin: impact of the chemical modification on the thermal stability and porous structure*, in *EWLP-2014: 13th European Workshop on Lignocellulosics and Pulp*, 2014.

45. U. Schwetmann, R. M. Cornell, *Iron Oxides in the Laboratory: Preparation and Synthesis*, 2000.

46. K. Taleb, J. Markovski, M. Milosavljević, M. Marinović-Cincović, J. Rusmirović, M. Ristić, A. Marinković, *Chemical Engineering Journal* **279** (2015).

47. Z. Veličković, G. D. Vuković, A. D. Marinković, M. S. Moldovan, A. A. Perić-Grujić, P. S. Uskoković, M. D. Ristić, *Chemical Engineering Journal* **181–182** (2012).

48. M. A. Ahmed, S. M. Ali, S. I. El-Dek, A. Galal, *Mater Sci Eng B Solid State Mater Adv Technol* **178** (2013).

49. H. Qiu, S. Zhang, B. Pan, W. Zhang, L. Lv, *Chemical Engineering Journal* **232** (2013).

50. K. Taleb, J. Markovski, Z. Veličković, J. Rusmirović, M. Rančić, V. Pavlović, A. Marinković, *Arabian Journal of Chemistry* **12** (2019).

51. Ł. Klapiszewski, T. J. Szalaty, B. Kurc, M. Stanisz, A. Skrzypczak, T. Jesionowski, *Int J Mol Sci* **18** (2017).

52. V. K. Gupta, A. Fakhri, S. Agarwal, N. Sadeghi, *Int J Biol Macromol* **102** (2017).

53. L. Wang, C. Shi, L. Pan, X. Zhang, J. J. Zou, *Nanoscale* **12** (2020).

54. W. Zou, R. Han, Z. Chen, J. Shi, L. Hongmin, *J Chem Eng Data* **51** (2006).

55. Y. Wang, X. Zhang, X. He, W. Zhang, X. Zhang, C. Lu, *Carbohydr Polym* **110** (2014).

56. S. Chatterjee, A. Ja, A. Subramanian, S. Subramanian, *Journal of Industrial Pollution Control* **33** (2017).

57. X. Zhang, T. Wang, C. Jiang, F. Zhang, W. Li, Y. Tang, *Electrochim Acta* **187** (2016).

58. B. Podkościelna, O. Gordobil, A. V. Riazanova, G. Dobele, J. Labidi, M. E. Lindström, V. M. Gun'ko, O. Sevastyanova, *ChemistrySelect* **2** (2017).

59. B. Yu, Z. Chang, Y. Zhang, C. Wang, *Mater Chem Phys* **203** (2018).

60. J. Sameni, S. Krigstin, S. A. Jaffer, M. Sain, *Ind Crops Prod* **117** (2018).

61. D. Dax, M. S. Chávez, C. Xu, S. Willför, R. T. Mendonça, J. Sánchez, *Carbohydr Polym* **111** (2014).

62. C. Wang, H. Wang, G. Gu, *Carbohydr Polym* **182** (2018).

63. P. J. Strong, H. Claus, *Crit Rev Environ Sci Technol* **41** (2011).

64. M. L. Niku-Paavola, E. Karhunen, P. Salola, V. Raunio, *Biochem J* **254** (1988).

65. V. Madhavi, S. S. Lele, *Bioresources* **4** (2009).

66. D. Wesenberg, I. Kyriakides, S. N. Agathos, *White-rot fungi and their enzymes for the treatment of industrial dye effluents*, in *Biotechnol Adv*, 2003.

67. P. Baldrian, *FEMS Microbiol Rev* **30** (2006).

68. B. Viswanath, M. Subhosh Chandra, H. Pallavi, B. Rajasekhar Reddy, *Afr J Biotechnol* **7** (2008).

69. https://ultimate-mushroom.com/edible/345-lentinus-tigrinus.html, (n.d.).

70. U. Hölker, J. Dohse, M. Höfer, *Folia Microbiol (Praha)* **47** (2002).

71. M. A. Velázquez-Cedeño, A. M. Farnet, E. Ferré, J. M. Savoie, *Mycologia* **96** (2004).

72. C. F. Thurston, *Microbiology (N Y)* **140** (1994).

73. O. V. Morozova, G. P. Shumakovich, S. V. Shleev, Y. I. Yaropolov, *Appl Biochem Microbiol* **43** (2007).

74. R. A. Sheldon, *Adv Synth Catal* **349** (2007).

75. E. P. Cipolatti, M. J. A. Silva, M. Klein, V. Feddern, M. M. C. Feltes, J. V. Oliveira, J. L. Ninow, D. De Oliveira, *J Mol Catal B Enzym* **99** (2014).

76. A. Kunamneni, F. Plou, A. Ballesteros, M. Alcalde, *Recent Pat Biotechnol* **2** (2008).

77. A. Givaudan, A. Effosse, D. Faure, P. Potier, M. L. Bouillant, R. Bally, *FEMS Microbiol Lett* **108** (1993).

78. N. Jimenez-Juarez, R. Roman-Miranda, A. Baeza, A. Sánchez-Amat, R. Vazquez-Duhalt, B. Valderrama, *J Biotechnol* **117** (2005).

79. M. E. Arias, M. Arenas, J. Rodríguez, J. Soliveri, A. S. Ball, M. Hernández, *Appl Environ Microbiol* **69** (2003).

80. F. Xu, W. Shin, S. H. Brown, J. A. Wahleithner, U. M. Sundaram, E. I. Solomon, *Biochimica et Biophysica Acta - Protein Structure and Molecular Enzymology* **1292** (1996).

81. C. Eggert, U. Temp, K. E. L. Eriksson, *Appl Environ Microbiol* **62** (1996).

82. T. Suzuki, K. Endo, M. Ito, H. Tsujibo, K. Miyamoto, Y. Inamori, *Biosci Biotechnol Biochem* **67** (2003).

83. K. L. Min, Y. H. Kim, Y. W. Kim, H. S. Jung, Y. C. Hah, *Arch Biochem Biophys* **392** (2001).

84. J. A. Wahleithner, F. Xu, K. M. Brown, S. H. Brown, E. J. Golightly, T. Halkier, S. Kauppinen, A. Pederson, P. Schneider, *Curr Genet* **29** (1996).

85. D. S. Yaver, F. Xu, E. J. Golightly, K. M. Brown, S. H. Brown, M. W. Rey, P. Schneider, T. Halkier, K. Mondorf, H. Dalbøge, *Appl Environ Microbiol* **62** (1996).

86. D. A. Wood, *J Gen Microbiol* **117** (1980).

87. H. A. Ernst, L. J. Jørgensen, C. Bukh, K. Piontek, D. A. Plattner, L. H. Østergaard, S. Larsen, M. J. Bjerrum, *PLoS One* **13** (2018).

88. K. Piontek, M. Antorini, T. Choinowski, *Journal of Biological Chemistry* **277** (2002).

89. N. Zouari, J. L. Romette, D. Thomas, *Appl Biochem Biotechnol* **15** (1987).

90. M. M. Rodríguez-Delgado, G. S. Alemán-Nava, J. M. Rodríguez-Delgado, G. Dieck-Assad, S. O. Martínez-Chapa, D. Barceló, R. Parra, *TrAC - Trends in Analytical Chemistry* **74** (2015).

91. N. Durán, M. A. Rosa, A. D'Annibale, L. Gianfreda, *Enzyme Microb Technol* **31** (2002).

92. F. J. Enguita, L. O. Martins, A. O. Henriques, M. A. Carrondo, *Journal of Biological Chemistry* **278** (2003).

93. L. Arregui, M. Ayala, X. Gómez-Gil, G. Gutiérrez-Soto, C. E. Hernández-Luna, M. Herrera De Los Santos, L. Levin, A. Rojo-Domínguez, D. Romero-Martínez, M. C. N. Saparrat, M. A. Trujillo-Roldán, N. A. Valdez-Cruz, *Microb Cell Fact* **18** (2019).

94. A. E. Palmer, D. W. Randall, F. Xu, E. I. Solomon, *J Am Chem Soc* **121** (1999).

95. I. Matera, A. Gullotto, S. Tilli, M. Ferraroni, A. Scozzafava, F. Briganti, *Inorganica Chim Acta* **361** (2008).

96. P. Giardina, V. Faraco, C. Pezzella, A. Piscitelli, S. Vanhulle, G. Sannia, *Cellular and Molecular Life Sciences* **67** (2010).

97. M. Alcalde, *Laccases: Biological functions, molecular structure and industrial applications*, in *Industrial Enzymes: Structure, Function and Applications*, 2007.

98. E. I. Solomon, U. M. Sundaram, T. E. Machonkin, *Chem Rev* **96** (1996).

99. M. M. Atalla, H. K. Zeinab, R. H. Eman, A. Y. Amani, A. A. E. A. Abeer, *Saudi J Biol Sci* **20** (2013).

100. S. Sondhi, P. Sharma, S. Saini, N. Puri, N. Gupta, *PLoS One* **9** (2014).

101. C. Johannes, A. Majcherczyk, A. Hüttermann, *J Biotechnol* **61** (1998).

102. S. Ilyas, A. Rehman, *Iranian J Environ Health Sci Eng* **10** (2013).

103. B. Viswanath, B. Rajesh, A. Janardhan, A. P. Kumar, G. Narasimha, *Enzyme Res* **2014** (2014).

104. R. C. Minussi, G. M. Pastore, N. Durán, *Trends Food Sci Technol* **13** (2002).

105. F. Xu, *Biochemistry* **35** (1996).

106. D. M. Mate, M. Alcalde, *Microb Biotechnol* **10** (2017).

107. R. C. Minussi, M. A. Miranda, J. A. Silva, C. V. Ferreira, H. Aoyama, S. Marangoni, D. Rotilio, G. M. Pastore, N. Durán, *Afr J Biotechnol* **6** (2007).

108. T. González, M. C. Terrón, S. Yagüe, E. Zapico, G. C. Galletti, A. E. González, *Rapid Communications in Mass Spectrometry* **14** (2000).

109. A. Majcherczyk, C. Johannes, A. Hüttermann, *Enzyme Microb Technol* **22** (1998).

110. M. Alcalde, M. Ferrer, F. J. Plou, A. Ballesteros, *Trends Biotechnol* **24** (2006).

111. M. Hartmann, X. Kostrov, *Chem Soc Rev* **42** (2013).

112. M. Fernández-Fernández, M. Á. Sanromán, D. Moldes, *Biotechnol Adv* **31** (2013).

113. M. H. Penner, *Expression And Measurement Of Enzyme Activity*, in *Handbook of Food Analytical Chemistry*, 2005.

114. R. C. Rodrigues, C. Ortiz, Á. Berenguer-Murcia, R. Torres, R. Fernández-Lafuente, *Chem Soc Rev* **42** (2013).

115. C. Mateo, J. M. Palomo, G. Fernandez-Lorente, J. M. Guisan, R. Fernandez-Lafuente, *Enzyme Microb Technol* **40** (2007).

116. R. A. Sheldon, S. van Pelt, *Chem Soc Rev* **42** (2013).

117. H. T. Imam, P. C. Marr, A. C. Marr, *Green Chemistry* **23** (2021).

118. T. Jesionowski, J. Zdarta, B. Krajewska, *Adsorption* **20** (2014).

119. N. R. Mohamad, N. H. C. Marzuki, N. A. Buang, F. Huyop, R. A. Wahab, *Biotechnology and Biotechnological Equipment* **29** (2015).

120. Y. A. Rodríguez-Restrepo, C. E. Orrego, *Environ Chem Lett* **18** (2020).

121. S. Datta, R. Veena, M. S. Samuel, E. Selvarajan, *Environ Chem Lett* **19** (2021).

122. B. Li, L. Zhao, H. Chen, D. Sun, B. Deng, J. Li, Y. Liu, F. Wang, *PLoS One* **11** (2016).

123. G. M. Shaul, T. J. Holdsworth, C. R. Dempsey, K. A. Dostal, *Chemosphere* **22** (1991).

124. H. Forootanfar, A. Moezzi, M. Aghaie-Khouzani, Y. Janlou, F. Niknejad, M. A. Faramarzi, *Res J Chem Environ* **17** (2013).

125. R. D. Saini, *International Journal of Chemical Engineering Research* **9** (2017).

126. A. Gürses, M. Açıkyıldız, K. Güneş, M. S. Gürses, *A. Gürses et al., Dyes and Pigments, SpringerBriefs in Green Chemistry for Sustainability* (2016).

127. A. Kumar, U. Dixit, K. Singh, S. Prakash Gupta, M. S. Jamal Beg, *Structure and Properties of Dyes and Pigments*, in *Dyes and Pigments - Novel Applications and Waste Treatment*, 2021.

128. T. Chairin, T. Nitheranont, A. Watanabe, Y. Asada, C. Khanongnuch, S. Lumyong, *Appl Biochem Biotechnol* **169** (2013).

129. T. Kenzom, P. Srivastava, S. Mishra, *Appl Environ Microbiol* **80** (2014).

130. W. Przystaś, E. Zabłocka-Godlewska, E. Grabińska-Sota, *Brazilian Journal of Microbiology* **49** (2018).

131. B. Legerská, D. Chmelová, M. Ondrejovič, *J Biotechnol* **285** (2018).

132. S. Sharma, A. Kaur, *Indian J Sci Technol* **11** (2018) 1–21.

133. V. J. Inglezakis, S. G. Poulopoulos, *Elsevier Science B V* (2006).

134. G. Newcombe, *Adsorption from aqueous solutions: Water purification*, in *Adsorption by Carbons*, 2008.

135. M. Králik, *Chemical Papers* **68** (2014).

136. M. Iqbal, N. Iqbal, I. A. Bhatti, N. Ahmad, M. Zahid, *Ecol Eng* **88** (2016).

137. J. N. Miller, J. M. Miller, *Pearson Education Limited* (2010).

138. M. A. Al-Ghouti, D. A. Da'ana, *J Hazard Mater* **393** (2020).

139. T. W. Weber, R. K. Chakravorti, *AIChE Journal* **20** (1974).

140. I. Langmuir, *J Am Chem Soc* **39** (1917).

141. K. I. Aika, A. Ozaki, *J Catal* **19** (1970).

142. F. Ghaznavi, S. Fatemi, M. Joda, W. J. Weber, J. C. Morris, S. Y. Elovich, G. M. Zhabrova, H. M. F. Freundlich, A. R. Khan, R. Ataullah, A. AlHaddad, S. Lagergren, I. Langmuir, R. Sips, J. Toth, *J Chem Phys* **24** (1971).

143. C. H. Liu, Y. H. Chuang, T. Y. Chen, Y. Tian, H. Li, M. K. Wang, W. Zhang, *Environ Sci Technol* **49** (2015).

144. J. Wang, X. Guo, *J Hazard Mater* **390** (2020).

145. S. Fan, Y. Wang, Z. Wang, J. Tang, J. Tang, X. Li, *J Environ Chem Eng* **5** (2017).

146. L. Dolatyari, M. R. Yaftian, S. Rostamnia, *J Environ Manage* **169** (2016).

147. F. C. Wu, R. L. Tseng, R. S. Juang, *Chemical Engineering Journal* **150** (2009).

148. L. Largitte, R. Pasquier, *Chemical Engineering Research and Design* **109** (2016).

149. S. Nethaji, A. Sivasamy, A. B. Mandal, *International Journal of Environmental Science and Technology* **10** (2013).

150. J. Wang, X. Guo, *Chemosphere* **258** (2020).

151. K. Pantić, Z. J. Bajić, Z. S. Veličković, J. Z. Nešić, M. B. Đolić, N. Z. Tomić, A. D. Marinković, *Environmental Science and Pollution Research* **26** (2019).

152. M. Zheng, C. Xu, H. Hu, Z. Ye, X. Chen, *RSC Adv* **6** (2016).

153. Q. Huang, M. Liu, J. Zhao, J. Chen, G. Zeng, H. Huang, J. Tian, Y. Wen, X. Zhang, Y. Wei, *Appl Surf Sci* **427** (2018).

154. L. Sellaoui, M. Bouzid, L. Duclaux, L. Reinert, S. Knani, A. Ben Lamine, *RSC Adv* **6** (2016).

155. L. Sellaoui, G. L. Dotto, J. O. Gonçalves, L. A. A. Pinto, S. Knani, A. Ben Lamine, *J Mol Liq* **222** (2016).

156. G. Alberti, V. Amendola, M. Pesavento, R. Biesuz, *Coord Chem Rev* **256** (2012).

157. H. C. Thomas, *J Am Chem Soc* **66** (1944).

158. Y. H. Yoon, J. H. Nelson, *Am Ind Hyg Assoc J* **45** (1984).

159. G. S. Bohart, E. Q. Adams, *J Am Chem Soc* **42** (1920).

160. R. M. Clark, *Environ Sci Technol* **21** (1987).

161. M. Ghasemi, A. R. Keshtkar, R. Dabbagh, S. Jaber Safdari, *J Hazard Mater* **189** (2011).

162. Z. Aksu, F. Gönen, *Process Biochemistry* **39** (2004).

163. A. Aichour, H. Zaghouane-Boudiaf, F. B. Mohamed Zuki, M. Kheireddine Aroua, C. V. Ibbora, *J Environ Chem Eng* **7** (2019).

164. E. B. Simsek, D. Duranoglu, U. Beker, *Separation Science and Technology (Philadelphia)* **47** (2012).

165. G. Athanasaki, L. Sherrill, K. D. Hristovski, *Environ Sci (Camb)* **1** (2015).

166. D. Yan, D. D. Gang, N. Zhang, L. Lin, *Journal of Environmental Engineering* **139** (2013).

167. J. C. Crittenden, N. J. Hutzler, D. G. Geyer, J. L. Oravitz, G. Friedman, *Water Resour Res* **22** (1986).

168. D. W. Hand, J. C. Crittenden, D. R. Hokanson, J. L. Bulloch, *Water Science and Technology* **35** (1997).

169. A. Goudarzi, L. T. Lin, F. K. Ko, *J Nanotechnol Eng Med* **5** (2014).

170. D. Brandon, W. D. Kaplan, *Microstructural Characterization of Materials: 2nd Edition*, 2008.

171. Y. Lei, Y. Cui, Q. Huang, J. Dou, D. Gan, F. Deng, M. Liu, X. Li, X. Zhang, Y. Wei, *Ceram Int* **45** (2019).

172. Slobodan Milosavljević, *Strukturne instrumentalne metode*, University of Belgrade-Faculty of chemistry, Belgrade, 1996.

173. B. J. Inkson, *Scanning Electron Microscopy (SEM) and Transmission Electron Microscopy (TEM) for Materials Characterization*, in *Materials Characterization Using Nondestructive Evaluation (NDE) Methods*, 2016.

174. E. Niwa, C. Uematsu, T. Hashimoto, *Journal of the American Ceramic Society* **95** (2012).

175. K. S. W. Sing, *Assessment of Surface Area by Gas Adsorption*, in *Adsorption by Powders and Porous Solids: Principles, Methodology and Applications: Second Edition*, 2013.

176. R. R. Mather, *Surface modification of textiles by plasma treatments*, in *Surface Modification of Textiles*, 2009.

177. A. A. Qaiser, M. M. Hyland, *Materials Science Forum* **657** (2010).

178. T. Bhaskar, A. Pandey, S. V. Mohan, D. J. Lee, S. K. Khanal, *Waste biorefinery: Potential and perspectives*, 2018.

179. L. Brečević, D. Kralj, *Croatica Chemica Acta* **80** (2007).

180. R. Salih, Z. Veličković, M. Milošević, V. P. Pavlović, I. Cvijetić, I. V. Sofrenić, J. D. Gržetić, A. Marinković, *J Environ Manage* **326** (2023) 116838.

181. R. Salih, K. Banjanac, A. Vukoicic, J. Grzetic, A. Popovic, M. Veljkovic, D. Bezbradica, A. Marinkovic, *J Environ Chem Eng* **11** (2023) 109077.

182. B. Podkościelna, M. Sobiesiak, Y. Zhao, B. Gawdzik, O. Sevastyanova, *Holzforschung* **69** (2015).

183. R. J. A. Gosselink, A. Abächerli, H. Semke, R. Malherbe, P. Käuper, A. Nadif, J. E. G. Van Dam, *Ind Crops Prod* **19** (2004).

184. A. Jablonskis, A. Arshanitsa, A. Arnautov, G. Telysheva, D. Evtuguin, *Ind Crops Prod* **112** (2018).

185. A. Jablonskis, A. Arshanitsa, A. Arnautov, G. Telysheva, D. Evtuguin, *Ind Crops Prod* **112** (2018) 225–235.

186. O. Trott, A. J. Olson, *J Comput Chem* (2009).

187. J. J. P. Stewart, *J Mol Model* **19** (2013).

188. A. Pedretti, A. Mazzolari, S. Gervasoni, L. Fumagalli, G. Vistoli, *Bioinformatics* **37** (2021).

189. L. Wu, S. Dutta, M. Mascal, *ChemSusChem* **8** (2015).

190. J. Rusmirović, V. Lukić, T. Kovačević, M. Bogosavljević, S. Brzić, A. Marinković, T. Stevanović, *Scientific Technical Review* **69** (2019).

191. D. Kołodyńska, M. Gęca, I. V. Pylypchuk, Z. Hubicki, *Nanoscale Res Lett* **11** (2016) 152.

192. C. Fernández-Costas, S. Gouveia, M. A. Sanromán, D. Moldes, *Biomass Bioenergy* **63** (2014).

193. I. V. Pylypchuk, P. A. Lindén, M. E. Lindström, O. Sevastyanova, *ACS Sustain Chem Eng* **8** (2020).

194. Y. X. An, N. Li, H. Wu, W. Y. Lou, M. H. Zong, *ACS Sustain Chem Eng* **3** (2015).

195. K. P. Kringstad, R. Mörck, *Holzforschung* **37** (1983).

196. M. Y. Balakshin, E. A. Capanema, *RSC Adv* **5** (2015).

197. M. M. Nassar, G. D. M. MacKay, *Wood and Fiber Science* (1984).

198. A. R. J. Gosselink, *Lignin as a Renewable Aromatic Resource for the Chemical Industry* (2011).

199. I. Bykov, *Construction* (2008).

200. J. Bebić, K. Banjanac, M. Ćorović, A. Milivojević, M. Simović, A. Marinković, D. Bezbradica, *Chin J Chem Eng* **28** (2020).

201. C. Zhang, L. Gong, Q. Mao, P. Han, X. Lu, J. Qu, *RSC Adv* **8** (2018).

202. C. Garcia-Galan, Á. Berenguer-Murcia, R. Fernandez-Lafuente, R. C. Rodrigues, *Adv Synth Catal* **353** (2011).

203. V. J. Inglezakis, A. A. Zorpas, *Desalination Water Treat* **39** (2012).

204. V. J. Inglezakis, A. A. Zorpas, *Desalination Water Treat* **39** (2012) 149–157.

205. P. Pillewan, S. Mukherjee, T. Roychowdhury, S. Das, A. Bansiwal, S. Rayalu, *J Hazard Mater* **186** (2011) 367–375.

206. Y. Jia, R. Wang, A. G. Fane, *Chemical Engineering Journal* **116** (2006).

207. C. S. Bețianu, P. Cozma, M. Roșca, E. D. C. Ungureanu, I. Mămăligă, M. Gavrilescu, *Processes* **8** (2020) 1–19.

208. C. Valderrama, X. Gamisans, X. de las Heras, A. Farrán, J. L. Cortina, *J Hazard Mater* **157** (2008) 386–396.

209. W. I. Weber, H. Sontheimer, J. C. Crittenden, S. Summers, *Activated Carbon for Water Treatment*, DVGW-Forschungsstelle, Engler-Bunte Institut, Universitat Karlsruhe, Karlsruhe, Germany, 1988.

210. C. CHEN, C. LU, Y. CHUNG, J. JAN, *J Hazard Mater* **141** (2007) 520–528.

211. Q. Qu, Q. Gu, Z. Gu, Y. Shen, C. Wang, X. Hu, *Colloids Surf A Physicochem Eng Asp* **415** (2012).

212. J. Perendija, Z. S. Veličković, I. Cvijetić, J. D. Rusmirović, V. Ugrinović, A. D. Marinković, A. Onjia, *Cellulose* **27** (2020).

7. BIOGRAFIJA

Rabab Salih je rođena 20.10.1985. godine u Alzavija (Alzawiyah), država Libija (Libya). Rabab Salih je diplomirala 2009. godine na Prirodno-matematičkom fakultetu u Alzavija, država Libija. Tokom 2010. godine završila je međunarodni kurs za kompjuterske programe (International Computer Driving Licence - ICDL) (Excel, Word, PowerPoint, Access, Internet), kao i kurs obuke u medicinskoj laboratoriji, bolnica Alzavija i obuku iz oblasti serologije u Nacionalnom centru medicinskih nauka. Master studije, u oblasti zaštite životne sredine, završila je na Univerzitetu FUTURA 2017. godine, u Republici Srbiji. Školske 2018/2019. godine Rabab Salih je upisala doktorske studije na Tehnološko-metalurškom fakultetu Univerziteta u Beogradu, smer Inženjerstvo zaštite životne sredine. Položila je sve ispite kao i završni ispit na doktorskim studijama. Govori arapski i engleski jezik. U Novembru 2022. godine prijavila je temu za izradu doktorske disertacije Nastavno-naučnom veću Tehnološko-metalurškog fakulteta.

Naučno istraživački rad Rabab Salih pripada oblasti inženjerstva zaštite životne sredine i usmeren je sintezu i funkcionalizaciju visoko efikasnih adsorbenata na bazi prirodnog materijala lignina i njegovu modifikaciju sa akrilnim umreživačima koji su dobijeni iz prirodnih resursa.

Rabab Salih je objavila dva naučna rada u časopisima medjunarodnog značaja (dva rada kategorije M21) i jedno saopštenje na skupu međunarodnog značaja (kategorije M33).

8. LIST OF PUBLICATION

Radovi objavljeni u časopisima medjunarodnog značaja (M20):

Radovi u vrhunskom medjunarodnom časopisu (M21):

1. **Salih R.**, Veličković Z., Milošević M., Pavlović P. V., Cvijetić I., Sofrenić V.I., Gržetić D. J., Marinković A.: *Lignin based microspheres for effective dyes removal: Design, synthesis and adsorption mechanism supported with theoretical study*, - Journal of Environmental Management, Vol. 326, No. 0, 2023, pp. 116838. (IF(2021)=8,910; ISSN 0301-4797), DOI: 10.1016/j.jenvman.2022.116838.

2. **Salih R.**, Banjanac K., Vukoičić A., Gržetić J., Popović A., Veljković M., Bezbradica D., Marinković A.: *Acrylic modified kraft lignin microspheres as novel support for immobilization of laccase from M. thermophila expressed in A. oryzae (Novozym*® 51003) *and application in degradation of textile dyes*, - Journal of Environmental Chemical Engineering, Vol. 11, No. 1, 2023, Article number 109077. (IF(2021)=7,968; ISSN 2213-2929), DOI: 10.1016/j.jece.2022.109077

Saopštenje sa međunarodnog skupa štampano u celini (M33):

1. Bošnjaković J., Bugarčić M., Milošević M., Prlainović N., **Salih R.**, Batinić P., Popović A., Đolić M.: *Application of nano- MnO_2 modified lignin – based adsorbent for removal of dichromate ions and diclofenac from water*, Proceedings of the 29th International Conference Ecological Truth and Environmental Research - EcoTER'22, Sokobanja 2022., pp. 49 - 54, ISBN: 978-86-6305-123-2.

9. ИЗЈАВА О АУТОРСТВУ

Име и презиме аутора Рабаб Салих (Rabab Salih)
Број индекса 4036/18

Изјављујем

да је докторска дисертација под насловом
Лигнин микросфере као адсорбенти за уклањање текстилних боја и носачи за имобилизацију ензима
Lignin microspheres as adsorbents for textile dyes removal and supports for immobilization of enzymes

- резултат сопственог истраживачког рада;
- да дисертација у целини ни у деловима није била предложена за стицање друге дипломе према студијским програмима других високошколских установа;
- да су резултати коректно наведени и
- да нисам кршио/ла ауторска права и користио/ла интелектуалну својину других лица.

У Београду, 08.03.2023

Потпис аутора

RABAB SALIH

10. ИЗЈАВА О ИСТОВЕТНОСТИ ШТАМПАНЕ И ЕЛЕКТРОНСКЕ ВЕРЗИЈЕ ДОКТОРСКОГ РАДА

Име и презиме аутора Рабаб Салих (Rabab Salih)
Број индекса 4036/18
Студијски програм Инжењерство заштите животне средине
Наслов рада
Лигнин микросфере као адсорбенти за уклањање текстилних боја и носачи за имобилизацију ензима
Lignin microspheres as adsorbents for textile dyes removal and supports for immobilization of enzymes

Ментори: др Александар Маринковић и др Катарина Бањанац

Изјављујем да је штампана верзија мог докторског рада истоветна електронској верзији коју сам предао/ла ради похрањена у **Дигиталном репозиторијуму Универзитета у Београду.**
Дозвољавам да се објаве моји лични подаци везани за добијање академског назива доктора наука, као што су име и презиме, година и место рођења и датум одбране рада. Ови лични подаци могу се објавити на мрежним страницама дигиталне библиотеке, у електронском каталогу и у публикацијама Универзитета у Београду.

У Београду, 08.05.2023

Потпис аутора

RABAB SALIH

11. ИЗЈАВА О КОРИШЋЕЊУ

Овлашћујем Универзитетску библиотеку „Светозар Марковић“ да у Дигитални репозиторијум Универзитета у Београду унесе моју докторску дисертацију под насловом:

Лигнин микросфере као адсорбенти за уклањање текстилних боја и носачи за имобилизацију ензима

Lignin microspheres as adsorbents for textile dyes removal and supports for immobilization of enzymes

која је моје ауторско дело.

Дисертацију са свим прилозима предао/ла сам у електронском формату погодном за трајно архивирање.

Моју докторску дисертацију похрањену у Дигиталном репозиторијуму Универзитета у Београду и доступну у отвореном приступу могу да користе сви који поштују одредбе садржане у одабраном типу лиценце Креативне заједнице (Creative Commons) за коју сам се одлучио/ла.

1. Ауторство (CC BY)
2. Ауторство – некомерцијално (CC BY-NC)
3. Ауторство – некомерцијално – без прерада (CC BY-NC-ND)
4. Ауторство – некомерцијално – делити под истим условима (CC BY-NC-SA)
5. Ауторство – без прерада (CC BY-ND)
6. Ауторство – делити под истим условима (CC BY-SA)

(Молимо да заокружите само једну од шест понуђених лиценци.

Кратак опис лиценци је саставни део ове изјаве).

Потпис аутора

У Београду, 08.03.2023.

RABAB SALIH

1. **Ауторство**. Дозвољавате умножавање, дистрибуцију и јавно саопштавање дела, и прераде, ако се наведе име аутора на начин одређен од стране аутора или даваоца лиценце, чак и у комерцијалне сврхе. Ово је најслободнија од свих лиценци.

2. **Ауторство – некомерцијално**. Дозвољавате умножавање, дистрибуцију и јавно саопштавање дела, и прераде, ако се наведе име аутора на начин одређен од стране аутора или даваоца лиценце. Ова лиценца не дозвољава комерцијалну употребу дела.

3. **Ауторство – некомерцијално – без прерада**. Дозвољавате умножавање, дистрибуцију и јавно саопштавање дела, без промена, преобликовања или употребе дела у свом делу, ако се наведе име аутора на начин одређен од стране аутора или даваоца лиценце. Ова лиценца не дозвољава комерцијалну употребу дела. У односу на све остале лиценце, овом лиценцом се ограничава највећи обим права коришћења дела.

4. **Ауторство – некомерцијално – делити под истим условима**. Дозвољавате умножавање, дистрибуцију и јавно саопштавање дела, и прераде, ако се наведе име аутора на начин одређен од стране аутора или даваоца лиценце и ако се прерада дистрибуира под истом или сличном лиценцом. Ова лиценца не дозвољава комерцијалну употребу дела и прерада.

5. **Ауторство – без прерада**. Дозвољавате умножавање, дистрибуцију и јавно саопштавање дела, без промена, преобликовања или употребе дела у свом делу, ако се наведе име аутора на начин одређен од стране аутора или даваоца лиценце. Ова лиценца дозвољава комерцијалну употребу дела.

6. **Ауторство – делити под истим условима**. Дозвољавате умножавање, дистрибуцију и јавно саопштавање дела, и прераде, ако се наведе име аутора на начин одређен од стране аутора или даваоца лиценце и ако се прерада дистрибуира под истом или сличном лиценцом. Ова пиценца дозвољава комерцијалну употребу дела и прерада. Слична је софтверским лиценцама, односно лиценцама отвореног кода.

ПРОВЕРА ОРИГИНАЛНОСТИ ДОКТОРСКЕ ДИСЕРТАЦИЈЕ

На основу Правилника о поступку провере оригиналности докторских дисертација које се бране на Универзитету у Београду, коришћењем програма iThenticate извршена је провера оригиналности докторске дисертације кандидата Рабаб Салих (Rabab Salih) под називом **„Лигнин микросфере као адсорбенти за уклањање текстилних боја и носачи за имобилизацију ензима (Lignin microspheres as adsorbents for textile dyes removal and supports for immobilization of enzymes)“**. Извештај који садржи резултате провере оригиналности ментор је добио дана 03.02.2023. Утврђени проценат подударности је 23%. Овај проценат је последица општих места, односно употребе стручних термина и података који се тичу обрађене теме, назива коришћених метода и њихових скраћеница, личних имена, инструмената, цитиране литературе и изјава кандидата. Део подударности се односи на претходно публиковане резултате докторандових истраживања, који су проистекли из његове дисертације.

На основу свега изнетог, а у складу са чланом 8. став 2. Правилника о поступку провере оригиналности докторских дисертација које се бране на Универзитету у Београду, изјављујемо да извештај указује на оригиналност докторске дисертације, те се прописани поступак припреме за њену одбрану може наставити.

У Београду, 08.03.2023. године

Ментори

1. Др Александар Маринковић, редовни професор Универзитета у Београду, Технолошко–металуршки факултет

2. Др Катарина Бањанац, научни сарадник Универзитета у Београду, Иновациони центар Технолошко–металуршког факултета у Београду доо